
Doctoral Dissertations

Student Theses and Dissertations

Spring 2021

Convective-diffusive transport in Krogh cylinders: A model for pharmacokinetics

Xianjie Qiu

Follow this and additional works at: https://scholarsmine.mst.edu/doctoral_dissertations



Part of the [Chemical Engineering Commons](#)

Department: Chemical and Biochemical Engineering

Recommended Citation

Qiu, Xianjie, "Convective-diffusive transport in Krogh cylinders: A model for pharmacokinetics" (2021). *Doctoral Dissertations*. 2981.

https://scholarsmine.mst.edu/doctoral_dissertations/2981

This thesis is brought to you by Scholars' Mine, a service of the Missouri S&T Library and Learning Resources. This work is protected by U. S. Copyright Law. Unauthorized use including reproduction for redistribution requires the permission of the copyright holder. For more information, please contact scholarsmine@mst.edu.

CONVECTIVE-DIFFUSIVE TRANSPORT IN KROGH CYLINDERS: A MODEL
FOR PHARMACOKINETICS

by

XIANJIE QIU

A DISSERTATION

Presented to the Graduate Faculty of the
MISSOURI UNIVERSITY OF SCIENCE AND TECHNOLOGY

In Partial Fulfillment of the Requirements for the Degree

DOCTOR OF PHILOSOPHY

in

CHEMICAL ENGINEERING

2021

Approved by:

Parthasakha Neogi, Advisor

Daniel Forciniti

Chen Hou

Cheng Wang

Jee-Ching Wang

© 2021

Xianjie Qiu

All Rights Reserved

PUBLICATION DISSERTATION OPTION

This dissertation consists of the following three articles, formatted in the style used by the Missouri University of Science and Technology:

Paper I, “Convection in a Krogh cylinder: Putting back fluid in the extravascular tissue”, found on pages 15–42, has been published in *American Institute of Chemical Engineers Journal*. (Qiu et al., 2019).

Paper II, “Effect of flow on mass transfer in targeted drug delivery”, found on pages 43–73, is under journal review.

Paper III, “A convection transport model for transfer of solute to the extravascular tissue” found on pages 74–93, is under journal review.

ABSTRACT

Drug delivery to inside of the tumor is the important problem. The dynamics of drug delivery is presented here. Previously and particularly for directed delivery, a stirred tank model has been used, which appears to have worked well when compared to experiments. However, the stirred tank models do not include all the mass transfer resistances and towards that end we have used a distributed system called Krogh cylinder. This study focuses on the Krogh cylinder model simulation, both on the fluid flow and the mass transfer. The capillary network is broken down into cylindrical cells, each containing a capillary and appropriate amount of extravascular tissue. An organ is built with several of these connected in parallel. These models use the experimental data and apply many formulations, such as dynamics, through the capillary membrane, through the porous media. The result emphasizes convective mass transfer, in major disagreement with Krogh cylinder models available so far. It predicts the flow more closely to obtain a higher amount of convection in keeping with non-quantitative discussions in physiology. The equations of motion, continuity and conservation of species to obtain pressure distribution and drug distribution.

ACKNOWLEDGMENTS

First of all, I would like to thank my advisor, Dr. Parthasakha Neogi, for his invaluable guidance and help me through so many challenges during my graduate studies at Missouri University of Science and Technology. Along with him, all my committee members, Dr. Forciniti, Dr. Hou, Dr. Isaac, and Dr. Wang, helped me by providing helpful comments and by encouraging me constantly. I also would like to extend my appreciation to Dr. Dipak Barua and Dr. Joontaek Park, although they left my committee group.

I am grateful to my parents, Mr. Zuguo Qiu, Mrs. Xiaolan Luo, and my wife, Ms. Linrui Han, for all the unconditional support and encouragement. They provided to me to pursue my graduate work.

Finally, I would like to thank all the current and former faculty and staff in our chemical and biochemical engineering department for assisting, contributing to my research, and taking care of the administrative work during my graduate studies. I would say my experience at Missouri S&T was simply great.

I am very grateful again to have Dr. Neogi in my graduate studies and definitely believe he can help me grow to a stronger academic presence.

TABLE OF CONTENTS

	Page
PUBLICATION DISSERTATION OPTION	iii
ABSTRACT.....	iv
ACKNOWLEDGMENTS	v
LIST OF ILLUSTRATIONS.....	ix
LIST OF TABLES.....	xi
NOMENCLATURE	xii
 SECTION	
1. INTRODUCTION.....	1
1.1. SIGNIFICANCE OF THIS STUDY	1
1.2. MACRO AND MICRO-CIRCULATORY SYSTEM	2
1.2.1. Circulatory System.....	2
1.2.2. Microenvironment in Tumor Vascular.....	7
1.3. MODELS FOR DRUG DELIVERY	9
1.4. KROGH CYLINDER.....	11
1.5. RHEOLOGY OF BLOOD	14
1.6. PREVIEW.....	14
 PAPER	
I. CONVECTION IN A KROGH CYLINDER: PUTTING BACK FLUID FLOW IN THE EXTRAVASCULAR TISSUE.....	15
ABSTRACT	15

1. INTRODUCTION.....	16
2. METHODS (MODELS).....	22
3. RESULTS AND DISCUSSION	24
3.1. LIVER WITH NO NET LOSS.....	24
3.2. THE TRANSCAPILLARY PRESSURE DROP.....	28
3.3. FLOW IN A TUMOR	29
3.4. LIVER REVISITED.....	29
3.5. RESIDENCE TIMES	31
3.6. SUMMARY.....	32
4. CONCLUSION	33
APPENDICES	
A. GENERAL SOLUTION IN THE TISSUE	34
B. COMPLETE SOLUTION.....	36
REFERENCES.....	40
II. EFFECT OF FLOW ON MASS TRANSFER IN A TUMOR IN TARGETED DRUG DELIVERY	43
ABSTRACT.....	43
1. INTRODUCTION.....	44
2. TRACER TRANSPORT	51
3. REACTIVE SYSTEM	55
4. RESULTS AND DISCUSSION	59
5. CONCLUSIONS.....	64

APPENDICES	
A. REACTIVE SYSTEM.....	66
B. LINEAR RESPONSE THEORY.....	69
REFERENCES.....	71
III. A CONVECTIVE TRANSPORT MODEL FOR TRANSFER OF SOLUTE TO THE EXTRAVASCULAR TISSUE.....	74
ABSTRACT.....	74
1. INTRODUCTION.....	75
2. FLUID MECHANICS.....	78
3. MASS TRANSFER.....	82
4. RESULTS AND DISCUSSION.....	85
5. CONCLUSIONS.....	92
REFERENCES.....	92
SECTION	
2. CONCLUSIONS AND RECOMMENDATIONS.....	94
2.1. CONCLUSIONS.....	94
2.2. RECOMMENDATIONS.....	96
APPENDIX.....	97
BIBLIOGRAPHY.....	99
VITA.....	104

LIST OF ILLUSTRATIONS

SECTION	Page
Figure 1.1. A schematic view of human circulation system and transport to organs	3
Figure 1.2. The mesenteric capillary bed schematic view	4
Figure 1.3. Schematic view of the capillary membrane.....	5
Figure 1.4. The schematic view of fundamental pressures in intravascular and extravascular space at every single point on the capillary.....	6
Figure 1.5. The schematic view of the pharmacokinetics, the concentration versus time in human body absorption and elimination profile.....	10
Figure 1.6. The Organ Vascular and Extravascular Sub-Compartments (CSTR), the capillary membrane separates the two compartments.....	11
Figure 1.7. Schematic view drawing by Krogh presented at his Nobel lecture 1920.....	12
Figure 1.8. Schematic view of capillary in organ in parallel	13
Figure 1.9. Schematic view of Krogh cylinder	13
 PAPER I	
Figure 1. Schematic view of a Krogh cylinder.....	17
Figure 2. The fluid mechanical quantities have been shown for normal liver where ω has been set to zero as the actual value is very low.....	26
Figure 3. The fluid mechanical quantities, have been shown for tumor where ω has been set to 0.1.....	27
Figure 4. Only the tissue side has been shown.	30
 PAPER II	
Figure 1. Schematic representation of the states of antibodies from Baxter et al.....	56
Figure 2. Hapten holdup in the liver tissue as a function of time (s).....	59

Figure 3. Hapten holdup in the tumor tissue as a function of time (s)..... 60

Figure 4. Specifically bound BFA holdup in the tumor as a function of time t s. 63

Figure 5. The concentration of θ_a^b in tissue at time 60s after the mixture of free bifunctional antibody fragment \hat{c}_a^f and nonspecifically bound (B) fragment \hat{c}_a^B is injected into the capillary. 65

PAPER III

Figure 1. (a) v_r in the liver tissue, (b) v_z in the liver tissue, (c) pressure in the liver tissue..... 86

Figure 2. (a) v_r in the tumor tissue, (b) v_z in the tumor tissue, (c) pressure in the tumor tissue 88

Figure 3. Hapten holdup in the liver tissue as a function of time (s)..... 89

Figure 4. Hapten holdup in the tumor tissue as a function of time (s)..... 90

Figure 5. Specifically bound BFA holdup in the tumor as a function of time t (s). 91

Figure 6. The concentration of θ_a^b in tissue at time 60s after the mixture of free bifunctional antibody fragment \hat{c}_a^f and nonspecifically bound (B) fragment \hat{c}_a^B is injected into the capillary..... 91

LIST OF TABLES

PAPER I	Page
Table 1. Properties of the Krogh Cylinder for Liver and Tumor for a 70 kg adult	19
PAPER II	
Table 1. Properties of the Liver and Tumor model for fluid flow for a 70 kg adult human	49
Table 2. Estimated parameters for a 70 kg adult human used to simulate hapten of mol. wt. 600 as a tracer	53
Table 3. Reaction rate constants taken mainly from Baxter et al (1995).....	54

NOMENCLATURE

Symbol	Description
γ	As defined as in paper I Eq. (PAPER I APPENDIX B-11)
μ_r	As defined as in paper I Eq. (PAPER I APPENDIX B-13)
\hat{v}_z	Axial velocity in the capillary
v_z	Axial velocity in the extravascular space
K	Conductivity
a_n	Constant of separation
\hat{c}_i	Constants of integration for solution in the capillary
\hat{a}_i	Constants of integration for solution in the capillary
c_i	Constants of integration for solution in the extravascular space
α_i	Constants of integration for solution in the extravascular space
L_y	Flow to the lymphatic system
ω	Fraction fluid lost
r_i	Inner radius of the capillary
\bar{r}	is the mean tube radius
L	Length of the capillary
L_p	Membrane hydraulic coefficient
ξ_i	Non-dimensional r_i, sr_i
ξ_0	Non-dimensional r_o, sr_o
Λ	Non-dimensional L, sL
ξ	Non-dimensional r, sr

ζ	Non-dimensional z , sz
Π	Osmotic pressure difference
r_o	Outer radius of the capillary
C_{pl}	Plasma in the capillary
k	Porous medium of permeability
s	Porous medium of permeability in the value of the length scale \sqrt{k}
$\Delta\phi$	Pressure difference
Δp	Pressure drop
$\hat{\phi}$	Pressure in the capillary
ϕ	Pressure in the interstitial
Q_i	Quantity plasma input
\hat{v}_r	Radial velocity in the capillary
v_r	Radial velocity in the extravascular space
R	Radius of total tissue
α	Ratio of resistance to flow in porous medium to resistance of flow through the capillary wall
β	Ratio of resistance to flow through the capillary to resistance of flow through the capillary wall
σ	Reflection coefficient
$\hat{\psi}$	Stream function of flow through the capillary
ψ	Stream function of flow through the extravascular space
Z	Total Length of capillary and tissue
U	Urinary excretion
μ	Viscosity of plasma

1. INTRODUCTION

1.1. SIGNIFICANCE OF THIS STUDY

Cancer has high death rate, shortens life expectancy and the process of cure is long and painful. There are many new methods that cure cancer, such as chemotherapy, surgery, immunotherapy, radiation therapy, nanomedicine, and targeted therapies. The treatment usually combines options in above. The chemotherapies are often used in cancer treatment and are effective in treating many types of tumors. In order to completely remove the cancer cells, the chemotherapy is considered to be an adjuvant therapy as well. The chemotherapy drug is powerful in striking down the fast-growing cells but carries danger for the healthy cell as well. Accordingly, the pharmaceutical treatment requires accurate dosing for each patient because the people have different body volumes, metabolism, and excretion. The over dosage destroys the healthy organs and cells and endangers the health of patient as well. However, the drug flow in the tumor has problems in permeability and retention (Jain 2010). The tumor microenvironment has the hypoxia and high interstitial fluid pressure (IFP) symptoms, and lead to peritumor edema, blood vessels grow spontaneously, and accelerate the tumor progression (Jain 1989, 2007). In the microvascular environment, the fluid mechanics and transport problem have an impact. The object of this study is to analyze a mathematical model to simulate the microenvironment and provide the dosage strategies for the cancer.

1.2. MACRO AND MICRO-CIRCULATORY SYSTEM

In order to completely explain the simulation model, the thesis introduction in this part involved the basic human blood circulation and short physiology discussion.

1.2.1. Circulatory System. The human blood fluid system is a circuit. It is called the circulatory system. It is assumed to start from the heart, receives the blood with adequate oxygen from the heart at left atrium, and then at the left ventricle pumps to the system as shown Figure 1.1. The total quantity flow is Q_{total} , the normal adult approximately has 1.2-1.5 gallons of blood in their body, and approximately 10% of their weight. The blood enters the systemic circuit and carries the oxygen and nutrients to the brain and all body, and to capillaries are the main part of the blood and surrounding tissues for material exchange. The total area of human capillaries is very large. For an adult person, the total area of capillaries can reach 1000 square meters (Wolinsky, 1980). where no tissue is further than 30 μm from a capillary (Guyton and Hall, 2006). The capillaries have very thin walls and are very close to the surrounding cells. Capillaries are the smallest of the blood vessels in diameter, about 5-9 μm on average, and the most widely distributed. It connects arterioles and venules. The arterioles branch two to five times each and into the capillary network (Figure 1.2.). To ensure that all cells receive adequate nutrition, tissues are filled with many small blood vessels (capillaries). These capillaries deliver food to any cell within an adequate distance. The capillary tube has a thin permeable wall. Its function is to facilitate the exchange of substances between blood and tissues. The density of the capillary network in various organs and tissues vary greatly. Tissues and organs with strong metabolism such as skeletal muscle, myocardium, lung, kidney, and glands have a dense capillary network; otherwise, the capillary network

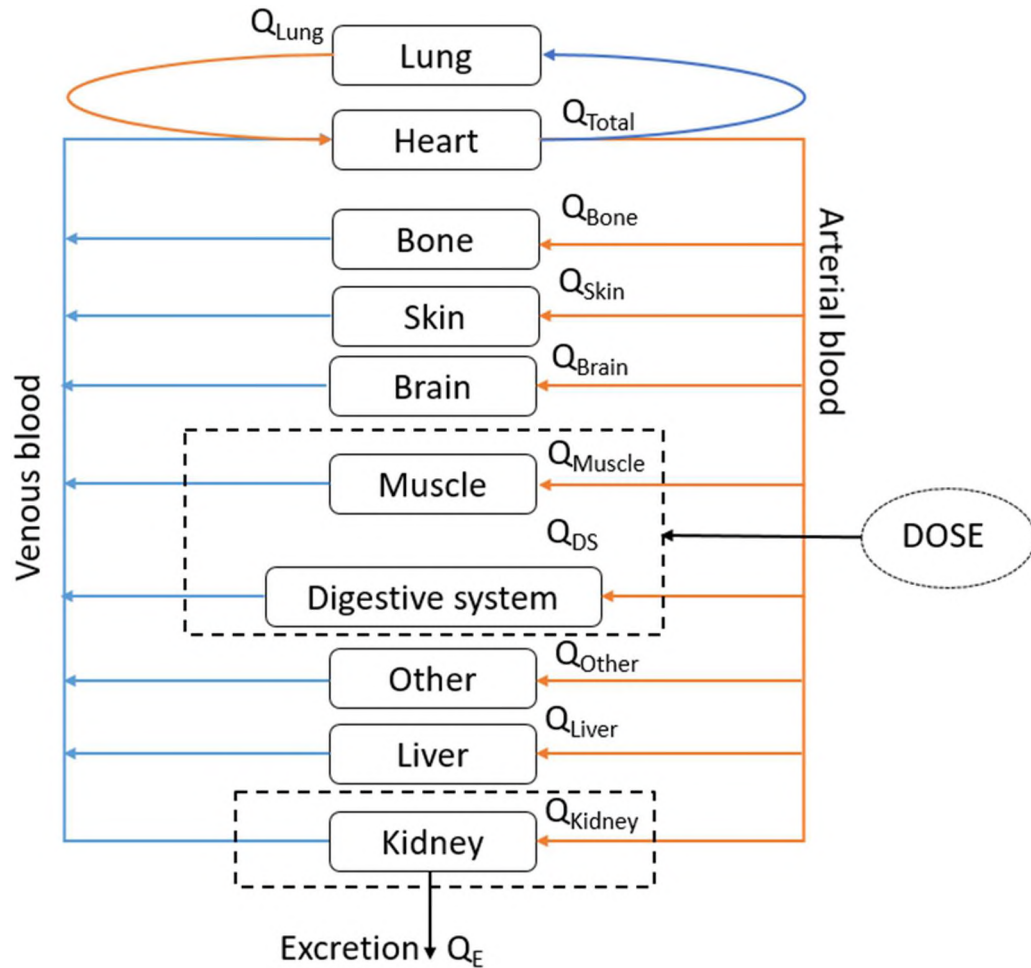


Figure 1.1. A schematic view of human circulation system and transport to organs

is sparse and for tissues with weak metabolism, such as bone, tendons, and ligaments.

There are no capillaries in cartilage, cornea, hair epithelium and tooth enamel. The blood flow rate in the capillaries is slow, the elasticity is small, and the permeability is large.

These characteristics are conducive to the full exchange of substances between blood and tissues.

The ability of a substance to penetrate the capillary wall is called capillary permeability. Studies on the relationship between capillary wall structure (as shown Figure 1.3.) and permeability have shown that the liquid can flow through the pores

between the endothelial cells and can carry some macromolecular solutes. The vesicles and vesicular channels can also allow movement of plasma and solutes. The capillary membrane can be penetrated by small molecules, but hinder the movement of substances such as proteins. Other substances, such as O_2 , CO_2 , and fat-soluble substances, can directly penetrate the endothelial cell membrane and cytoplasm (Guyton and Hall, 2000).

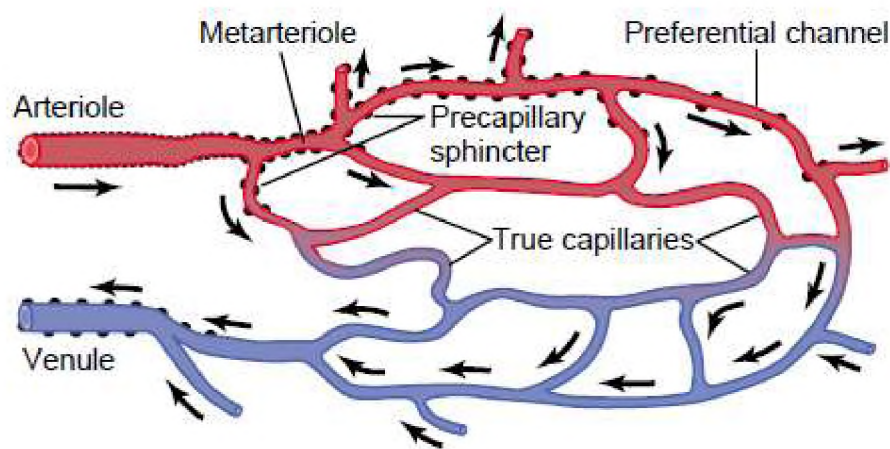


Figure 1.2. The mesenteric capillary bed schematic view (Redrawn from Zweifach, 1950, reproduced from Guyton and Hall, 2000)

Substances in the liquid inside and outside of the capillaries can diffuse through the tube wall as long as the molecular diameter is smaller than the pores in the capillary wall. The diffusion rate is proportional to the concentration difference of the substance on both sides of the capillary wall. The concentration of oxygen and glucose in the blood is higher in the capillary than in the tissue fluid, so oxygen and glucose diffuse from the capillary into the tissue fluid. The carbon dioxide concentration in the plasma is lower than the tissue fluid, and it diffuses from the tissue fluid into the plasma. The speed of

diffusion is related to the concentration difference of the solute molecules on both sides, the diffusion distance, the area of the diffusion interface, temperature, and the size of the solute molecules. In animals, tissue fluid is a part of the fluid that penetrates from the arterial end of capillaries into the interstitial space. After material exchange with tissue, it flows back into the blood in the venous beginning of capillary, some of the fluid in the tissue goes into the lymphatic system.

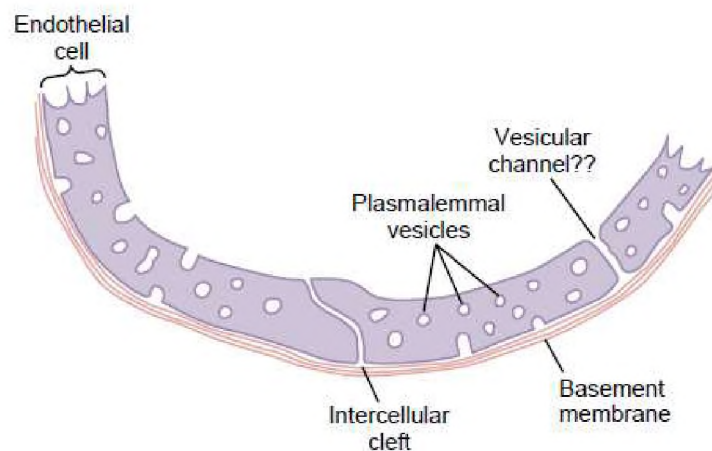


Figure 1.3. Schematic view of the capillary membrane (Redrawn from Zweifach, 1950, reproduced from Guyton and Hall (2006).

Water molecules and solute molecules go through the small pores of the capillary membrane from the side with high pressure to the side with low pressure. When the capillary pressure is higher, the plasma fluid is filtered out through the capillary walls to the tissue fluid. The tissue fluid is reabsorbed back to the blood vessel from the interstitial space into the capillary when the interstitial pressure is higher.

Besides the hydrostatic pressure, there is also the osmotic pressure. It acts in the opposite direction to the hydrostatic pressure as shown in Figure 1.4. The osmotic pressure is the pressure equivalent of the chemical potential difference and have been calculated from the compositions of the plasma in Guyton and Hall (2006).

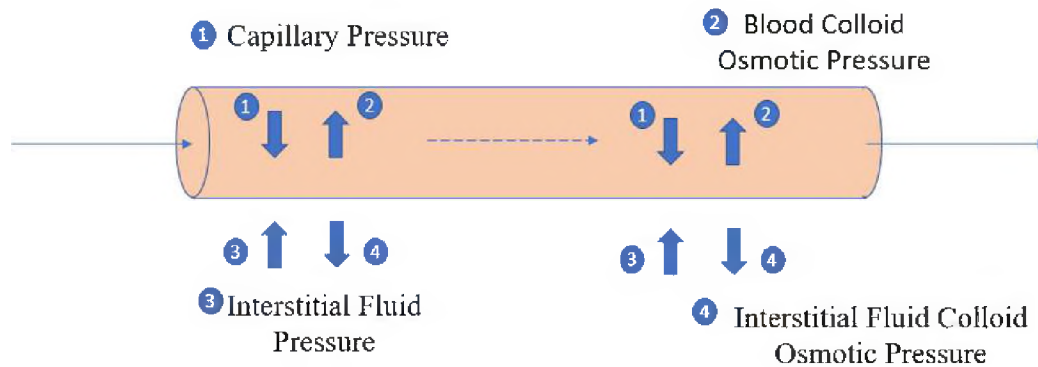


Figure 1.4. The schematic view of fundamental pressures in intravascular and extravascular space at every single point on the capillary.

Human plasma colloid osmotic pressure is mainly due to albumin in plasma, generally about 3.33kPa (25mmHg). The blood pressure of capillary vessels is about 4.0kPa (30mmHg) at the arterial end, 2.0kPa (15mmHg) at the venous end, the colloidal osmotic pressure of tissue fluid is about 2.0kPa (15mmHg), and the hydrostatic pressure of tissue fluid is about 1.33kPa (10mmHg). If these numbers are substituted into the above formula, the effective filtration pressure at the arterial end of the capillaries is 1.33kPa (10mmHg), and the effective filtration pressure at the venous end is 1.07kPa (-8mmHg). Therefore, at the capillary arterial end, the fluid is filtered out of the capillaries, and the fluid is reabsorbed at the venous end. In the work below, a reference hydrostatic pressure of zero has been used at the entrance.

In general, most (about 90%) of the fluid filtered out at the arterial end of the capillaries can be reabsorbed back into the blood at the venous end, and a small amount of fluid enters the lymphatic capillaries to the lymph node (Guyton and Hall, 2006).

1.2.2. Microenvironment in Tumor Vascular. For this thesis study, the micro-environmental of the tumor vessel is the key to the understanding the physiological mechanism background and to build the simulation model. The tumor vessels are usually not as organized as normal blood vessels, and leak more easily than normal blood vessels (see Jain, 2013 in his Figure 2). All cells require continuous oxygen, glucose, and nutrients; the transport happens through the blood and across the capillary membrane. Nutrients and oxygen are transported through the circulatory system throughout the body. Nutrients cross the blood vessel wall and enter the space around the cells in the extravascular side. Even if cancer cells are abnormal, they still need oxygen and nutrients. The development of blood vessels is a necessary step in tumor growth. The oxygen and nutrient content decrease as the region increases in the number of cells in the tumor, they move further away from the capillaries and the supply of oxygen and nutrients fall. The outer part of the tumor also has higher leakage than normal and loses fluids much faster, the leakage is approximately 5 – 10% (Gullino, 1961). In the inner part of the tumor the drainage is lower, increasing the interstitial fluid pressure (IFP) in the absence of proper lymphatic function. The experiments of Boucher et al (1996) showed the tumor to grow up from avascular stage to the vascularized tumor (see their Figure 1), and their research result show the tumor IFP to increase at the onset of angiogenesis. Angiogenesis is another issue of increase the tumor size. Tumor cells produce or cause nearby cells to produce the growth factors and stimulate blood vessel to

release the vascular endothelial growth factor (VEGF) to form new blood vessel to supply the nutrient. VEGF or other angiogenic factors produced by tumor cells or nearby cells lead the angiogenesis, and then promote tumor growth again. VEGF is a normal signal for that forms blood vessels in animal, and they are just doing their own job. Tumors "cheat" the animal body to form new blood vessels spontaneously in local area or organ. The blood vessels produced in this way are not exactly the same as normal blood vessels.

The abnormal vascular structure changes the IFP, and the tumor solid pressure as well. The pressure gradients and tortuosity become complicated in the extracellular matrix region and generates a compression pressure to the capillary. As Boucher and Jain mentioned (Boucher et al, 1992), IFP in tumor tissue is as high as 20 to 50 mmHg. As a result the plasma avoids the high-pressure region and forces blood fluid flow to be limited in the pinched vessel. The blood with abundant oxygen becomes very limited for the surrounding tissue. The decreased oxygen level in the extravascular is called hypoxia, and the hypoxia triggers changes in the behavior of tumor cells. Jain has said that the hypoxia is a critical biomarker of treatment resistance (Martin and Jain, 2020). Hypoxia induces genetic instability, angiogenesis, immunosuppression, and inflammation, and also confers resistance to oxygen delivery, as oxygen is necessary during the various treatment methods (such as radiation, certain chemotherapy, photodynamic therapy, and even immunotherapy). Hypoxia gives rise to necrosis and the necrotic region has a very high density. This heterogeneity makes the transport in tumors difficult to study. Therefore, the study of using the empirical equation and experiment data to simulate the fluid model of tumor capillary arise.

1.3. MODELS FOR DRUG DELIVERY

Pharmacokinetic model (PK) is a mathematical model which applies empirical equations and experimental data to predict the effect of drug in the human or animal body. It analyzes the absorption, distribution, metabolism, and excretion (ADME) of the drug and its concentration level. According to the principle of pharmacokinetics, numerical values of the concentrations can be used to describe the in vivo process of the drug and provide information of the drug plasma concentration. It helps to formulate a reasonable dosing plan and maintain the drug level in therapeutic range. It is necessary to adjust the dosing plan based on the body condition and avoid the maximum safe (toxic level) and the minimum effective concentration level (sub-therapeutic level). Only a standard mature human at 70 kgs is analyzed here.

The PK model is used to predict the bioavailability of the drug. The pharmaceutical solute we ingest is absorbed in the stomach or injected to the veins as input to a closed system, the concentration of drug increases initially, and decreases after the C_{\max} (the peak concentration) is reached. Concentration of the blood is the blood titer and the blood titer can be measured as a function of time from the time that the drug is introduced to its eventual elimination. This is shown schematically in Figure 1.5. The area under the curve (AUC) is taken to be the bioavailability.

The easier PK model to determine the dynamics of the solute in the blood and organs is the continuous stirred tank reactor (CSTR). The simpler early models used (Welling, 1997) became more complicated to allow every organ to be a stirred tank (Cooney, 1976). Eventually, each stirred tank was subdivided into two compartments, the blood and the extravascular tissue separated by a capillary membrane. It is only

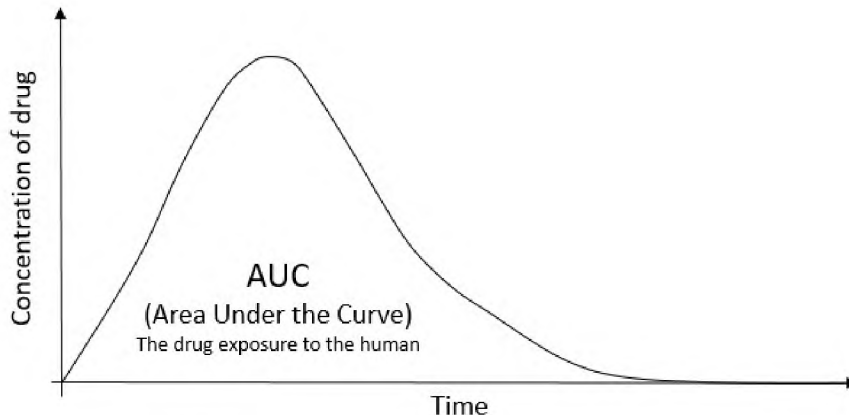


Figure 1.5. The schematic view of the pharmacokinetics, the concentration versus time in human body absorption and elimination profile

across the capillary membrane that exchange of plasma and solute can take place. The sum of the volume of the extravascular tissue and the volume inside the capillaries make up the total volume of the organ in this model as shown in Figure 1.6. One important feature here is a slow leak from the organ to the lymphatic system as shown. This feature turns out to be very important in drug delivery. This form of CSTR model is used by Baxter et al (1995). They simulated the results of first injecting a bifunctional antibody (BFA) which anchored mainly in the tumor, and after a while injected a hapten. The concentration of hapten (which was radioactive) was monitored for a long time. It is important to note that an extended period after the drug delivery, was a period of washout. The hapten is anchored to the tumor by the BFA for a long time. The comparison with experimental data was very good.

The problem with the stirred tank model is that it is a lumped system, that is, there are no spatial variations. However, spatial changes are known and some of them have

been measured. For instance, pressure drop across a standard capillary is known to be 20 mm of mercury (Guyton and Hall, 2006). When we look at AUC, it does not tell us how much of the solute has gone into the extravascular tissue, which would tell us of the effectiveness of drug delivery.

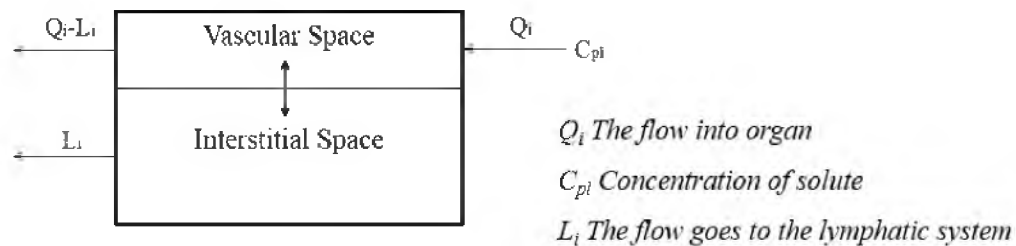


Figure 1.6. The Organ Vascular and Extravascular Sub-Compartments (CSTR), the capillary membrane separates the two compartments.

1.4. KROGH CYLINDER

Schack August Steenberg Krogh (Appendix A) made a remarkable contribution on the capillary circulation and gas exchange in the lungs, and was awarded the Noble Prize in 1912 for his work. He made further contributed on the mechanism and regulation in skeletal muscle. The below Figure 1.7. shows substantially the skeletal muscle tissue and the blood vessel. Krogh chose the skeletal muscle because the distribution of the capillary distribution is irregular. The capillaries in the skeletal muscle are actively dilating and contracting, and as illustrated of figure some of capillaries fairly regulated when tissue is in rest (Krogh, 1919 a and b). The closed capillaries are shown

with small dots, and all capillaries are distributed in the model with regularity in his model.

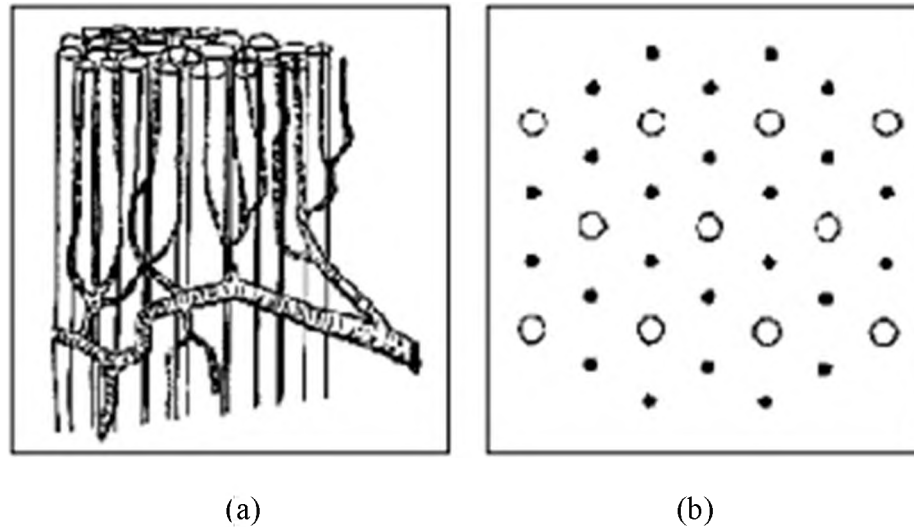


Figure 1.7. Schematic view drawing by Krogh presented at his Nobel lecture 1920. A small portion of muscle with arterial branches. Cross-section of muscle: o open and • closed capillaries

A second feature was in decoupling a single capillary from a network shown in Figure 1.4. If the network is stretched, then the smallest distance is taken to be the length of the cylinder where a capillary is modeled as one. This length L was determined from capillaries in bat wings to be 0.23 mm (Wiedeman, 1963). Smaje et al (1970) obtained a value of about 0.0615 cm cremaster muscle in rats. Kubinova et al (2013) show rat brain is 0.167 to 0.7200 cm in 3D imaging methods which appear to be very high. The present model is essentially a cell model and has been used successfully by Happel (1958) to account for a pressure drop in a packed bed. It has also been extended to mass transfer by Pfeiffer (1964). Other cell models such as tessellations, including Wigner-Seitz cell

abound in physics. Figure 1.8. is the idealized schematic view of vertical cross section cut of whole skeletal muscle (Figure 1.7. a).

As presented, the blood flow goes through the parallel capillaries. Thus, an organ is made of many Krogh cylinders in parallel. The Krogh cylinder model is shown in Figure 1.9. Krogh was able to show that in oxygen transport and consumption in the extravascular issue, all of the tissue was oxygenated.

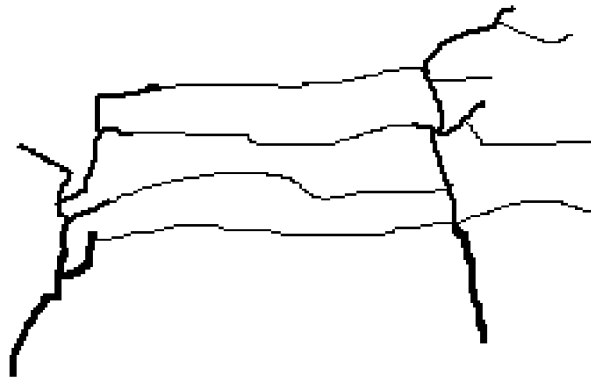


Figure 1.8. Schematic view of capillary in organ in parallel

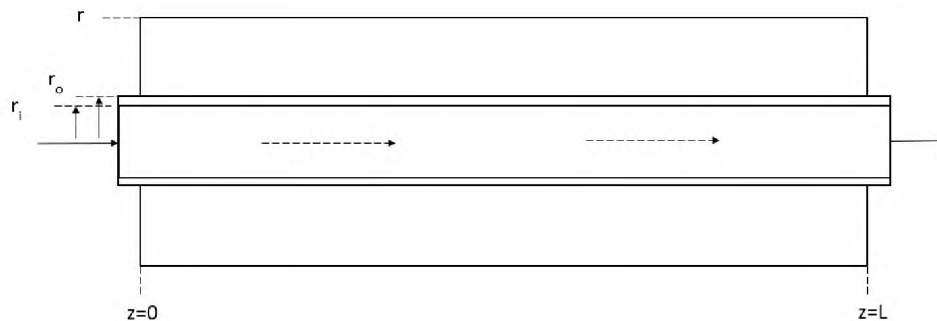


Figure 1.9. Schematic view of Krogh cylinder

1.5. RHEOLOGY OF BLOOD

The blood comprises of high weight fraction of red blood cells (RBC). Whole blood shows a small threshold stress, which is due to fibrinogen in the blood and in its absence shows only a Newtonian behavior with a viscosity of 6 mPa.s (Repløge, 1967). The long diameter of RBC is approximately 8 μm (Fournier, 1999). In studies on flow of blood into small capillaries (Fournier, 1999), the viscosity of blood is seen to decrease with decreasing diameters of the capillary. The reason is that less RBC enter the capillary. The apparent viscosities reported were volume averaged values and along with the averaged velocities the RBC concentrations in the tube were also measured. This decrease goes down to a little below tube diameter of 10 μm after which the viscosity increases sharply (Gaehtgen, 1980). At a microscopic scale, the RBC go in one by one (single file), they are bent and stay away from the walls. The walls have a thin film of plasma, which is Newtonian. Secomb et al (2006) has made a micromodel where the plasma exerts a force on the elastic membrane of the RBC to bend it, as well as a shear stress on the capillary walls. This shear stress was equated to that for Hagen-Poiseuille flow to calculate a viscosity. The values of the calculated viscosities agreed well with the experimentally measured values. In addition, the flow rate Q is proportional to Δp .

1.6. PREVIEW

In Paper I, is discussed the work in fluid flow; II is discussed present results in convective-diffusive mass transfer; and III is discussed the results when the action of the lymphatic system is included.

PAPER**I. CONVECTION IN A KROGH CYLINDER: PUTTING BACK FLUID FLOW
IN THE EXTRAVASCULAR TISSUE**

Xianjie Qiu, Nandini Sane, and Parthasakha Neogi

Department of Chemical and Biochemical Engineering, Missouri University of Science
and Technology, Rolla, MO 65409

ABSTRACT

Models for drug delivery are based on the use of stirred tanks to represent organs, that contain no mass transfer resistances. In the original Krogh cylinder model, a mass transfer resistance shows up but there is no convection in the tissue where convection should matter. In the present work, a two-dimensional flow field is used to show that when a liquid enters the capillary, some leave through the walls into the tissue at the arterial end and then doubles back into the capillary at the venous end. Some flow does not return which is taken to be the flow to the lymphatic system. We can get the measured transcapillary pressure drop of about 2666 Pa if in addition the compliance of the tube wall is taken into account. Very realistic flow fields have been shown for a model liver and a tumor.

1. INTRODUCTION

Study of pharmacokinetics or drug delivery uses two different models. In one model various organs are seen as stirred tanks. Each organ is divided into two compartments, a vascular space and an interstitial space with both stirred tanks separated by a semi-permeable membrane. The plasma comes into the vascular space and leaves from it. Most of it goes in and out of the interstitial space to return to the vascular space, but a small part is lost to the lymphatic system from the interstitial space (Baxter et al., 1995). Baxter et al (1995) also provided a very detailed compilation of physicochemical constants and we will refer to those quite often. Because the tanks are well stirred, there is no mass transfer resistance in the system except in the membrane. In contrast, there is a distributed system called the Krogh cylinder (Fournier, 1999). Krogh's model was originally used to quantify oxygen transport in the body (Krogh, 1999 a and b). However, the convective flow in the extravascular tissue is not considered. Now, the extravascular tissue is where the therapeutic drugs bind to drug-specific sites. Consequently, the convective-diffusive transport there is the key to the drug effectiveness. If it is assumed that diffusion is hindered in the tissue by both the interstitium and the cells, then Chauhan et al (2009) observe that the effective diffusivities can fall to 10^{-8} cm²/s. Consequently, even a small convection will compete with diffusion.

We analyze here fluid flow in a model Krogh cylinder. The geometry of Krogh cylinder is shown in Figure 1. It consists of a capillary surrounded by extravascular tissue. The dimensions are given in Table 1 using references listed. In the table, we have named the source used. In addition, values of parameters vary with the organ, and we

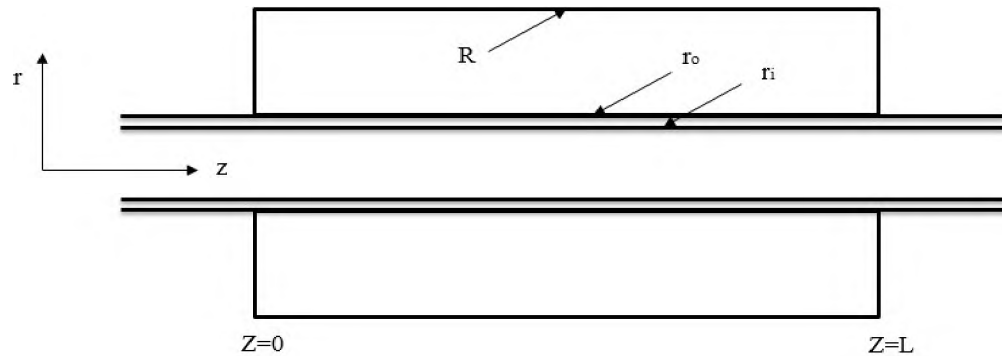


Figure 1. Schematic view of a Krogh cylinder.

have picked liver and Tumor. The vascular volumes and the tissue volumes are known for different organs and for an organ the ratio is $\frac{\pi r_i^2 L}{(R^2 - r_i^2)L}$ from which the outer radius of Krogh cylinder R has determined for the organ. Capillaries form networks between the arterial and venule ends. Most of the network has walls that are permeable to plasma and solutes. Although the length between neighboring two nodes (where the capillary bifurcates or merge) is very small, the length traced by blood from arteriole to venule ends is taken to be the length L suitable for use in a Krogh cylinder. It is often called the length of the capillary. We have used one (Table 1) and have seen somewhat longer dimension used. Fournier (1999) discusses how the capillaries/Krogh cylinders can be joined in parallel to represent a whole organ. Cell models are important in engineering, and Happel's cell model provides a good account of pressure drops in packed beds and has also been extended to mass transfer in packed beds. Some have gone further with the idea that the transport can be averaged over the network using a random or geometric arrangement (Shipley et al., 2010; Penta et al., 2015; Penta et al., 2015; Mascheroni et al,

2017; Cattaneo et al, 2014; Kojic et al, 2017 and 2018). Other models that pursue Krogh cylinders have not offered much improvement as they use one-dimensional velocity in the capillary (Goldman, 2008; Bassingthwaight et al, 1992) or side-step convection altogether (Secomb, 2014), or supplement some of the response using experimental data (Baxter et al., 1992). Whereas such approximations hold in some regime, we either do not know what the conditions are or what happens where they do not hold.

Before going into the details of the Krogh cylinder model, we note that it has been known that the pressure drop in a capillary, from the arteriole end to the venule end, is about 2666 Pa (20 mm Hg). Such a prediction cannot be made with stirred tanks where this pressure drop would be zero. Hence, one important object of the present model is to see if it is possible to predict the above pressure drop. Further, in a model similar to Krogh cylinder, Netti et al (1996) have also tried to predict this pressure drop. Their model decouples flow in the tissue from that in the capillary by setting the pressure in the tissue to a known constant. To get better results, they assumed that the capillary walls were elastic, that is, deformable. Expansion of the walls under pressure can lead to an increased and required pressure drop as shown by them. Along with showing that the pressure is 2666 Pa, it is also necessary to show that it occurs when the linear velocity of flow through the capillary to be $\sim 0.02\text{-}0.17$ cm/s (Fenster, 2015). Finally, some comparisons with the stirred tank are required, notably the residence times of fluid in stirred tank versus that in the Krogh cylinder. The flow through a membrane is given by $2\pi\bar{r}.L_p(\Delta P - \sigma\Delta\Pi)$ in $\text{cm}^3/(\text{s}. \text{cm length})$ where \bar{r} is the mean tube radius, ΔP is the difference in pressure between inside and outside and $\Delta\Pi$ is the osmotic pressure difference, which is generally fixed at 2666 Pa. L_p is the hydraulic coefficient and

Table 1. Properties of the Krogh Cylinder for Liver and Tumor for a 70 kg adult

L	Length of the capillary	0.02 cm	Healthy tissue (Netti et al., 1996)
r_o	Outer radius of the capillary	0.00055 cm	Healthy tissue (Netti et al., 1996)
L_p	Membrane hydraulic coefficient	2.700×10^{-10} m/(Pa.s)	Liver (Baxter et al., 1989)
L_p	Membrane hydraulic coefficient	21.003×10^{-10} m/(Pa.s)	Tumor (Baxter et al., 1989)
r_i	Inner radius of the capillary	0.0005 cm	Healthy tissue (Netti et al., 1996)
R	Outer radius of Krogh cylinder	0.000866 cm	Liver (Baxter et al., 1995)
R	Outer radius of Krogh cylinder	0.001482 cm	Tumor (Baxter et al., 1995)
μ	Viscosity of plasma	1 mPa.s	Similar to water
$\hat{\mu}$	Viscosity of blood	6 mPa.s	Similar to water (Fournier, 1999)
Δp	Pressure drop	2666.4 Pa	Healthy tissue (Guyton et al., 2006)
Δp	Pressure drop		Tumor
$K = k/\mu$	Conductivity	6.398×10^{-13} m ² /(Pa.s)	Liver (Swabb et al., 1974)
$K = k/\mu$	Conductivity	2.250×10^{-11} m ² /(Pa.s)	Tumor (Boucher et al., 1988)
ω	Fraction fluid lost	5-10%	Tumor (Gullino et al., 1961)
ω	Fraction fluid lost	0.01%	Liver space (Baxter et al., 1995)

represents the resistance to flow. Further, σ is the reflection coefficient which varies from 0 to 1, generally close to 1. This flux through the membrane is a local one and its value can vary on the surface. The osmotic pressure difference is due to the fact that large

molecules such as serum albumin are available in the capillary but cannot cross the membrane into the extravascular tissue. When liquid enters the capillary, plasma flows out through the permeable wall near the arterial end but 90% of it returns near the venous end of the capillary because the pressure there is now low. As a result, a circulation in the tissue is expected. Most of the discussion in this section along with some quantification can be found in Guyton and Hall (2006).

The viscosity of blood has received a lot of attention. It has a small threshold stress after which the increased shear rates, the slope in stress versus shear rate curve reaches 6 mPa.s (centipoise). So that it is a reasonable approximation to take whole blood to be Newtonian at 6 cp. Nature of flow of blood in a narrow capillary has more complications. As the tube diameter decreases below 100 μm , the red blood cells cannot all enter the capillary. There is a difference in the cell concentrations in connected tubes with large and tubes with small diameters which is the Fåhræus effect. In addition, a film of clear plasma is seen next to the wall and red blood cells collect in the central region. If we calculate the effective viscosity, then it is seen to decrease with the decreasing tube diameter reaching a minimum at 10 μm . Below that tube diameter, the effective viscosity rises and this is the Fåhræus-Lindqvist effect. At still lower diameters the red blood cells distort and flow along the centerline in a single file. Secomb et al (2006), have modeled the cells as covered with an elastic material that deforms and obtained the fluid flow resistance around the cells and the wall. This fluid is the plasma which is Newtonian and results in apparent viscosity which fits the apparent viscosity curve of Fåhræus-Lindqvist who assumed blood to be Newtonian a priori. When the apparent viscosity rises with decreasing diameter of the capillary, they do not show the viscosity to recover its original

value of 6 mPa.s although the trend suggests so. For simplicity the fluid has been assumed here to be Newtonian and a viscosity 6 mPa.s has been used here, although this value could be lower. The information in this section has been discussed by Fournier (1999). Since then, there have been many theoretical calculations made to obtain effective viscosities (Secomb et al., 2006).

Schmidt-Schobein (1999) has shown that inside the capillaries, the Reynolds numbers are very small. As a result, the continuity and momentum equations become

$$\nabla \cdot \hat{\mathbf{v}} = 0 \quad (1)$$

$$\mathbf{0} = -\nabla \hat{p} + \hat{\mu} \nabla^2 \hat{\mathbf{v}} \quad (2)$$

where vectors have been shown in bold and quantities inside the capillary with carats, thus $\hat{\mathbf{v}}$ and \hat{p} are the velocity and pressure in the capillary. The flow in the extravascular tissue is governed by the continuity and by Brinkman equation (1947).

$$\nabla \cdot \mathbf{v} = 0 \quad (3)$$

$$\mathbf{0} = -\frac{\mu}{k} \mathbf{v} - \nabla p + \mu \nabla^2 \mathbf{v} \quad (4)$$

If the viscous term, that is, the last term in Eq. (4) is ignored, then we get Darcy's law.

Here, k is the permeability and quantities without the carats are those outside the capillary. Note that the velocity \mathbf{v} in the extravascular tissue is the superficial velocity.

If $\langle \hat{v}_{zo} \rangle$ is the average inlet velocity into the capillary, then the flow rate out of the capillary is $\pi r_i^2 (1 - \omega) \langle \hat{v}_{zo} \rangle$ where ω is the fraction lost to the lymphatic system and is the ratio between the flow rate to the lymphatic system from the organ and the flow rate into the organ.

2. METHODS (MODELS)

The flow in two dimensions inside the capillary is given by the radial velocity

$$\hat{v}_r = \frac{1}{r} \frac{\partial \hat{\psi}}{\partial z} \quad \text{and the axial velocity } \hat{v}_z = -\frac{1}{r} \frac{\partial \hat{\psi}}{\partial r} \text{ where } \hat{\psi} \text{ is the stream function, and the}$$

continuity Eq. (1), is automatically satisfied and the equation of motion, Eq. (2), becomes

$$E^4 \hat{\psi} = 0 \quad (5)$$

where $E^4 = E^2 E^2$ and $E^2 = \frac{\partial^2}{\partial r^2} + \frac{1}{r} \frac{\partial}{\partial r} + \frac{\partial^2}{\partial z^2}$ (Haberman et al., 1958). Eq. (5) is

broken up into

$$E^2 \hat{\psi} = \hat{\psi}_1 \quad (6)$$

$$E^2 \hat{\psi}_1 = 0 \quad (7)$$

This is now solved using separation of variables and they report the complete solution.

Once $\hat{\psi}$ has been determined, \hat{v}_z and \hat{v}_r are obtained and substituted into Eq. (1) to

calculate \hat{p} . Stream function is defined inside the tissue as $v_r = \frac{1}{r} \frac{\partial \psi}{\partial z}$ and

$v_z = -\frac{1}{r} \frac{\partial \psi}{\partial r}$ and Eq. (4) becomes

$$E^4 \psi = \frac{E^2 \psi}{k} \quad (8)$$

which is broken down to

$$E^2 \psi_1 = k^{-1} \psi_1 \quad (9)$$

and

$$E^2\psi = k^{-1}\psi_1 \quad (10)$$

The value of the length scale \sqrt{k} is very small ~ 7 nm. In comparison, all other length scales in Table 1 are of the order of 1-10 μm . The two very disparate length scales make the differential equations stiff and exceedingly difficult to solve numerically.

However, the equations are linear, and exact solutions are possible. We assume that $s = k^{-1/2}$ and use dimensionless $\xi = sr$ and $\zeta = sz$ in both Eqs. (9) and (10) and Eqs. (6) and (7). The solutions to Eqs. (9) and (10) are given in Appendix A.

The two solutions for flow in the vascular space and tissue have to satisfy boundary conditions. These are that at the entrance of the vascular space $\hat{v}_r = 0$ and

$$\hat{v}_z = 2 \langle \hat{v}_{z0} \rangle \left[1 - \left(\frac{\xi}{\xi_i} \right)^2 \right] \text{ at } \zeta = 0 \quad (11)$$

and at the exit $\hat{v}_r = 0$ and

$$\hat{v}_z = 2 \langle \hat{v}_{z0} \rangle (1 - \omega) \left[1 - \left(\frac{\xi}{\xi_i} \right)^2 \right] \text{ at } \zeta = \Lambda \quad (12)$$

where ω is the fraction lost to the lymphatic system and $\Lambda = sL$. Eq. (11) represents Hagen-Poiseuille flow, a fully developed laminar flow of a Newtonian liquid at an average velocity of $\langle \hat{v}_{z0} \rangle$. Other conditions are of finiteness at the centerline $\xi = 0$ and that the tangential velocity \hat{v}_z at the wall $\xi = \xi_i$ is zero.

For the tissue, we take that no fluid enters or leaves the system at $\zeta = 0$ nor Λ , that is, $v_z = 0$. Like inside the capillary, the tangential velocity $v_z = 0$ on the outer surface of the capillary $\xi = \xi_o$. Further, we make the overall balance that all the fluid

that leaves the Krogh cylinder (integral of $2\pi R v_r$ at $r = R$ over z from 0 to L) is given by

$\pi r_i^2 \omega \langle \hat{v}_{zo} \rangle$, which is the loss to the lymphatic system.

Notice that we do not require that $v_r = 0$ at $\xi = Z$, that is, fluid can leave the Krogh cylinder, which is what we take to be the fluid that leaves for the lymphatic system. We do insist that the net loss be specified as noted earlier.

One very important boundary condition is mentioned earlier.

$$2\pi r_i \hat{v}_r \Big|_{r=r_i} = 2\pi \bar{r} L_p (\hat{p} \Big|_{r=r_i} - p \Big|_{r=r_o} - \sigma \Delta \Pi) = 2\pi r_o v_r \Big|_{r=r_o} \quad (13)$$

The results are given in Appendix B.

3. RESULTS AND DISCUSSION

3.1. LIVER WITH NO NET LOSS

The fluid mechanical quantities were evaluated by taking $\langle \hat{v}_{zo} \rangle = 1$ cm/s.

Matlab was used to calculate and plot, which we found gave overflow errors for $k = 6.398 \times 10^{-14}$ cm² which has a large $s = 2.529 \times 10^7$ cm⁻¹. The value of s was lowered to 10^6 cm⁻¹ about the largest value for which there is no numerical overflow. It appears in Appendix B, that the term $\sigma \Delta \Pi$ only affects the pressure in the tissue, that is, does not have a direct bearing on the fluid flow. As a results all equations are linear and we eventually calculate

$$\begin{aligned} \hat{p} \Big|_{\xi=0} - \hat{p} \Big|_{\xi=\Lambda} = \Delta \hat{p} = 2s^3 \hat{\mu} \sum_{m=1}^{\infty} a_n [\hat{c}_2 \hat{c}_5 I_0(a_n \xi)] [1 - 2(-1)^n] \\ + s \hat{\mu} \frac{8 \langle \hat{v}_{zo} \rangle \Lambda}{\xi_i^2} [1 - \omega] + \frac{2L_p \Delta p^*}{(2\mu_r \alpha + \xi_i)} s \hat{\mu} \end{aligned} \quad (14)$$

where Δp^* is the Hagen-Poiseuille pressure drop or

$$\Delta p^* = \frac{8\hat{\mu} \langle \hat{v}_{zo} \rangle L}{r_i^2} \quad (15)$$

where we have averaged the first and last terms on the right-hand side of Eq. (14) over the cross-section. All notations are explained in Appendix A. The first term in Eq. (14) is negligible. ω is set to zero here. The choice of $\langle \hat{v}_{zo} \rangle = 1$ cm/s is convenient, and if it is changed then all other fluid mechanical quantities can be changed by the same proportion in this linear problem with the exception of \hat{p} as it contains the osmotic pressure term.

Sixteen plots are shown below, eight for $\omega = 0$ for liver (actual value of ω for liver is 10^{-4}) in Figure 2 and eight for $\omega = 0.1$ for tumor in Figure 3. Most of the implications of the figures are given in the captions, however, it is worth emphasizing some. The reason for setting ω to 0.0 here is not just because ω is low but also because it would show the maximum amount of circulation in the tissue. This circulation is seen but it is weak. All parameters were taken from Table 1 except for ω which was set to zero and k that was increased by two orders of magnitude. Hence approximately, the flow would drop by two orders of magnitude if the value of k is restored to that in Table 1. Netti et al (1996) have suggested the use of the ratio between the resistance to the axial flow in the capillary to the resistance to the flow through the membrane as $\beta = 16\pi^2 r_i \hat{\mu} L_p L^2 / A_i^2$ where the inside cross-sectional area is $A_i \approx \pi r_i^2$. β is used to determine the leakiness of the membrane. We calculate β for the values used here from Table 2.1 as $\beta = 6.5 \times 10^{-11}$ which makes the membrane practically impermeable. Another ratio is the resistance of the flow

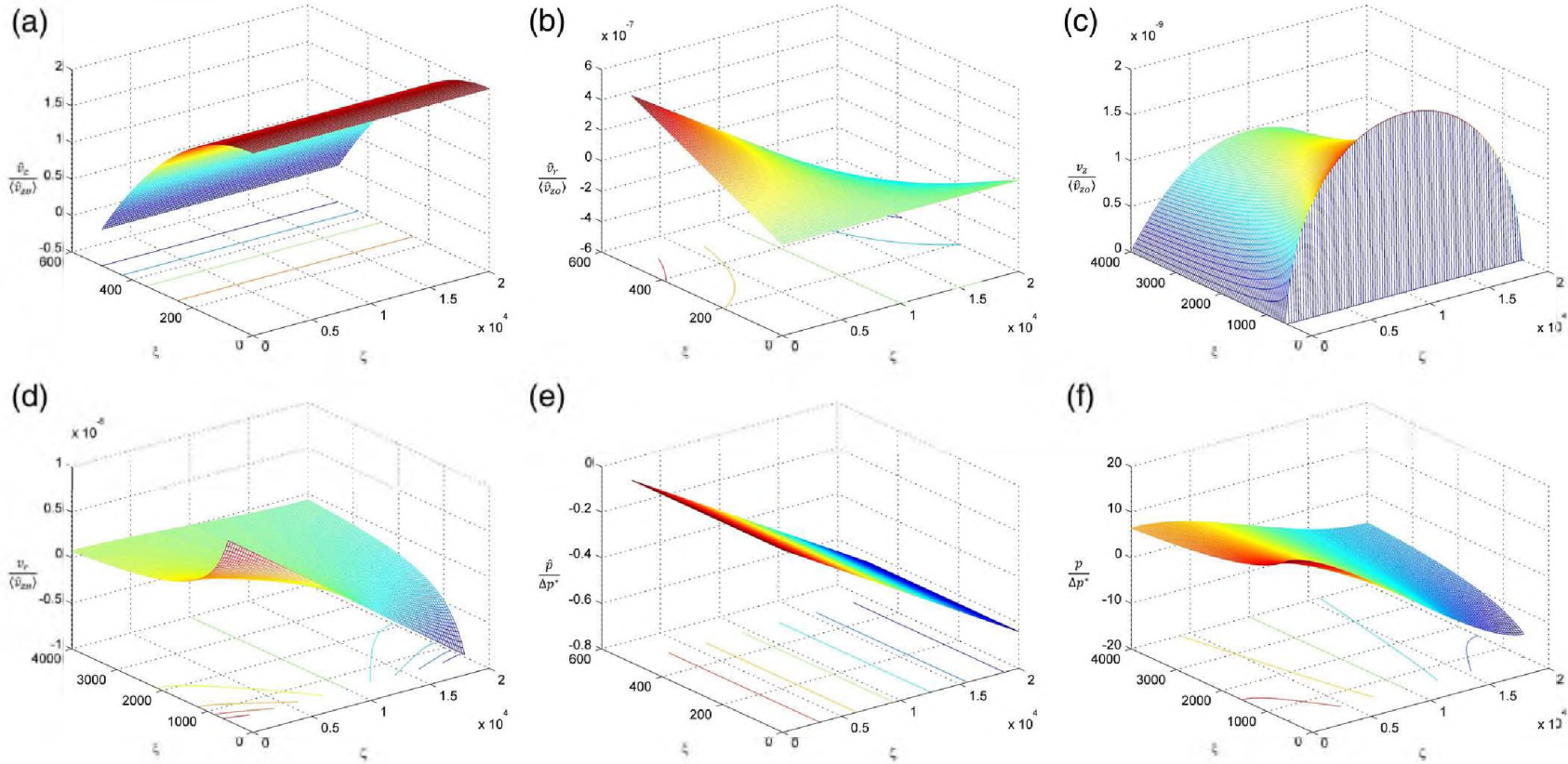


Figure 2. The fluid mechanical quantities have been shown for normal liver where ω has been set to zero as the actual value is very low. (a) The axial flow in the capillary is seen to be parabolic, and ~ 1 cm/s, that is, very high compared to (b) the radial flow. It is seen here that the flow exits radially at the arterial end and reenters at the venous end. The velocities in the tissue are shown in (c) and (d) where the axial velocity in the tissue (c) shows the circulation that takes place in the tissue and (d) shows that fluid enters the tissue at the arterial end and exits at the venous end. Pressure drop is linear inside in (e) as expected of flows with parabolic profile, and in the tissue (f) the pressures actually have negative values as measurements indicate in Guyton et al. (2006). Note that except for flow in the capillary in the axial directions, all velocities are very small.

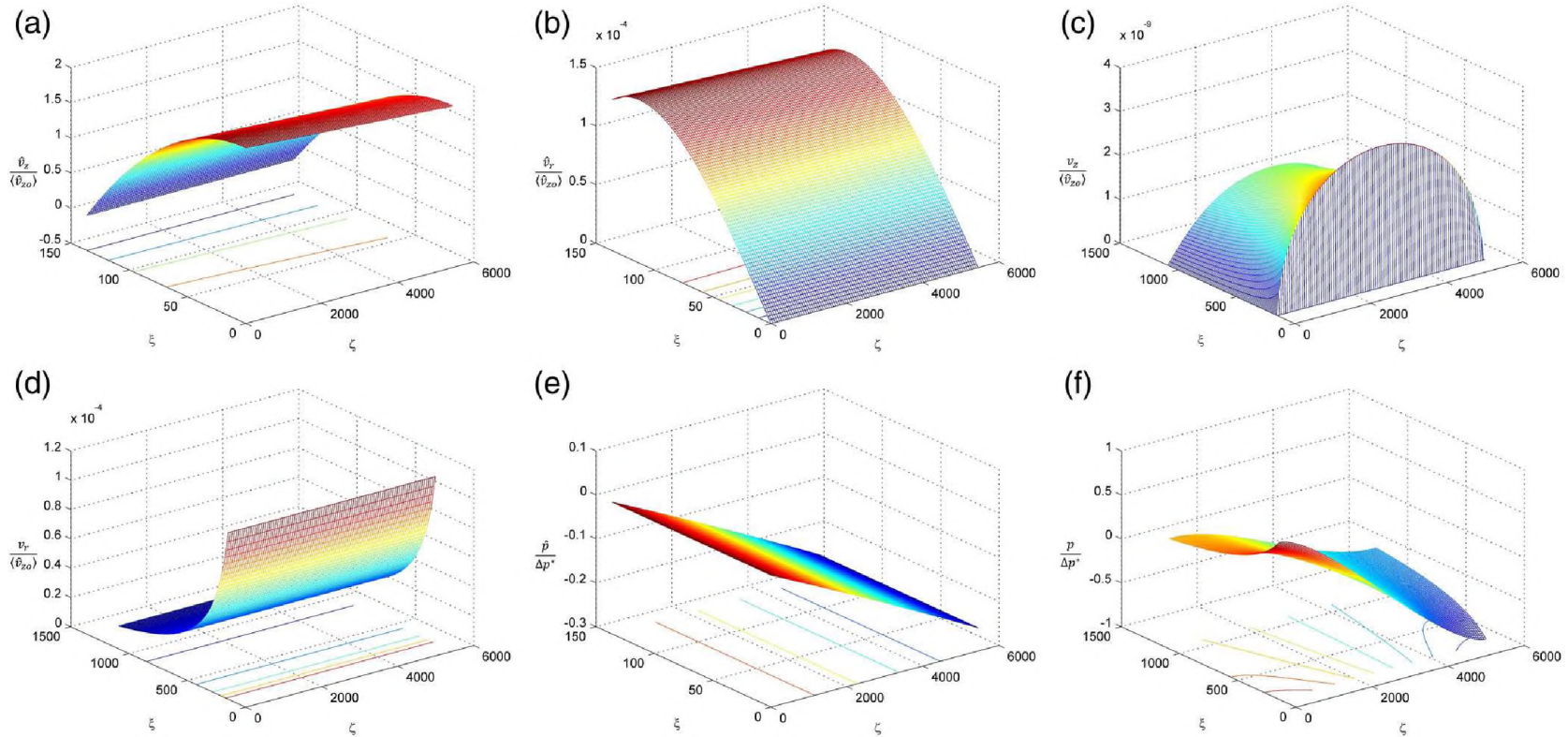


Figure 3. The fluid mechanical quantities, have been shown for tumor where ω has been set to 0.1. The sequence follows Fig. 2 but the tissue appears awash with plasma. (a) The axial flow in the capillary shows some distortion from the parabolic velocity profile and (b) the radial flow in the capillary shows a significant flux out of the capillary. (c) The axial velocity in the extravascular tumor tissue shows circulation and (d) shows radial velocity in the extravascular tumor tissue which demonstrates that a significant amount of plasma is exiting. (e) and (f) show the pressures inside and outside. Pressure drop is linear inside in (e) and shows negative pressures outside in (f). Note that due to lymphatic flow, the velocities in the radial direction are much larger. Other than axial flow in the capillary all other velocities remain very small.

in the tissue to that across the membrane in form of $\alpha = L_p S \mu = 1.06 \times 10^{-6}$ which explains why so little fluid enters the tissue.

Further decrease in the values of all velocities will take place by a factor of 10, if $\langle \hat{v}_{zo} \rangle$ is set to be 0.1 cm/s and not 1 cm/s used here. Hence, the actual flow in the tissue will now fall by 3 to 4 orders of magnitude total of Figure 2.

3.2. THE TRANSCAPILLARY PRESSURE DROP

For $\hat{\mu}$ equal to 1, 6 and 10 mPa.s we get $\Delta\hat{p}$ in Eq. (14) to be equal to 640, 3840 and 6400 Pa, whereas from Table 1 it should be 2666 Pa (20 mm Hg). If we take $\langle \hat{v}_{zo} \rangle$ to be 0.1 cm/s (instead of 1 cm/s), which falls in the 0.02-0.17 cm/s domain²⁴, then for the viscosity of blood at 6 cp, $\Delta\hat{p}$ is 384 Pa (2.9 mm Hg). Note that $\Delta\hat{p}$ is almost identical to that for Hagen-Poiseuille flow Δp^* given in Eq. (15). In Eq. (14), both first and last terms are negligible, and the middle term is identical to Eq. (15). Netti et al (1996) have argued that the compliance of the capillary walls can play a role. Smaller the elastic modulus, the enlargement of the inlet end of tube will be higher and will give rise to higher pressure drops. However, their model is not suitable here, so we put together a model in words that $\Delta\hat{p}$ is the sum of a part which is a constant and equal to 384 Pa and a part that is inversely proportional to the modulus of elasticity. Thus, if the modulus of elasticity is infinite, the value of the pressure drop of 384 Pa is returned which is the pressure drop for a tube that is rigid. Netti et al (1996) show that much larger and more appropriate values of pressure drop can be reached using a finite modulus, and they used a modulus of 8.66×10^3 Pa. Compared to material properties (1973) the value of

compliance used by Netti et al (1996) is similar the modulus of elasticity of a glassy polymer which is rigid when it should correspond with that for a rubbery polymer, which is about 100 times less. Lower compliance will raise the deformation but lower pressure drop. Thus, it is possible to come up with a pressure drop of 2666 Pa (20 mm Hg) if the capillary tube is considered to be compliant.

3.3. FLOW IN A TUMOR

We look next at a tumor. In Figure 3, $\langle \hat{v}_{zo} \rangle = 0.1$ cm/s and $\omega = 0.1$, and k and L_p have been taken from Table 1. Everything appear to be similar except in Figure 3. (b) where the radial velocity of the fluid out of the capillary is large as well as in Figure 3. (d) where the radial velocity out of the Krogh cylinder is seen to be large. The circulation in the tissue is drowned out in face of relatively large amount of fluid that flows out radially. The radial velocity in the tissue is sufficiently large that it will compete with diffusion there.

3.4. LIVER REVISITED

With this knowledge of dynamics from Figure 3, we return to Figure 2, where we set $\omega = 10^{-4}$ from Table 1. All values of the parameters are from Table 1 with the exception of k . We have to use $s = 10^6$ cm⁻¹ to prevent overflow. We also take $\langle \hat{v}_{zo} \rangle$ to be 0.1 cm/s. The results are shown in Figure 4.

The flow through the capillary is very high, comparatively speaking. Thus even if 10^{-4} of it flows out to the tissue, it will make a large contribution. Keeping in mind that

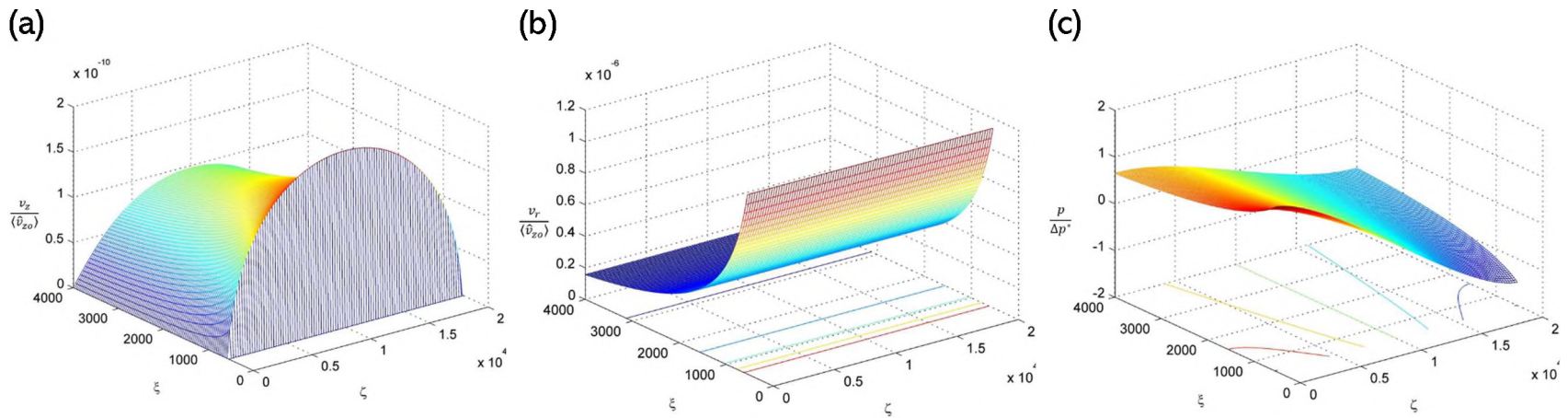


Figure 4. Only the tissue side has been shown. Both velocities in the tissue are up by two orders of magnitude in (a) and (b) in this case where $\omega = 10^{-4}$ as opposed to Fig. 2 where $\omega = 0$. The absolute value of radial velocity in (b) is also larger due to the lymphatic flow. In (c) the pressures are seen to be smaller in magnitude.

on using the correct value of permeability k , the values of velocities in Figure 4 will drop be one to two orders of magnitude, the convective transport can still be comparable to diffusion. Now, the flow behavior in Figure 4 inside the capillaries remain unchanged from Figure 2, and as a result the calculated $\Delta\hat{p} = 384 \text{ Pa}$ (2.88 mm Hg), same as for Figure 4. Consequently, we will need to consider compliance to get the transcapillary pressure up to 2666 Pa (20 mm Hg) here as well.

3.5. RESIDENCE TIMES

One important conclusion is that lymphatic flow is very important to drug delivery as mass transfer in the tissue will be convective-diffusive and lymphatic flow leads to significant convection even at small ω . This importance of lymphatic flow cannot be concluded from the stirred tank model. One other feature is the residence times which gives us the time scale of how long the fluid resides in that part of the organ. The higher this value, the better will be the absorption of a drug in that region. The residence time in a capillary is $L / \langle \hat{v}_{zo} \rangle = 0.2 \text{ s}$. For a stirred tank it is (volume of vascular space)/(volumetric flow rate out of the vascular space) = 13.6 s for liver and 148.9 s for the tumor. The residence times in the tissue in Krogh cylinder are $\frac{R-r_0}{v_r}$, which are of the order of $3.16 \times 10^4 \text{ s}$ for liver and $9.32 \times 10^4 \text{ s}$ for tumor. In contrast, the residence times in stirred tanks (volume of the tissue)/(flow rate to the lymphatic system) are $2.50 \times 10^5 \text{ s}$ for the liver and $2.18 \times 10^4 \text{ s}$ for the tumor. Thus, except for the fact that the fluid clears the vascular space remarkably fast in Krogh cylinder, all the remaining residence times are similar in the two models. In the conventional model of a Krogh

cylinder with no convection in the tissue (1999) the residence time there can be considered to be infinite.

3.6. SUMMARY

Convection in the tissue has been shown to be significant in the present model of the Krogh cylinder. Much of the flow there is due to the flow that leaves for the lymphatic system. There is a great difference between the residence times of the fluid in the capillary in the Krogh cylinder model and a similar residence time in the stirred tank model. This is probably because the vascular space defined for an organ will contain a large domain where no transport can take place through the walls, that is, vessel space before arterioles and after venules. Further, we were interested in being able to predict the transcapillary pressure of 2666 Pa but the calculated pressures for a rigid capillary was short, and to reach 2666 Pa, the walls have to be compliant.

Using the above, we can make a simple model for the flow in the system. We

take $\hat{v}_z = 2 \langle \hat{v}_{zo} \rangle [1 - \frac{r^2}{r_i^2}]$ to be the inlet velocity in the capillary and

$\hat{v}_z = (1 - \omega) 2 \langle \hat{v}_{zo} \rangle [1 - \frac{r^2}{r_i^2}]$ to be the outlet velocity in the capillary as taken in all

calculations. We also take the flow to decrease linearly from the entrance to the exit. In addition, in the capillary we can take $\hat{v}_r \approx 0$. In the tissue $v_z \approx 0$ and

$2\pi r_o L v_r|_{r=r_o} = \omega \pi r_i^2 \langle \hat{v}_{zo} \rangle$. Further, the continuity equation, Eq. (3) shows in this

case that $v_r \propto 1/r$, making complete a very reasonable view of the flow. This

approximation is almost the same as that used by Netti et al (1996). However, if we

phrase the results in terms of asymptotics, then some errors emerge. The velocities \hat{v}_z and v_r are correct to the order ω . However, v_z and \hat{v}_r have errors of the order of ω , which should be their leading order. How good the different tiers of approximations are can eventually determine through mass transfer calculations which we have started. In this connection it should be noted that the detailed calculations here, were carried out using measurements over large scale, to fit observations on large scale, averages, etc. For instance, the flow through a capillary does not satisfy pointwise velocity profile given by Hagen-Poiseuille flow, but will satisfy a measured apparent viscosity. It is not clear if this will affect mass transfer because most of the effects of mass transfer lie outside in tissue.

4. CONCLUSION

It is possible to use values of physical parameters of the system that are known and apply to the Krogh cylinder model. As a result, some of the predicted quantities can be calculated to be close some of the measured quantities. That is, Krogh cylinder model can mimic a real system. Details of the flow can be determined and in addition, the fact that flow to the lymph is important to drug delivery is seen here for the first time.

APPENDIX A.

GENERAL SOLUTION IN THE TISSUE

$$\begin{aligned} \psi = & (c_3\xi I_1(\gamma\xi) + c_4\xi K_1(\gamma\xi) + c_5\xi I_1(b\xi) + c_6\xi K_1(b\xi))(c_1\cos(b\zeta) \\ & + c_2\sin(b\zeta)) \\ & + \left(\alpha_3\xi I_1(\xi) + \alpha_4\xi K_1(\xi) + \alpha_5\frac{\xi^2}{2} + \alpha_6 \right) (\alpha_1\zeta + \alpha_2) \end{aligned} \quad (\text{A-1})$$

$$v_z = -s^2[c_3\gamma I_0(\gamma\xi) - c_4\gamma K_0(\gamma\xi) + c_5bI_0(b\xi) - c_6bK_0(b\xi)][c_1b\cos(b\zeta) + c_2\sin(b\zeta)] - s^2[\alpha_3I_0(\xi) - \alpha_4K_0(\xi) + \alpha_5][\alpha_1\zeta + \alpha_2] \quad (\text{A-2})$$

$$\begin{aligned} v_r = s^2 \left\{ [c_3I_1(\gamma\xi) + c_4K_1(\gamma\xi) + c_5I_1(b\xi) + c_6K_1(b\xi)][c_2b\cos(b\zeta) \right. \\ \left. - c_1b\sin(b\zeta)] + \alpha_1 \left[\alpha_3I_1(\xi) + \alpha_4K_1(\xi) + \alpha_5\frac{\xi}{2} + \frac{\alpha_6}{\xi} \right] \right\} \end{aligned} \quad (\text{A-3})$$

$$\begin{aligned} \frac{p}{s^3\mu} = & [c_5I_0(b\xi) - c_6K_0(b\xi)][c_1\sin(b\zeta) - c_2\cos(b\zeta)] \\ & + \alpha_5 \left[\alpha_1\frac{\zeta^2}{2} + \alpha_2\zeta \right] - \alpha_1 \left[\alpha_5\frac{\xi^2}{4} + \alpha_6\ln\xi \right] + \alpha_7 \end{aligned} \quad (\text{A-4})$$

where $c_i, i = 1, 6, \alpha_i, i = 1, 7$ are constants. I_i and K_i are modified Bessel functions of first and second kind and order i ²⁸.

APPENDIX B.
COMPLETE SOLUTION

$$\frac{v_z}{\langle \hat{v}_{z0} \rangle} = \beta \sum_{m=1}^{\infty} \sin(a_n \zeta) [c_{2n} c_{4n} \gamma_n K_0(\gamma_n \xi) - c_{2n} c_{5n} a_n I_0(a_n \xi) + c_{2n} c_{6n} a_n K_0(a_n \xi)] \quad (\text{B-1})$$

$$\frac{v_r}{\langle \hat{v}_{z0} \rangle} = \beta \sum_{m=1}^{\infty} a_n \cos(a_n \zeta) [c_{2n} c_{4n} K_1(\gamma_n \xi) + c_{2n} c_{5n} I_1(a_n \xi) + c_{2n} c_{6n} K_1(a_n \xi)] + \frac{\omega \xi_i^2}{2\Lambda} \frac{1}{\xi} \quad (\text{B-2})$$

$$\frac{p}{\Delta p^*} = \alpha \sum_{m=1}^{\infty} \cos(a_n \zeta) [-c_{2n} c_{5n} I_0(a_n \xi) + c_{2n} c_{6n} K_0(a_n \xi)] + \frac{\omega}{16\hat{\mu}} \frac{\xi_i^4}{\Lambda^2} \ln \xi \quad (\text{B-3})$$

$$\frac{\psi}{\langle \hat{v}_{z0} \rangle \xi_i^2} = \beta \sum_{m=1}^{\infty} \sin(a_n \zeta) \frac{\xi}{\xi_i^2} [c_{2n} c_{4n} K_1(\gamma_n \xi) + c_{2n} c_{5n} I_1(a_n \xi) + c_{2n} c_{6n} K_1(a_n \xi)] + \frac{\omega \xi_i^2}{2\Lambda} \zeta \quad (\text{B-4})$$

$$\frac{\hat{v}_z}{\langle \hat{v}_{z0} \rangle} = \beta \sum_{m=1}^{\infty} -\sin(a_n \zeta) [\hat{c}_{2n} \hat{c}_{3n} a_n I_0(a_n \xi) + \hat{c}_{2n} \hat{c}_{5n} a_n \xi I_1(a_n \xi) + 2\hat{c}_{2n} \hat{c}_{5n} I_0(a_n \xi)] + 2 \left(1 - \frac{\xi^2}{\xi_i^2}\right) \left[1 - \omega \frac{\zeta}{\Lambda}\right] + \frac{\beta \zeta}{(2\mu_r \alpha + \xi_i)} \left(\frac{\zeta}{\Lambda} - 1\right) \quad (\text{B-5})$$

$$\frac{\hat{v}_r}{\langle \hat{v}_{z0} \rangle} = \beta \sum_{m=1}^{\infty} a_n \cos(a_n \zeta) [\hat{c}_{2n} \hat{c}_{3n} I_1(a_n \xi) + \hat{c}_{2n} \hat{c}_{5n} \xi I_0(a_n \xi)] + \frac{\omega}{\Lambda} \xi \left(1 - \frac{1}{2} \frac{\xi^2}{\xi_i^2}\right) + \beta \frac{\xi}{(2\mu_r \alpha + \xi_i)} \left(\frac{1}{2} - \frac{\zeta}{\Lambda}\right) \quad (\text{B-6})$$

$$\frac{\hat{p}}{\Delta \rho^*} = 2\alpha \sum_{m=1}^{\infty} \cos(a_n \zeta) a_n \hat{c}_{2n} \hat{c}_{5n} I_0(a_n \xi) - \frac{\omega(2\zeta^2 - \xi^2)}{4\Lambda^2} - \frac{\zeta}{\Lambda} \left[\frac{2(\mu_r + 1)\alpha + \xi_i}{2\mu_r \alpha + \xi_i} \right] - \frac{\xi_i^2 L_p \sigma \Delta \Pi}{8\hat{\mu} \langle \hat{v}_{z0} \rangle \Lambda s} \quad (\text{B-7})$$

$$\frac{s^2 \hat{\psi}}{\langle \hat{v}_{zo} \rangle} = \beta \sum_{m=1}^{\infty} \sin(a_n \zeta) [\hat{c}_{2n} \hat{c}_{3n} \xi I_1(a_n \xi) + \hat{c}_{2n} \hat{c}_{5n} \xi^2 I_0(a_n \xi)] \quad (\text{B-8})$$

$$+ \beta \frac{\zeta \xi^2}{2(\xi_i + 2\mu_r \alpha)} \left(1 - \frac{\zeta}{\Lambda}\right) - \xi^2 \left(1 - \frac{\omega \zeta}{\Lambda}\right) \left(1 - \frac{1}{2} \frac{\xi^2}{\xi_i^2}\right)$$

where $n = 2m-1$

$$\alpha = L_p s \hat{\mu} \quad (\text{B-9})$$

$$\beta = \frac{L_p \Delta \wp}{\langle \hat{V}_{zo} \rangle} \quad (\text{B-10})$$

$$\gamma_n = \sqrt{a_n^2 + 1} \quad (\text{B-11})$$

$$a_n = \frac{\pi n}{\Lambda} \quad (\text{B-12})$$

$$\mu_r = \frac{\hat{\mu}}{\mu} \quad (\text{B-13})$$

$$\hat{\alpha}_1 \hat{\alpha}_4 = -\frac{\langle \hat{V}_{zo} \rangle}{s^2} \quad (\text{B-14})$$

$$\hat{\alpha}_5 \hat{\alpha}_7 = \frac{1}{2} \frac{\langle \hat{V}_{zo} \rangle}{\xi_i^2 s^2} \quad (\text{B-15})$$

$$\hat{\alpha}_6 \hat{\alpha}_7 = -\frac{1}{2} \frac{\omega \langle \hat{V}_{zo} \rangle}{\xi_i^2 s^2 \Lambda} \quad (\text{B-16})$$

$$\hat{\alpha}_2 \hat{\alpha}_4 + \hat{\alpha}_8 \Lambda = \frac{\omega \langle \hat{V}_{zo} \rangle}{s^2 \Lambda} \quad (\text{B-17})$$

$$\alpha_7 = -\frac{L_p \sigma \Delta \Pi}{\alpha s^2} \quad (\text{B-18})$$

$$\hat{\alpha}_8 = -\frac{L_p \Delta p^*}{2s^2 (2\mu_r \alpha + \xi_i) \Lambda} \quad (\text{B-19})$$

where the Fourier series (Mangulis, 1965)

$$\frac{\zeta}{\Lambda} - \frac{\zeta^2}{\Lambda^2} = \frac{8}{\pi^3} \sum_{m=0}^{\infty} \frac{\sin(2m+1)\pi \frac{\zeta}{\Lambda}}{(2m+1)^3} \quad (\text{B-20})$$

$$\frac{1}{3} - \frac{\zeta^2}{\Lambda^2} = \frac{4}{\pi^2} \sum_{n=1}^{\infty} (-1)^{n+1} \frac{\cos\left(n\pi \frac{\zeta}{\Lambda}\right)}{n^2} \quad (\text{B-21})$$

$$\frac{\zeta}{\Lambda} - \frac{1}{2} = \frac{4}{\pi^2} \sum_{m=0}^{\infty} -\frac{\cos(2m+1)\pi \frac{\zeta}{\Lambda}}{(2m+1)^2} \quad (\text{B-22})$$

have been used.

REFERENCES

- Abramowitz, M., Stegun, I. (1968) Handbook of Mathematical Functions. With Formulas, Graphs, and Mathematical Tables. U.S. Dept. of Commerce National Bureau of Standards; 374.
- Bassingthwaighe, J.B., Chan, I.S.J., Wang, C.J. (1992). Computationally efficient algorithms for convection-permeation-diffusion models for blood-tissue exchange. *Annals Biomedical Eng.* 20, 687-725.
<https://doi.org/10.1007/BF02368613>
- Baxter, L.T., Jain, R.K. (1989). Transport of fluid and macromolecules in tumors. I. Role of interstitial pressure and convection. *Microvasc. Res.* 37: 77-104.
- Baxter, L.T., Yuan, F., Jain, R.K. (1992). Pharmacokinetic analysis of the perivascular distribution of bifunctional antibodies and haptens: Comparison with experimental data. *Cancer Res.* 52, 5838-5844.
- Baxter, L.T., Zhu, H., Mackensen, D.G., Butler, W.F., Jain, R.K. (1995). Biodistribution of monoclonal antibodies: Scale-up from mouse to human using a physiologically based pharmacokinetic model. *Cancer Res.* 55. 4611-4622.
<https://doi.org/10.1016/j.dmpk.2018.11.002>
- Boucher, Y., Brekken, C., Netti, P.A., Baxter, L.T., Jain, R.K., (1988). Intratumoral infusion of fluid: estimation of hydraulic conductivity and implications for the delivery of therapeutic agents. *Brit. J. Cancer.* 78: 1442-1448.
- Brinkman, H.C. (1947) A calculation of the viscous force exerted by a flowing fluid on a dense swarm of particles. *Applied Scientific Research.* 1:27.
- Cattaneo, L., Zunino, P. (2014). A computational model of drug delivery through microcirculation to compare different tumor treatments. *Int. J. Numer. Meth. Biomed. Engng.* 30. 1347-1371. <https://doi.org/10.1002/cnm.2661>
- Chauhan, V.P., Lanning, R.M., Diop-frimpong, B., Mok, W., Brown, E.B., Padera, T.P., Boucher, Y., Jain, R. (2009) Multiscale measurements distinguish cellular and interstitial hindrances to diffusion in vivo. *Biophys. J.* 97: 330-336.
<https://doi.org/10.1016/j.bpj.2009.03.064>
- Fenster, A., Lacefield, J.C., (2015). *Ultrasound Imaging and Therapy.* CRC Press, Taylor & Francis, Boca Raton, FL; 2015: 67.
- Fournier, R.L. (1999) *Basic Transport in Biomedical Engineering,* Taylor and Francis, Philadelphia. 24, 44, 71.

- Goldman, D. (2008). Theoretical models of microvascular oxygen transport to tissue. *Microcirculation*. 15, 795-811. <https://doi.org/10.1080/10739680801938289>
- Gullino, P., Grantham, F. (1961). Studies on the exchange of fluids between host and tumor. I. A method for growing "tissue-isolated" tumors in laboratory animals. *J. Natl. Cancer Inst.* 27, 679–693.
- Guyton, A.C., Hall, J.E., (2006). *Textbook of Medical Physiology*, 11th ed., Saunders.
- Haberman, W.L., Sayre, R.M. (1958). Motion of rigid fluid spheres in stationary and moving liquids inside cylindrical tubes. U.S. Department of Navy, David Taylor Model Basin Report. 1143 NS 715-102.
- Haward, R.N. (1973). Introduction (The nature of polymer glasses, their packing density and mechanical behavior) in *The Physics of Glassy Polymers*, R.N. Haward, ed., Applied Sci. Pub., London; 1-53 (see Table 5, p. 43).
- Kojic, M., Milosevic, M., Simic, V., Koay, E.J., Fleming, J.B., Nizzero, S., Kojic, N., Ziemys, A., Ferrari, M. (2017). A composite smeared finite element for mass transport in capillary systems and biological tissue. *Comput. Methods Appl. Mech. Engng.* 324, 413-437. <https://doi.org/10.1016/j.cma.2017.06.019>
- Kojic, M., Milosevic, M., Simic, V., Koay, E.J., Ziemys, A., Ferrari, M. (2018). Multiscale smeared finite element model for mass transport in biological tissue: From blood vessels to cells and cellular organelles. *Comput. Biology Medicine.* 99, 7-23. <https://doi.org/10.1016/j.compbiomed.2018.05.022>
- Krogh A. (1919). The supply of oxygen to the tissues and the regulation of the capillary circulation. *The Journal of physiology*, 52(6), 457–474. <https://doi.org/10.1113/jphysiol.1919.sp001844>
- Mangulis, V. (1965) *Handbook of Series for Scientists and Engineers*, Academic Press Inc., New York, 90, 95.
- Mascheroni, P., Penta, R. (2017). The role of microvascular network structure on diffusion and consumption of anticancer drugs. *Int. J. Numer. Meth. Biomed. Engng.* 33: e2857. <https://doi.org/10.1002/cnm.2857>
- Netti, P.A., Roberge, S., Boucher, Y., Baxter, L.T., Jain, R.K. (1996). Effect of transvascular fluid exchange on pressure-flow relationship in tumors: a proposed mechanism for tumor blood flow heterogeneity. *Microvasc. Res.* 52. 27-46. <https://doi.org/10.1006/mvre.1996.0041>
- Penta, R., Ambrosi, D. (2015) The role of microvascular tortuosity in tumor transport phenomena. *J. Theor. Biol.* 364, 80-97. <https://doi.org/10.1016/j.jtbi.2014.08.007>

- Penta, R., Ambrosi, D., Quateroni, A. (2015) Multiscale homogenization for fluid and drug transport in vascularized malignant tissues. *Math. Models and Methods Appl. Sci.* 25, 79-108. <https://doi.org/10.1142/S0218202515500037>
- Schmid-Schönbein, G.W. (1999) Biomechanics of microcirculatory blood perfusion. *Annual Review of Biomedical Engineering.* 1:73-102. <https://doi.org/10.1146/annurev.bioeng.1.1.73>.
- Secomb, T.W., Hsu, R., Pries, A.R. (2006) Tribology of capillary blood flow. *Proc. IMechE v.220 Part J: J. Engineering Tribology.* 767-774. <https://doi.org/10.1243/13506501JET121>
- Secomb, T.W. (2014). Krogh-cylinder and infinite domain models for washout of an inert diffusible solute from tissue. *Microcirculation.* 22, 91-98. <https://doi.org/10.1111/micc.12180>
- Shiple, R., Chapman, S.J. (2010) Multiscale modelling of fluid and drug transport in vascular tumours. *Bull. Math. Biol.* 72, 1464-1491. <https://doi.org/10.1007/s11538-010-9504-9>
- Swabb, E.A., Wei, J., Gullinon P.M. (1974). Diffusion and convection in normal and neoplastic tissue. *Cancer Res.* 34, 2814-2822.

II. EFFECT OF FLOW ON MASS TRANSFER IN A TUMOR IN TARGETED DRUG DELIVERY

Xianjie Qiu and Parthasakha Neogi

Department of Chemical and Biochemical Engineering, Missouri University of Science and Technology, Rolla, MO 65409

ABSTRACT

The targeted delivery of a drug to a tumor is generally considered using a stirred tank model, which does not include all the mass transfer resistances. A distributed system called Krogh cylinder has been used here. The complex capillary network is broken down into cylindrical cells, each containing a capillary and appropriate amount of extravascular tissue. The flow in the cylinder model has two-dimensional velocities, which are in the axial direction and the radial direction. Whereas the area under the curve (A.U.C.) describes the bioavailability, it does not describe how much or how fast the drug is being absorbed in the extravascular tissue where therapeutic effects are expected to take place. For a given bioavailability, the uptakes of reactive and nonreactive solutes have been obtained. The diffusion in the tissue appears to be low. Most of the drug uptake happens through convection, which is actually slowed down in the presence of a reaction. For the case where a reaction takes place, a modeling effort based on local equilibrium is made, which both cuts down the computation times and provides good results for the case of reactive solutes. The full results of a distributed system have been obtained for the first time, and the mechanics of how A.U.C. can be used to calculate the

actual solute uptake has also been determined. The results emphasize the need for a higher rate of perfusion in the tumor because of the importance of convection.

1. INTRODUCTION

A pharmaceutical solute is introduced into the body plasma, and it travels to the heart and then to other organs. In chemotherapy, the drug damages all organs and not just the tumor that it was meant for. To handle this problem investigators have focused on targeted drug delivery, and a particular prescription is followed by Baxter et al (1995). The procedure uses a bifunctional antibody (BFA) that reacts selectively with the tumor. Hapten is introduced next which contains radioactive iodine. It attaches to the other arm of the BFA. Thus, it is a form of radiation therapy for the tumor. It is noteworthy that both BFA and hapten go to all parts of the body but are eventually washed out by the plasma that goes into the lymphatic system. However, the BFA-hapten unit is more strongly tied to the tumor and takes more time to dissociate and get washed out. Thus the tumor continues to be irradiated long after all the material is washed out from the other parts. In general, the predictions of their model for drug distribution show good comparison with experimental results obtained from radiation dosimetry. Their model also shows that the heart receives a smaller dosage as a result. It is noteworthy that this is a special case of the general area of drug delivery (Welling, 1997, Cooney, 1976).

Baxter et al (1995) use a stirred tank model with no adjustable parameters to predict the efficacy of the process. However, stirred tank models are lumped systems that do not include spatial variations. We use below a distributed system called Krogh

cylinder (1919), which does include model spatial variations. One shortcoming in stirred tanks is that mass transfer resistance exists only in the membranes. If the drug concentration in the blood (blood titer) is measured as a function of time, then the area under the curve (A.U.C.) is taken to represent the bioavailability of the solute. A.U.C. does not tell us how much of the drug has entered the extravascular tissue, where usually the receptors or target sites for the drug lie. It only provides a potential for such a move, where the plasma and the solute can go from the capillary to the extravascular tissue only through the walls of the capillary. It is a complex process and one main purpose here has been to relate A.U.C. to the actual delivery of the drug to the receptor which is a very lengthy problem to solve. If there is no such transport, A.U.C. will be large, but the effectiveness of the drug will be zero as one extreme. In contrast, the Krogh cylinder model (Krogh, 1919), is a distributed system that can include the resistances due to convective and diffusive transport, but so far have not been used in an inclusive way. The presence of reaction will affect concentration distribution in the extravascular tissue and hence the transport. Eventually, there is no new solute that is brought in, and plasma continues into the tissue and washes out the solute there. There is also another feature in the model of interest, namely the residence times of a solute in the capillaries, which tell us how much time is allowed for the reactions as well as the ease of transport. As will be discussed later, they are quite different in the two models because the fluid mechanical resistances to the flow of plasma are different.

Many parameters are needed to quantify the process, most of which have been amassed by Jain and coworkers as described later. However, a few more are needed here as discussed below. Blood flows through the inner cylinder of Krogh cylinder. The

capillary diameter is smaller than the size of red blood cells (RBC), and hence the RBC bend to enter into the capillary. Based on volume averaged shear rates and shear stresses, Gaehtgens (1980) found experimentally that the apparent viscosity of the whole blood was a steeply increasing function of decreasing tube diameter in the range of interest, reaching 3 mPa.s. The concentration of RBC here is much higher than normal, but they keep away from the walls and flow along the centerline in single file. Secomb et al (2006) modeled the flow of plasma as a Newtonian fluid. The RBC were considered to be covered by an elastic membrane which makes them deform due to stresses from the plasma. In the resulting flow, the shear stress at the wall is calculated and equated to that under Newtonian flow to obtain an apparent viscosity. The results fit the measured values in both magnitude and trend with decreasing tube diameters. Consequently, in the earlier work for blood flow, Qiu et al (2019) took the viscosity of blood to be Newtonian at 6 mPa.s which is its bulk viscosity. Such a value of viscosity is in line with the trend.

The capillary is enclosed in a membrane that is lined with endothelial cells. In between neighboring cells is the endothelial cleft, which forms the pore through which plasma and solute flow. Actual pores also exist, and large ones are seen in the liver, one organ that is considered below. One significant contribution is by Rippe and Haraldsson (1987) who showed that the pores were mainly bimodal at diameters of 22.5 and 4.5 nm. Baxter et al (1994) showed that the use of a bimodal pore model gave superior results when compared to experiments.

The extravascular tissue contains cells that are not permeable to the plasma that flows out of the capillary. In between the cells is a gelatinous material reinforced by proteoglycan filaments and some collagen fibers (Guyton and Hall, 2006). It is assumed

that the fluid and the solute that come out of the capillary do not flow into the cells and that the small molecules of plasma exhibit a water-like viscosity in the gel. The solute concentration c is based on the void volume of the tissue. The flow in the extravascular tissue is usually found in the form of superficial velocity as in Darcy's law (Qiu et al, 2019; Netti et al, 1996) and needs to be converted to interstitial velocity to be used in the conservation of species equation involving solute concentration c . Diffusivities in the gel are usually measured in vitro using 5% agarose gel (Iwata et al, 1996), and some researchers have also measured values in the tissue (Chauhan et al, 2009).

The main arteries enter an organ and breakdown into small blood vessels and eventually to an arteriole that generates a network of capillaries which again merge to join a venule. Smaje et al (1970) used the shortest distance traveled by blood between an arteriole and a venule to define a length for the capillaries. The results vary but a standard value of 0.02 cm is used (Netti et al, 1996) for a Krogh cylinder and an organ can be represented by Krogh cylinders in parallel (Smaje et al, 1970, Fournier et al, 1999) a feature that we use to calculate the drug availability time, that is, the micro-dosing time, t^* given below. Some researchers have assumed in their models random or geometric structures (Shipley and Chapman, 2010; Penta et al, 2015; Penta and Ambrosi, 2015; Mascheroni and Penta, 2017; Cattaneo and Zunio, 2014; Kojic et al, 2017; Kojic et al, 2018) for the capillary networks with the idea of eventually averaging the results. Averaging is done in packed beds to get Darcy's law where the details of the arrangement of the packing in the bed, do not appear. The alternate method has been to use a cell model for individual packing and Happel's cell model (Happel, 1958) works quite well. It is a fluid mechanical model that has been extended to mass transfer by Pfeffer (1964).

The latter is what a Krogh's cylinder represents, a cell, and a distributed system that provides more information.

We have chosen the system of Baxter et al (1994) both because of the complexity of the process and very many parameters in the system that are all known. In fact, it is probably the only case known to us all the information are available. There are two stages to the delivery, in the first it has to reach the tumor and then it has to penetrate the tumor. It is the latter that is being considered here.

Previously Qiu et al (2019) solved continuity and momentum balance equations in such systems and a simplified flow profile obtained there is given below

$$\hat{v}_z / \langle \hat{v}_{z0} \rangle = 2 [1 - \xi^2] [1 - \omega \zeta / \Lambda] \quad (1)$$

$$\hat{v}_r / \langle \hat{v}_{z0} \rangle = \frac{\omega}{\Lambda} \left[\xi - \frac{\xi^3}{2} \right] \quad (2)$$

$$\frac{v_r}{\langle \hat{v}_{z0} \rangle} = \frac{1}{2\xi} \frac{\omega}{\Lambda} \quad (3)$$

where a carat denotes quantities inside the capillary and quantities without a carat are in the extravascular tissue. $\langle \hat{v}_{z0} \rangle$ is the average velocity of blood entering a capillary. $\zeta = \frac{z}{r_i}$ and $\xi = \frac{r}{r_i}$ represent the dimensionless distances in the axial and radial directions, ω is the leak, that is, the fraction of fluid that is lost. Λ is the dimensionless length of the capillary L/r_i . v_r is a superficial velocity. There is a loss of plasma through the walls of the capillary which eventually leaves the Krogh cylinder. This loss is small and constitutes the fluid that is taken up by the lymphatic system (Jain, 2013, see his Figure 2). We can take the flow rate to drop linearly in the axial direction as shown in Eq. (1) because the loss in above occurs at almost a constant rate in the axial direction. Eq. (2)

results from the use of the continuity equation. Eq. (3) also results from the use of continuity between the fluxes in the tissue and the capillary at the membrane. It is assumed that the target for a drug lies in the tissue and hence this convection will play an important role in the efficacy of drug delivery. We have chosen the liver and tumor, and the values of parameters and sources are shown in Table 1. As is apparent from Table 1, values of many parameters are needed but may not be available. It is often assumed that some physiological properties do not change among mammals, some properties scale with the standard bodyweight and others with the molecular weight of the species or both.

Table 1. Properties of the Liver and Tumor model for fluid flow for a 70 kg adult human

		Liver	Tumor	Ref.
L	Length of the capillary	0.02 cm	0.02 cm	Netti et al. (1996)
r_i	Inner radius of the capillary	0.0005 cm	0.0005 cm	Netti et al. (1996)
r_o	Outer radius of the capillary	0.00055 cm	0.00055 cm	Netti et al. (1996)
R^a	Outer radius of Krogh cylinder	0.000866 cm	0.001482 cm	Baxter et al. (1995)
ω^b	Fraction of fluid lost	0.01%	5-10%	Baxter et al. (1995), Gullino and Grantham (1961)
$\langle \hat{v}_{zo} \rangle$	Blood inlet velocity	0.02-0.17 cm/s		Secomb et al. (2014)
L_p	Membrane hydraulic coefficient	2.700×10^{-10} m/(Pa.s)	21.003×10^{-10} m/(Pa.s)	Netti et al. (1996)

- a. calculated from (volume of the tissue)/(volume of the vascular space) = $\pi(R^2 - r_o^2)L / \pi r_o^2 L$. This value should be larger because not all that is considered to be the volume of the vascular space have permeable walls.
- b. calculated from (volumetric flow rate of the blood out to the lymphatic system from the organ)/(volumetric flow rate of blood into the organ) = ω

Often properties are normalized by the mass of the organ; then this value is considered to be independent of the organ. References in Table 1 contain references which discuss the details of how these numbers were arrived at. The total number of parameters for a single organ are many. Some organs have one or more of these parameters that are very much out of the range of standard values and hence much of the overall parameter space is empty. For these reasons and for directed drug delivery, the simulations are best done for specific organs, here the liver and tumor have been chosen. The tumor chosen is 20g but the data for the tumor is based on studies in mice for a small tumor of 0.7g. At this size, the tumor can be treated as homogeneous and when scaled up to 20 g in humans is also treated as homogeneous (Baxter et al, 1995).

Mass transfer calculations for the Krogh cylinder, which is a distributed system are given below. Two systems are considered. In the first, the solute is an inert tracer that is described as hapten (MW ~ 600) by Baxter et al (1995) and, second a bifunctional antibody fragment $F(ab')_2$ (MW ~ 100, 000) that binds both specifically and nonspecifically. It should be mentioned that there have been efforts to solve the Krogh cylinder problem for a distributed system (Gullino and Grantham, 1961; Goldman, 2008; Bassingthwaight et al, 1992; Secomb, 2014; Baxter et al, 1992). However, some simplifications were made, notably a lack of convection in the tissue, that we avoid below.

Consider now the main artery to the liver. It brings in the solute at concentration c_0 over a time T . Then A.U.C. = $c_0 \cdot T$ and the total solute is $M = c_0 \cdot Q \cdot T$ where Q is the flow rate of blood into the liver. If this blood vessel breaks down into many (N) capillaries, then flow of solute into each capillary is $M / N = c_0 \cdot (Q / N) \cdot t^*$, or the

microscopic dosing time is $t^* = T = \frac{M}{c_o Q}$. It is also necessary to account for the fact that the solute is distributed to all organs, which is straightforward, and we have ignored this feature. As noted earlier, other than the capillaries, none of the blood vessels allow plasma or solute out through the walls.

2. TRACER TRANSPORT

The dimensionless conservation of species equation is

$$\frac{\partial \hat{\theta}}{\partial \tau} + f(\zeta, \xi) \hat{P}e \frac{\partial \hat{\theta}}{\partial \zeta} + g(\xi) \hat{P}e \frac{\partial \hat{\theta}}{\partial \xi} = \frac{\partial^2 \hat{\theta}}{\partial \xi^2} + \frac{1}{\xi} \frac{\partial \hat{\theta}}{\partial \xi} + \frac{\partial^2 \hat{\theta}}{\partial \zeta^2} \quad (4)$$

where $\hat{\theta} = \hat{c} / c_o$, $\tau = \hat{D}t / r_i^2$ and Peclet number $\hat{P}e = \frac{\langle \hat{v}_{zo} \rangle r_i}{\hat{D}}$. Further, $\xi = r/r_i$, $\zeta = z/r_i$, Λ

$= L/r_i$ where L is the length of the capillary, $f(\zeta, \xi) = 2(1 - \xi^2) \left(1 - \omega \frac{\zeta}{\Lambda} \right)$ and

$g(\xi) = \frac{\omega}{\Lambda} \left[\xi - \frac{\xi^3}{2} \right]$. As before, the carats indicate quantities in the capillary and the

functions f and g are from Eqs. (1) and (2). The conservation equation in the tissue is

$$\frac{\partial \theta}{\partial \tau} + \frac{\hat{P}e}{\varepsilon} h \frac{\partial \theta}{\partial \xi} = d \left[\frac{\partial^2 \theta}{\partial \xi^2} + \frac{1}{\xi} \frac{\partial \theta}{\partial \xi} + \frac{\partial^2 \theta}{\partial \zeta^2} \right] \quad (5)$$

where ε is the volume fraction not occupied by the cells, $h = \frac{\omega}{\Lambda} \cdot \frac{1}{2\xi}$ from Eq. (3), the

concentration is $\theta = c / c_o$ and c_o is a reference concentration used throughout. In

addition, the diffusivity ratio is $d = D / \hat{D}$. The boundary conditions are straightforward

with the exception of the condition at the membrane

$$\left(\hat{\theta}.g.\hat{P}e - \frac{\partial \hat{\theta}}{\partial \xi}\right)\Bigg|_{\xi=1} = \frac{j_{v-i}}{c_0 \hat{D} / r_i} = \left(\theta.h.\frac{\hat{P}e}{\varepsilon} - d \frac{\partial \theta}{\partial \xi}\right)\Bigg|_{\xi=r_0/r_i} \quad (6)$$

where the quantities to the left and to the right in Eq. (6) are the convective-diffusive transport from the capillary and the tissue, normal to the membrane. Now j_{v-i} is the flux of the solute through the membrane from the vascular space to the interstitial space which is described below. For large solute molecules, Rippe and Harraldsson (1987) note that the model predicts that transport through the membrane is mainly due to convection. The flow of solute across the membrane in moles per unit time is given by

$$\begin{aligned} J_{v-i} = & J_L (1 - \sigma_L) \hat{c}|_{\xi=1} + PS_L \left(\hat{c}|_{\xi=1} - \frac{c|_{\xi=r_0/r_i}}{R} \right) \frac{Pe_L}{e^{Pe_L} - 1} + J_S (1 - \sigma_S) \hat{c}|_{\xi=1} \\ & + PS_S \left(\hat{c}|_{\xi=1} - \frac{c|_{\xi=r_0/r_i}}{R} \right) \frac{Pe_S}{e^{Pe_S} - 1} \end{aligned} \quad (7)$$

where the subscripts L and S refer to large and small pores respectively. PS is the permeability times the membrane surface area. The rejection coefficient is R taken to be 1.0 here, and σ is the reflection coefficient. The effective porosity ε is taken to be 0.3. The fluxes through the pores are

$$J_L = J_{iso} + \alpha_L L_y \quad (8)$$

$$J_S = -J_{iso} + \alpha_S L_y \quad (9)$$

where L_y is the lymphatic flow. Note that J_{iso} cancels between the two pore types. Also, $\alpha_L + \alpha_S = 1.0$. The values of the parameters are given in Tables 2 and 3. The membrane Peclet numbers are given by $Pe_L = J_L(1 - \sigma_L)/PS_L$ and $Pe_S = J_S(1 - \sigma_S)/PS_S$. The term J_{iso} needs some explanation. Rippe and Harraldsson (1987) found some circulation

Table 2. Estimated parameters for a 70 kg adult human used to simulate hapten of mol. wt. 600 as a tracer

			Liver	Tumor	Ref
J_{iso}	Recirculation flow rate	ml/min	0.1214	2.14×10^{-4}	Baxter et al. (1995)
L_y	Lymphatic flow	ml/min	8.7×10^{-2}	3×10^{-2}	Baxter et al. (1995)
ω^a	Ratio between the lymphatic flow and entering flow		1.014×10^{-4}	0.05	Baxter et al. (1995)
σ_L^b	Reflection coefficient		0.1	0.1	Rippe and Harraldsson (1987)
σ_S^b	Reflection coefficient		0.1	0.1	Rippe and Harraldsson (1987)
α_L^c	Fraction L_y from large pores		0.056	0.056	Rippe and Harraldsson (1987)
α_S^c	Fraction L_y from small pores		0.944	0.944	Rippe and Harraldsson (1987)
PS_L^d	Permeability times surface area of large pores	ml/min	0.0199	0.00561	Baxter et al. (1995)
PS_S^d	Permeability times surface area of small pores	ml/min	0.00561	6.2×10^{-5}	Baxter et al. (1995)
S^e	Surface area of the capillaries	cm ²	126630	98	Renkin (1997)
\hat{D}^f	Diffusivity in the capillary	cm ² /s	5.78×10^{-6}	5.78×10^{-6}	Renkin (1977)
D^g	Diffusivity in the tissue	cm ² /s	2.2×10^{-6}	4.3×10^{-6}	Iwata et al. (1996) Baxter et al. (1992)

a L_y/Q_i both values from Baxter et al (1995) and not from Table 1.

b available only for serum albumin for dog paw

c available only for dog paw

d both liver and tumor are considered to be hyperpermeable with permeabilities/gram ten times the other organs

e interpolated from Renkin (1977)

f interpolated from Renkin (1977)

g interpolated from Iwata et al (1996) for normal tissue and from Baxter et al (1995) for the tumor

Table 3. Reaction rate constants taken mainly from Baxter et al (1995)

	Liver	Tumor
Forward nonspecific binding rate	$k_a^{f,ns} 2.0 \times 10^{-3} \text{ min}^{-1}$	0
Backward nonspecific rate	$k_a^{r,ns} 7.0 \times 10^{-4} \text{ min}^{-1}$	0
Forward specific binding rate	$k_a^{f,s} 0$	$0.16 \times 10^9 \text{ min}^{-1} \text{ M}^{-1}$
Reverse specific rate	$k_a^{r,s} 0$	0.0085 min^{-1}
Saturation in specific binding	B_{max} none	$1.18 \times 10^{-8} \text{ M}$
Diffusivity of (Fab') ₂ in water/plasma ^a	$7.854 \times 10^{-7} \text{ cm}^2/\text{s}$	$7.854 \times 10^{-7} \text{ cm}^2/\text{s}$
Diffusivity of (Fab') ₂ in tissue ^b	$1.58 \times 10^{-9} \text{ cm}^2/\text{s}$	$5 \times 10^{-8} \text{ cm}^2/\text{s}$

- a. extrapolated from Renkin (1977). When serum albumin (MW 66,500) is added, diffusivity falls to $2.8 \times 10^{-8} \text{ cm}^2/\text{s}$.
- b. from Nugent and Jain (1984). When serum albumin is added, diffusivity falls to 3.5×10^{-10} in liver and $9.348 \times 10^{-8} \text{ cm}^2/\text{s}$ in tumor.

across the membrane, which they attributed to the osmotic pressure difference. As their system is a lumped system, J_{iso} is independent of location. There is a larger circulation arch across the tissue in Krogh cylinder where the flow depends on location (Guyton and Hall, 2006). However, Qiu et al (2019) have found this circulation to be very small in their calculated results, and it has been ignored in Eqs. (1) – (3). Finally, $j_{v-i} = J_{v-i} / S$.

The solution is obtained numerically using finite differences, forward time and central space, and explicit scheme (Roache, 1998). Values of $\hat{P}e = 15$, $\hat{D} = 5.78 \times 10^{-6} \text{ cm}^2/\text{s}$ and $D = 2.2 \times 10^{-6} \text{ cm}^2/\text{s}$ in the liver and $4.3 \times 10^{-6} \text{ cm}^2/\text{s}$ in the tumor were used. It gives us a value of $\langle \hat{v}_{zo} \rangle = 0.0867 \text{ cm/s}$. At zero-time θ and $\hat{\theta}$ were set to zeros everywhere. At the entrance to the capillary $\hat{\theta}$ was set to 1.0 starting from zero time. The result is expressed as an average concentration of hapten in the tissue

$$F = \frac{2}{(Z^2 - \xi_i^2)\Lambda} \iint_{\xi=\xi_i, Z \& \zeta=0, \Lambda} \theta \xi d\xi d\zeta \quad (10)$$

which should go up with time to 1.0.

3. REACTIVE SYSTEM

One of the systems studied by Baxter et al (1995) has an antibody as a solute. Two different parts with differing affinities are joined back, and the main stem is missing. That is, it is a bifunctional antibody (BFA) fragment $F(ab')_2$. We have shortened the full computations and look only at the process that follows when the BFA has been introduced and not followed by hapten. Instead of a pulse as in the earlier case, we have a step up in the concentration of BFA.

Conservation equations for two species in the capillary and three in the tissue are considered. The species are free (f) bifunctional antibody fragment (a) \hat{c}_a^f and nonspecifically bound (B) fragment \hat{c}_a^B in the capillary. In the tissue, we have c_a^f , c_a^B and specifically bound c_a^b fragments in the tissue. $F(ab')_2$ and a are the same. They are shown schematically in Figure 1 following Baxter et al (1995). The nonselective binding happens, as an example, with human serum albumin (HSA). The binding is reversible, and some researchers have proposed using this form of binding to provide a focused delivery (Larsen et al, 2016, Tao et al, 2019). A 1:1 binding has been assumed below.

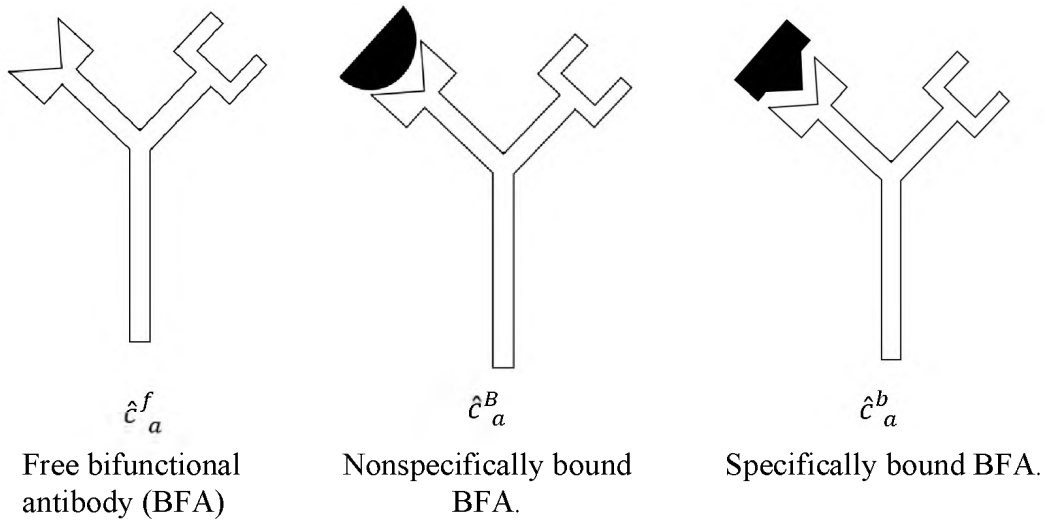


Figure 1. Schematic representation of the states of antibodies from Baxter et al (1995). The second arm is specific to hapten and in absence of hapten remains free.

The governing equations are quite lengthy, and in view of the large computation time taken for the previous case, some steps are taken to simplify the problem. In the capillary, we take \hat{c}_a^f and \hat{c}_a^B to be constants, or $c_o = \hat{c}_a^f + \hat{c}_a^B$. Taking into account the forward and the backward rate constants of binding lead to

$$\hat{\theta}_a^f = \frac{1}{1 + K_A} \quad (11)$$

$$\hat{\theta}_a^B = \frac{K_A}{1 + K_A} \quad (12)$$

where the equilibrium constant $K_A = k_a^f/k_a^r$. These are the concentrations with which the two species enter the capillary. Since the two species are pre-equilibrated, as a first approximation we can assume them to be at equilibrium everywhere. The unsteady state conservation equations in the extracellular extravascular space are lengthy and given in the Appendix A, where dimensionless groups are explained, and their values have been

defined using data in Tables 2 and 3. The reaction rate constants are given in Table 3.

The value of c_o is 2.0×10^{-8} M and the total specific binding site density is $B_{max} = 1.18 \times 10^{-8}$ M both from Baxter et al (1995, 1994).

The following relevant numbers are reported. \widehat{Pe} has been retained in the calculations as 15, and using the diffusivity of a free BFA, a value of $\langle \widehat{v}_{zo} \rangle = 0.0236$ cm/s is obtained. A value of $\langle \widehat{v}_{zo} \rangle = 0.1$ cm/s is used. The Damköhler number $Da = \frac{k_a^f r_i^2}{D}$ is 1.061×10^{-5} , a very small number. $K_A = \frac{k_a^f}{k_a^r}$ the reaction constant = 2.86. Further, d is the ratio of the diffusion coefficient of BFA bound to HSA to D is equal to 0.0020. The Damköhler number for the specific reaction is $Da' = \frac{k_a^{f'} c_o r_i^2}{D} = 1.019$, which is small and changes very little if B_{max} is used as the reference instead of c_o . Its equilibrium constant is $K_A' = \frac{k_a^{f'} c_o}{k_a^{r'}} = 376$. This is the only large number in above. The diffusion ratios are d_1 the ratio between the diffusivity of BFA in the tissue and in the capillary, and is 0.0020 for the liver and 0.064 for the tumor; d_2 is the ratio of the diffusivity between BFA bound to HSA in the tissue and the diffusivity D , and is 0.00045 for the liver and 0.119 for the tumor. These are all small numbers.

Because the nonspecific binding has been equilibrated and then introduced into the capillary, that reaction is considered to be in equilibrium in the conservation equations. Consequently, terms in the conservation equations involving this reaction have been ignored as well as in the conservation equation for the nonspecifically bound BFA. The latter has been replaced by the equilibrium relation as the specific binding has

a very high equilibrium constant. The governing equations for inside the capillaries are given below,

$$\frac{\partial \hat{\theta}_a^f}{\partial \tau} + f(\zeta, \xi) \hat{P}e \frac{\partial \hat{\theta}_a^f}{\partial \zeta} + \hat{P}e \cdot g(\xi) \frac{\partial \hat{\theta}_a^f}{\partial \xi} = \left[\frac{1}{\xi} \frac{\partial}{\partial \xi} \xi \frac{\partial \hat{\theta}_a^f}{\partial \xi} + \frac{\partial^2 \hat{\theta}_a^f}{\partial \zeta^2} \right] \quad (13)$$

$$\hat{\theta}_a^B = K_A \cdot \hat{\theta}_a^f \quad (14)$$

and in the tissue

$$\frac{\partial \theta_a^f}{\partial \tau} + \hat{P}e \cdot h(\xi) \frac{\partial \theta_a^f}{\partial \xi} = d_1 \left[\frac{1}{\xi} \frac{\partial}{\partial \xi} \xi \frac{\partial \theta_a^f}{\partial \xi} + \frac{\partial^2 \theta_a^f}{\partial \zeta^2} \right] \quad (15)$$

$$\theta_a^B = K_A \cdot \theta_a^f \quad (16)$$

$$\theta_a^b = b_{\max} K_A' \theta_a^f / [1 + K_A' \theta_a^f] \quad (17)$$

Also, $g(\zeta)$ and $h(\zeta)$ are given after Eq. (4). Eq. (16) shows that it does not matter where the active sites are located, outside the cells, inside on the cells or on the surface of the cells for this approximation, provided that the equilibrium constant does not change by a large amount in these locations.

To understand the results, we look at the extent by which the specific sites have reacted. This is given by the concentration θ_a^b or $\int_0^{\Lambda} \int_{\xi_o}^R \theta_a^b 2\pi\xi d\xi d\zeta$ where the saturation value is $\pi(R^2 - \xi_o^2)b_{\max}\Lambda$. The dimensionless form is

$$F' = \frac{\int_0^{\Lambda} \int_{\xi_o}^R \theta_a^b 2\pi\xi d\xi d\zeta}{\pi(R^2 - \xi_o^2)b_{\max}\Lambda} \quad (18)$$

4. RESULTS AND DISCUSSION

Figure 2 shows the holdup of hapten in the liver in the extravascular tissue as a function of time. The plot becomes fairly linear at large times showing that convection dominates except for a very short initial transient. The convection out of the tissue is outward in the radial direction and does not vary with the axial position. It follows that convection is the main transport mechanism in the tissue. The dosing time $t^* = 0.001042$ s which is well within the time showing the initial transients.

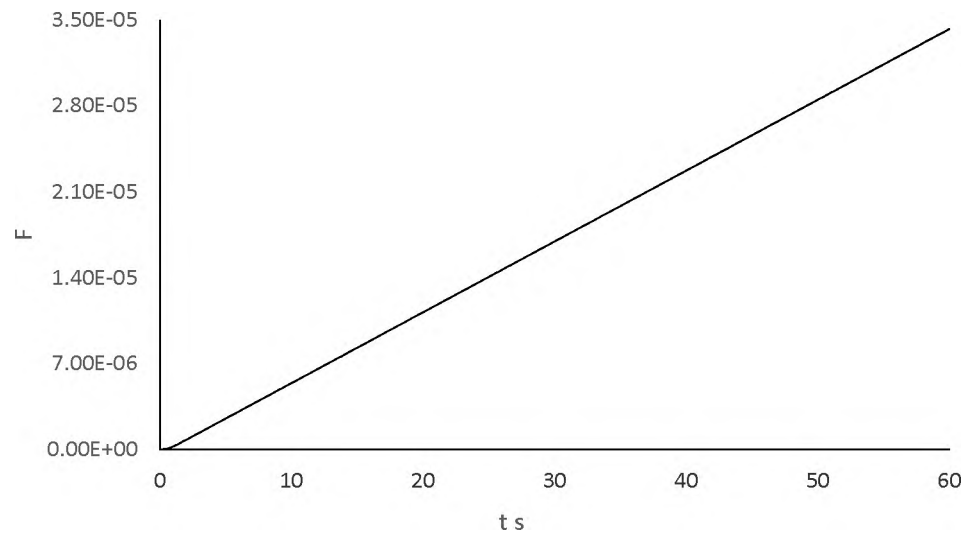


Figure 2. Hapten holdup in the liver tissue as a function of time (s). Dosing time is 0.001042 s.

Figure 3 shows the holdup of hapten in the tumor in the extravascular tissue as a function of time. The plot becomes fairly linear showing that convection dominates and the holdup increases at a faster rate than for the liver because of the higher flow rate in

the tumor. The dosing time $t^* = 0.3251$ s. The importance of the plots is clear.

Specifically, we can use the linear response theory (Appendix B) to show that F for a pulse lasting for a short t^* , is $t^* \frac{dF}{dt}$.

In cases where convection dominates, the penetration is described as a moving boundary problem where the boundary does not vary in the axial direction. The jump balance at the interface becomes for haptan

$$\left[\frac{v_r}{\varepsilon} \Big|_{r=r^*} - \frac{dr^*}{dt} \right] \cdot c_o = 0 \quad (19)$$

where $r = r^*$ describes the moving boundary in the tissue, diffusion is neglected and v_r can be obtained from Eq. (3). Integrating, we have

$$r^{*2} - r_o^2 = \langle \hat{v}_{zo} \rangle \frac{r_i^2}{\varepsilon L} \omega t \quad (20)$$

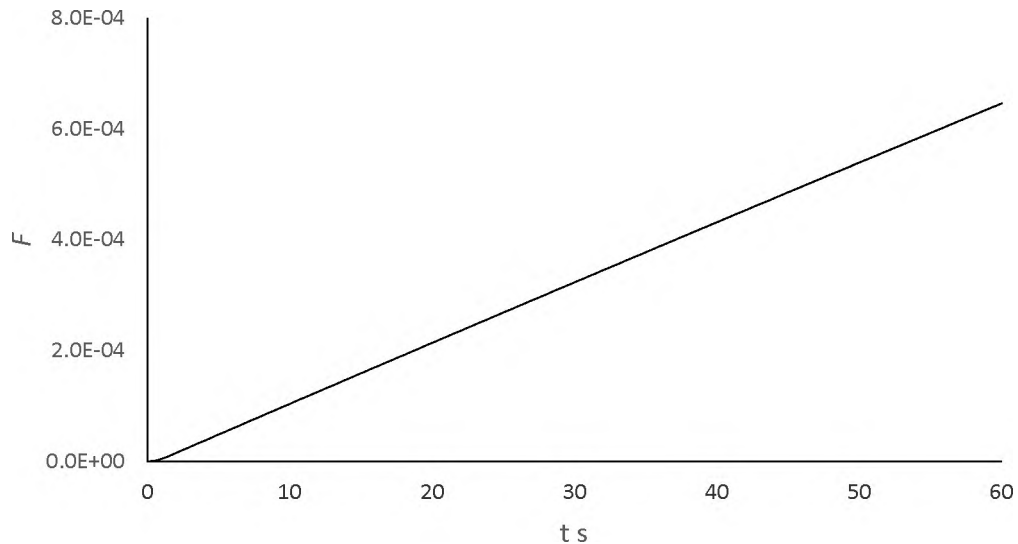


Figure 3. Haptan holdup in the tumor tissue as a function of time (s). Dosing time is 0.3251 s.

The process finishes when $r^* = R$, the outer radius of the Krogh cylinder. An assumption has been made in Eq. (19). Since the flow through the capillary is very rapid, the concentration c_o is attained at r_i at a short time. As the membrane has a rejection coefficient of 1, the concentration at the outer radius of the capillary r_o is taken to be c_o which is also attained in a very short time. Thus, the amount in the tissue as a fraction is

$$f = \langle \hat{v}_{zo} \rangle \frac{r_i^2}{\varepsilon(R^2 - r_o^2)L} \omega t \quad (21)$$

The slope of F versus t in Figure 2 in the linear region of $5.55 \times 10^{-7} \text{ s}^{-1}$, is far lower than the slope predicted by Eq. (21) of $9.31 \times 10^{-4} \text{ s}^{-1}$ (f versus t If a concentration profile exists in the tissue due to diffusion initially, then the convected amount will be less than the saturation amount assumed in Eq. (19). As a result, relating the average concentration with a saturation concentration in Eq. (18) with lower the rate of penetration. These remarks also apply to the non-reactive systems discussed earlier (Figures 2 and 3) where the fronts appear to move slower than the convection-only model.

In Figure 4, the uptake of BFA in the tumor has been shown as a function of time. At 60 s the initial transients are gone and the system settles to convective mass transfer. However, the initial transients are significant. In Figure 5, it is seen that the initial band of concentration gradients in the tumor that is established in the first 60 s, continues, at least upto 60 s as shown.

To model the reactive system, an additional assumption is needed, since the reaction is available in terms of per unit volume. It is assumed that the reaction occurs at the surface of cells of radius a_c which is 1-10 μm , and surrounded by void with an overall

radius a_o , then the volume per unit cell surface area is $\frac{a_c}{3(1-\varepsilon)}$. The jump balance

becomes for haptan

$$\left(\frac{v_r|_{r=r^*}}{\varepsilon} - \frac{dr^*}{dt}\right) \frac{c_o}{1+K_A} = k_a^{f,s} B_{\max} \frac{c_o}{1+K_A} \frac{a_c}{3(1-\varepsilon)} \quad (22)$$

which integrates to

$$t = -\frac{r^* - r_0}{b} - \frac{a}{b^2} \ln \frac{a - br^*}{a - br_0} \quad (23)$$

where $a = \frac{\langle \hat{v}_{z0} \rangle r_i \omega}{2\Lambda\varepsilon}$ and $b = k_a^{f,s} B_{\max} \frac{a_c}{3(1-\varepsilon)}$. Eq. (22) when compared to Eq. (19)

shows that $\frac{dr^*}{dt}$ decreases in presence of reaction. For small values of b Eq. (23) gives us

f in Eq. (20) that is linear in t just as shown in Figure 4 at large times. That is at large times, the convection dominates. When the reaction rate given by b is high, Eq. (23) is not valid. It is also known there that the front is characterized by zero reactant concentration. It now follows that large concentration gradients will arise and diffusion will remain important. The conclusion here is that the convection only model shows a much higher rate of penetration, which means that overall at even at later times, the diffusion is never really shaken off and results in a lower rate of penetration. Thus to increase the rate of solute penetration into the tumor, it is necessary to increase perfusion into the tumor. The rate of perfusion in the tumor is already lowered because many lymphatic ducts are damaged, blocking some of the flow out. Jain (2013) has pointed this out and provided some solutions to mitigate this problem.

The main thrust in the modeling by Baxter et al (1995) has been to look at what happens to the solute after the dosing time when only the plasma enters the extravascular tissue. Under the convection dominant model, for haptens, one would see a band that moving radially outwards with the local radial velocities, as given in Eq. (9). For the BFA, the reverse reaction rate constant is very low, so the lower edge of the band will move outwards at a very low speed, and the upper edge at the same speed as given in Eq. (23), at least to the first approximation.

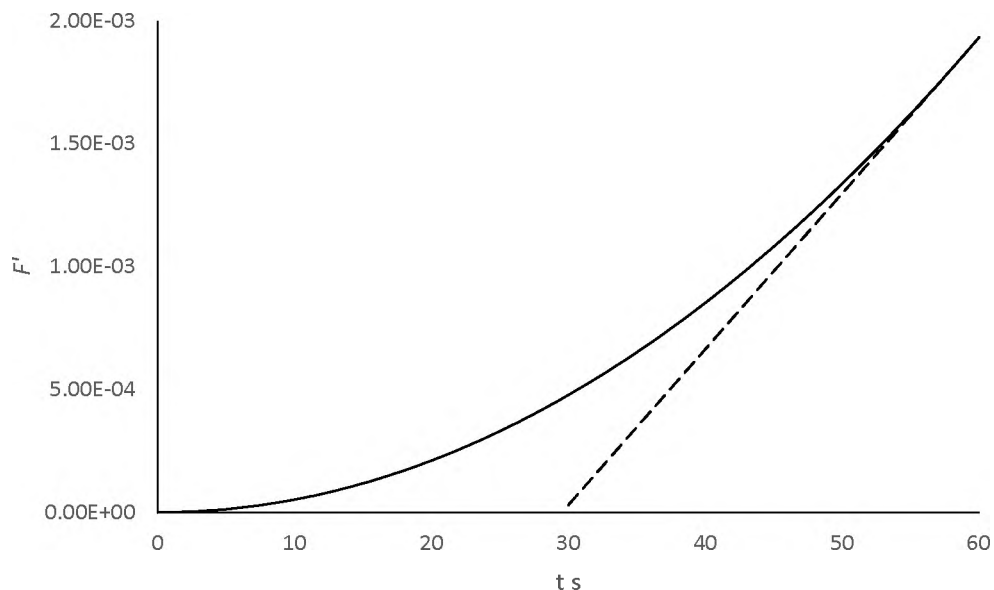


Figure 4. Specifically bound BFA holdup in the tumor as a function of time t s. The dashed line shows a linearity that is observed after an initial transient. The dosing t^* is 3.9 s.

We have confirmed that convection in the tissue is important to drug delivery even though the convection we have to work with is small. This conclusion could not be arrived at using stirred tanks. The results are also in contrast to Krogh's (1919) original

model which used only diffusion in the tissue. A key accomplishment is that of the use of local equilibrium, which not just gives us good results, but also brings down the computation time which still remain large but within limits. It is possible to calculate the residence times for the liver in the Krogh cylinder model for the capillary as

$$\tau_c = L / \langle \hat{v}_{z_0} \rangle = 0.2 \text{ s and of the extravascular tissue } \tau_e = \frac{(R^2 - r_o^2).L}{\omega.r_i^2 \langle \hat{v}_{z_0} \rangle} = 3790 \text{ s. For the}$$

stirred tank model from Baxter et al (1995), where $\tau_c = \frac{\text{vascular volume}}{\text{plasma flow rate}} = 13.56 \text{ s}$ and

$$\tau_e = \frac{\text{total volume} - \text{vascular volume}}{\text{lymphatic flow rate}} = 1.122 \times 10^6 \text{ s. They do not agree except in that the}$$

τ_e in either model is very large.

5. CONCLUSIONS

Convective transport is the most important factor in the mass transfer of a reactive solute in the tissue. The solution of the transport equations in the extravascular tissue demonstrates the above, and shows diffusion to be important at short times and reaction slows down the uptake. We have provided a link between A.U.C. and the actual uptake for the first time.

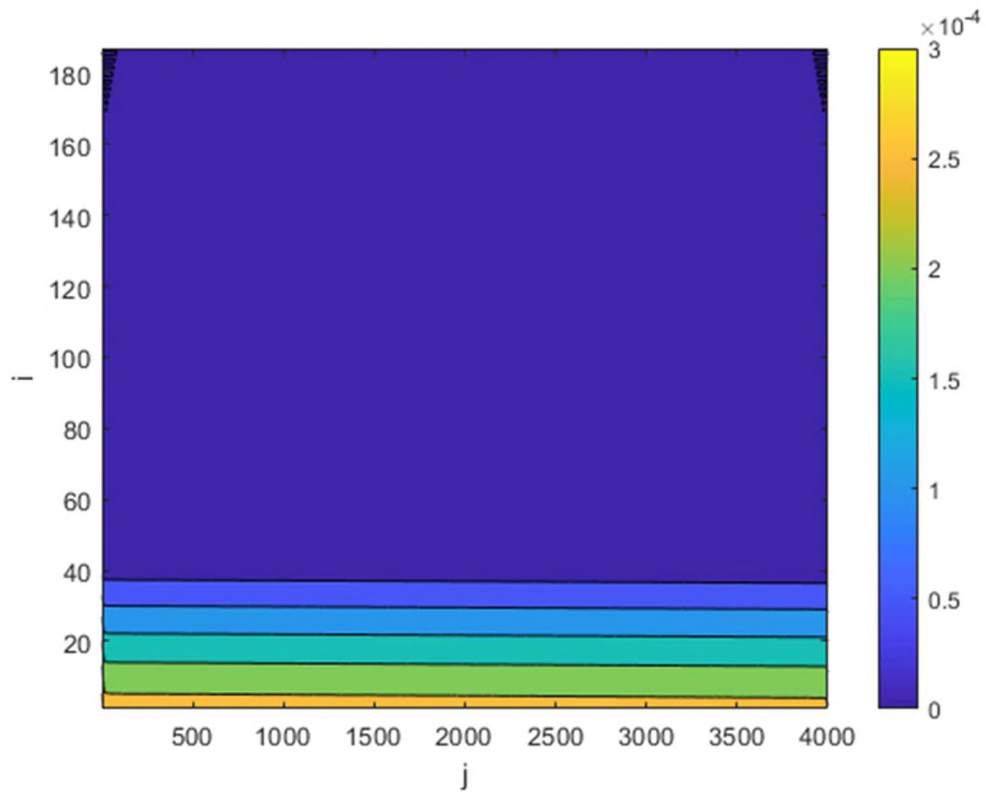


Figure 5. The concentration of θ_a^b in tissue at time 60s after the mixture of free bifunctional antibody fragment \hat{c}_a^f and nonspecifically bound (B) fragment \hat{c}_a^B is injected into the capillary. Here i and j represent the steps in the radial and axial directions. The steps in the radial direction have been made to start from the outer surface of the membrane. Note that the concentration is based on the void volume, though plotted uniformly. The time is 60 s.

APPENDIX A.
REACTIVE SYSTEM

In the capillary

$$\frac{\partial \hat{\theta}_a^f}{\partial \tau} + f(\zeta, \xi) \hat{P}e \frac{\partial \hat{\theta}_a^f}{\partial \zeta} + \hat{P}e \cdot g(\xi) \frac{\partial \hat{\theta}_a^f}{\partial \xi} = \left[\frac{1}{\xi} \frac{\partial}{\partial \xi} \xi \frac{\partial \hat{\theta}_a^f}{\partial \xi} + \frac{\partial^2 \hat{\theta}_a^f}{\partial \zeta^2} \right] - Da \left[\hat{\theta}_a^f - \frac{1}{K_A} \hat{\theta}_a^B \right] \quad (\text{A.1})$$

$$\frac{\partial \hat{\theta}_a^B}{\partial \tau} + \hat{P}e \cdot g(\xi) \frac{\partial \hat{\theta}_a^B}{\partial \xi} = d \cdot \left[\frac{1}{\xi} \frac{\partial}{\partial \xi} \xi \frac{\partial \hat{\theta}_a^B}{\partial \xi} + \frac{\partial^2 \hat{\theta}_a^B}{\partial \zeta^2} \right] + Da \left[\hat{\theta}_a^f - \frac{1}{K_A} \hat{\theta}_a^B \right] \quad (\text{A.2})$$

In the tissue

$$\frac{\partial \theta_a^f}{\partial \tau} + \hat{P}e \cdot h(\xi) \frac{\partial \theta_a^f}{\partial \xi} = d_1 \left[\frac{1}{\xi} \frac{\partial}{\partial \xi} \xi \frac{\partial \theta_a^f}{\partial \xi} + \frac{\partial^2 \theta_a^f}{\partial \zeta^2} \right] - Da \left[\theta_a^f - \frac{1}{K_A} \theta_a^B \right] - Da' \left[\left(b_{\max} - \theta_a^b \right) \theta_a^f - \frac{1}{K_A'} \theta_a^b \right] \quad (\text{A.3})$$

$$\frac{\partial \theta_a^B}{\partial \tau} + \hat{P}e \cdot h(\xi) \frac{\partial \theta_a^B}{\partial \xi} = d_2 \left[\frac{1}{\xi} \frac{\partial}{\partial \xi} \xi \frac{\partial \theta_a^B}{\partial \xi} + \frac{\partial^2 \theta_a^B}{\partial \zeta^2} \right] + Da \left[\theta_a^f - \frac{1}{K_A} \theta_a^B \right] \quad (\text{A.4})$$

$$\frac{\partial \theta_a^b}{\partial \tau} = Da' \left[\left(b_{\max} - \theta_a^b \right) \theta_a^f - \frac{1}{K_A'} \theta_a^b \right] \quad (\text{A.5})$$

where $\hat{P}e$ has been retained as 15, and using the diffusivity of a free BFA $\langle \hat{v}_{z_0} \rangle = 0.0236$

cm/s. $g(\xi)$ and $h(\xi)$ are given below Eq. (4). The Damköhler number $Da = \frac{k_a^f r_i^2}{D}$ where D

is the diffusivity of BFA. in the capillary and is the ratio between reaction and diffusion =

1.061×10^{-5} , a very small number. $K_A = \frac{k_a^f}{k_a'}$ is the reaction constant = 2.86. Further, d is

the ratio of the diffusion coefficient of BFA bound to HSA to D and equal to 0.0020.

This allows us to ignore the reaction term in Eq. (A-1) and replace (A-2) with reaction equilibrium.

The Eqs. (A.3) - (A.5) apply to the extravascular tissue. The Damköhler number for the specific reaction is $Da' = \frac{k_a^{f'} c_o r_i^2}{D} = 1.019$ and also low. Its equilibrium constant $K'_A = \frac{k_a^{f'} c_o}{k_a^{r'}} = 376$. This is the only large number in the system. The diffusion ratios are d_1 the ratio between the diffusivity of BFA in the tissue and in the capillary and is equal to 0.0020 for liver and 0.064 for the tumor; d_2 is the ratio between BFA bound to HSA in the tissue and diffusivity D equal to 0.00045 for the liver and 0.119 for the tumor. These are all small numbers with the exception of the last one. Consequently, we can ignore the reaction terms in Eq. (A.3) and assume reaction equilibria instead of Eqs. (A-4) and (A-5).

APPENDIX B.
LINEAR RESPONSE THEORY

If R_s is the response to a Dirac delta function $\delta(t)$, then the response to any input $\phi(t)$ is given by

$$R = \int_0^t R_s(t-t') \cdot \phi(t') dt' \quad (\text{B-1})$$

under the linear response theory. So the response to a Heaviside step function $H(t)$ where

$$H(t) = 0 \quad \text{for } t \leq 0 \quad (\text{B-2})$$

$$H(t) = 1 \quad \text{for } t > 0 \quad (\text{B-3})$$

Taking Laplace transforms of Eq. (A-1)

$$\bar{R} = \bar{R}_s \cdot \bar{\phi} \quad (\text{B-4})$$

where overbars indicate transformed quantities. The Laplace transform of $H = 1/s$ that results in the present case of

$$\bar{R}_H = \bar{R}_s \cdot \frac{1}{s} \quad (\text{B-5})$$

In the case of finite dosing, the input is $H(t) - H(t-t^*)$, and under Laplace transform, it gives us

$$\bar{R}^* = \bar{R}_s \cdot (1/s - e^{-st^*}/s) \quad (\text{B-6})$$

where t^* is the dosing time. Eliminating \bar{R}_s between the two A-5 and A-6 we have

$$\bar{R}^* = \bar{R}_H \cdot [1 - e^{-t^*s}] \quad (\text{B-7})$$

For small values of t^* will be

$$\bar{R}^* = t^* s \bar{R}_H \quad (\text{B-8})$$

which on inversion gives us

$$R^* = t^* \frac{d}{dt} R_H \quad (\text{B-9})$$

REFERENCES

- Bassingthwaighe, J.B., Chan, I.S.J., Wang, C.J. (1992). Computationally efficient algorithms for convection-permeation-diffusion models for blood-tissue exchange. *Annals Biomedical Eng.* 20, 687-725.
<https://doi.org/10.1007/BF02368613>
- Baxter, L.T., Yuan, F., Jain, R.K. (1992). Pharmacokinetic analysis of the perivascular distribution of bifunctional antibodies and haptens: Comparison with experimental data. *Cancer Res.* 52, 5838-5844.
- Baxter, L.T., Zhu, H., Mackensen, D.G., Butler, W.F., Jain, R.K. (1995). Biodistribution of monoclonal antibodies: Scale-up from mouse to human using a physiologically based pharmacokinetic model. *Cancer Res.* 55, 4611-4622.
<https://doi.org/10.1016/j.dmpk.2018.11.002>
- Baxter, L.T., Zhu, H., Mackenson, D.G, Jain, R.K. (1994). Physiologically based pharmacokinetic model for specific and nonspecific monoclonal antibodies and fragments in normal tissue and human tumor xenografts in nude mice. *Cancer Res.* 54, 1517-1528.
- Cattaneo, L., Zunino, P. (2014). A computational model of drug delivery through microcirculation to compare different tumor treatments. *Int. J. Numer. Meth. Biomed. Engng.* 30, 1347-1371. <https://doi.org/10.1002/cnm.2661>
- Chauhan, V.P., Lanning, R.M., Diop-frimpong, B., Mok, W., Brown, E.B., Padera, T.P., Boucher, Y., Jain, R. (2009) Multiscale measurements distinguish cellular and interstitial hindrances to diffusion in vivo. *Biophys. J.* 97: 330-336.
<https://doi.org/10.1016/j.bpj.2009.03.064>
- Cooney, D.O. (1976) *Biomedical Engineering Principles*, Marcel Dekker, N.Y.
- Fournier, R.L. (1999) *Basic Transport in Biomedical Engineering*, Taylor and Francis, Philadelphia. 24, 44, 71.
- Gaehtgens, P. (1980). Flow of blood through narrow capillaries: Rheological mechanisms determining capillary hematocrit and apparent viscosity. *Biorheology.* 17, 183-189. <https://doi.org/10.3233/bir-1980-171-220>
- Goldman, D. (2008). Theoretical models of microvascular oxygen transport to tissue. *Microcirculation.* 15, 795-811. <https://doi.org/10.1080/10739680801938289>
- Gullino, P.M., Grantham, F.H. (1961) Studies on the exchange of fluids between host and tumor. II. The blood flow of hepatomas and other tumors in rats and mice. *J. Nat. Cancer Institute.* 27, 1465-1491. <https://doi.org/10.1093/jnci/27.6.1465>

- Guyton, A.C., Hall, J.E., 2006. Textbook of Medical Physiology, 11th ed., Saunders.
- Happel, J. (1958). Viscous flow in a multiparticle systems: Slow motion of fluids relative to beds of spherical particles. *AIChE J.* 4, 197-201.
<https://doi.org/10.1002/aic.690040214>
- Iwata, H., Morikawa, N., Ikada, Y. (1996). Permeability of filters used for immunoisolation. *Tissue Eng.* 2, 289-298. <https://doi.org/10.1089/ten.1996.2.289>
- Jain, R.K. (2013). Normalizing tumor microenvironment to treat cancer: Bench to biomarkers. *J. Clinical Oncology.* 31, 2205-2218.
<https://doi.org/10.1200/JCO.2012.46.3653>
- Kojic, M., Milosevic, M., Simic, V., Koay, E.J., Fleming, J.B., Nizzero, S., Kojic, N., Ziemys, A., Ferrari, M. (2017). A composite smeared finite element for mass transport in capillary systems and biological tissue. *Comput. Methods Appl. Mech. Engng.* 324, 413-437. <https://doi.org/10.1016/j.cma.2017.06.019>
- Kojic, M., Milosevic, M., Simic, V., Koay, E.J., Ziemys, A., Ferrari, M. (2018). Multiscale smeared finite element model for mass transport in biological tissue: From blood vessels to cells and cellular organelles. *Comput. Biology Medicine.* 99, 7-23. <https://doi.org/10.1016/j.combiomed.2018.05.022>
- Krogh A. (1919). The supply of oxygen to the tissues and the regulation of the capillary circulation. *The Journal of physiology,* 52(6), 457-474.
<https://doi.org/10.1113/jphysiol.1919.sp001844>
- Larsen, M.T., Kuhlmann, M., Hvam, M.L., Howard, K.A. (2016). Albumin-based drug delivery: harnessing nature to cure disease. *Molecular Cellular Therapies.* 4(3), 1-12 <https://doi.org/10.1186/s40591-016-0048-8>
- Mangulis, V. (1965). *Handbook of Series for Scientists and Engineers*, Academic Press Inc., New York, 90, 95.
- Mascheroni, P., Penta, R. (2017). The role of microvascular network structure on diffusion and consumption of anticancer drugs. *Int. J. Numer. Meth. Biomed. Engng.* 33: e2857. <https://doi.org/10.1002/cnm.2857>
- Netti, P.A., Roberge, S., Boucher, Y., Baxter, L.T., Jain, R.K. (1996). Effect of transvascular fluid exchange on pressure-flow relationship in tumors: a proposed mechanism for tumor blood flow heterogeneity. *Microvasc. Res.* 52, 27-46.
<https://doi.org/10.1006/mvre.1996.0041>
- Nugent, L.J., Jain, R.K. (1984). Extravascular diffusion in normal and neoplastic tissues. *Cancer Res.* 44, 238-244.

- Penta, R., Ambrosi, D. (2015) The role of microvascular tortuosity in tumor transport phenomena. *J. Theor. Biol.* 364, 80-97. <https://doi.org/10.1016/j.jtbi.2014.08.007>
- Penta, R., Ambrosi, D., Quateroni, A. (2015) Multiscale homogenization for fluid and drug transport in vascularized malignant tissues. *Math. Models and Methods Appl. Sci.* 25, 79-108. <https://doi.org/10.1142/S0218202515500037>
- Pfeffer, R. (1964). Heat and mass transport in multiparticle systems. *I&EC Fundamentals.* 3, 308-383. <https://doi.org/10.1021/i160012a018>
- Qiu, X., Sane, N., Neogi, P. (2019). Convection in Krogh cylinder: Putting back fluid flow in the extravascular tissue. *AIChE J.* 65. e16720/1-7. <https://doi.org/10.1002/aic.16720>
- Renkin, E.M. (1977). Multiple pathways of capillary permeability. *Circulation Res.* 41, 735-743. <https://doi.org/10.1161/01.res.41.6.735>
- Rippe, B., Haraldsson, B. (1987). Fluid and protein fluxes across small and large pores in the microvasculatures. Application of two-pore equation. *Acta Physiol Scand.* 131, 411-428. <https://doi.org/10.1111/j.1748-1716.1987.tb08257.x>
- Roache, J., (1998). *Fundamentals of Computational Fluid Dynamics.* Hermosa Pub.
- Secomb, T.W. (2014). Krogh-cylinder and infinite domain models for washout of an inert diffusible solute from tissue. *Microcirculation.* 22, 91-98. <https://doi.org/10.1111/micc.12180>
- Secomb, T.W., Hsu, R., Pries, A.R. (2006) Tribology of capillary blood flow. *Proc. IMechE v.220 Part J: J. Engineering Tribology.* 767-774. <https://doi.org/10.1243/13506501JET121>
- Shipley, R., Chapman, S.J. (2010) Multiscale modelling of fluid and drug transport in vascular tumours. *Bull. Math. Biol.* 72, 1464-1491. <https://doi.org/10.1007/s11538-010-9504-9>
- Smaje, L., Zweifach, B.W., Intaglietta, M. (1970) Micropressures and capillary filtration coefficients in single vessels of the cremaster muscle of the rat. *Microvascular Res.* 2, 96-110. [https://doi.org/10.1016/0026-2862\(70\)90055-5](https://doi.org/10.1016/0026-2862(70)90055-5)
- Tao, C., Chuah, Y.J., Xu, C., Wang, D.A. (2019). Albumin conjugates and assemblies as versatile bio-functional additives and carriers for biomedical applications. *J. Material Chemistry B*, 7, 357-367. <https://doi.org/10.1039/c8tb02477d>
- Welling, P.G. (1997) *Pharmacokinetics.* 2nd ed., Amer. Chem. Soc., Washington, D.C.

III. A CONVECTIVE TRANSPORT MODEL FOR TRANSFER OF SOLUTE TO THE EXTRAVASCULAR TISSUE

Xianjie Qiu and Parthasakha Neogi

Department of Chemical and Biochemical Engineering, Missouri University of Science and Technology, Rolla, MO 65409

ABSTRACT

Delivery of a solute to different parts of the body is studied using a stirred tank model, a lumped systems model that cannot differentiate spatially distributed features. The distributed model in the Krogh cylinder model focuses on a capillary which is the only blood vessel that permits the transfer of solute and plasma through the walls. Previously, we could not show the appropriate transcapillary pressure drop and some of the circulations that is seen around the cylinder. The fluid flow in the short distance of capillary and peripheral space has been corrected here. The new velocity profiles inside the capillary and the extravascular tissue have been used to obtain a solute penetration into the extravascular tissue for both binding and non-binding solutes. In the model, all parameters that are known have been used, and there are no unknown parameters. The rate of penetration is low and is determined chiefly by convection. A conclusion is reached that we observe that increased convection is what is required for improved drug delivery.

1. INTRODUCTION

A therapeutic drug is inserted into plasma, from where it travels to all organs. As the chemotherapy drugs damage all organs and not just the tumor that it was meant for, and a targeted drug delivery route is preferred. In one of the procedures, a bifunctional antibody (BFA) is first introduced and it eventually attaches itself to the tumor by a specific reaction. In the second stage, is introduced the hapten which attaches specifically to the other arm of the BFA. The hapten molecule considered below contains a radioactive iodine, and the procedure constitutes a case of radiation therapy. A simple model for the study of the dynamics is that of Baxter et al (1995) who considered all organs to be stirred tanks separated in the middle by a membrane, the capillary wall, which separates the capillaries from the extravascular tissue. The plasma and solutes can cross from the blood vessels to the extravascular tissue only through the capillary at the capillary walls. In the last stage there is only perfusion, which drives out the BFA and hapten from other organs. In the tumor, the specific binding takes a longer time to dissociate and the radioactivity stays there for a longer time. Using this model Baxter et al (1995) were able to match their results to the experimental data obtained using x-ray dosimetry. However, the model is a lumped system model that cannot account for how the pressures are distributed in space and discounts the large mass transfer resistance in the tissue. Quantification of the process needs many parameters that Jain and coworkers have provided, and perhaps this is the only system where there are no adjustable parameters.

The present work focuses on another model called the Krogh cylinder (1999) which is a distributed model, and as a result spatially resolved quantities such as pressure drops and penetration of the solute into the extravascular tissue can be determined. One consequence of applying this model is to include a two-dimensional velocity field and a two-dimensional concentration field (Qiu et al., 2019). It was found for the first time that the solute transport in the extravascular tissue is dominated by convection, where the flow occurs mainly in form of a small loss of plasma to the lymphatic system. The work here emphasizes convection, which so far falls a little short of observations. A circulatory flow leaves the capillary at the arteriole end and most of it returns at the venule end (Guyton and Hall, 2006). The solution to equation of motion and continuity does show such a flow (Qiu et al., 2019) but barely visible as it is very low. Consequently, Qiu and Neogi (2021) ignored it in their calculations. The main flow is in the form of escape into the lymphatic system. However, as their results showed, the flow in general is very important to the drug delivery, hence a more informed attempt has been made here to account for all of the flow. It is noteworthy that a possible direct contribution of the lymphatic system, which acts as a sump, may exist in a way that affects the flow in the extravascular tissue.

The walls of capillaries are considered to be the only place where the plasma and solute are exchanged with the extravascular tissue. The capillaries form a network that are partially random but also follow some simple rules. Instead of looking at the network, Krogh looked at a single capillary with a defined amount of extravascular tissue around it. The organ is made up of these Krogh cylinders in parallel. This is a cell model that avoids looking at the full complex structure and has worked well in many disciplines.

The length of capillary is taken to be $200 \mu\text{m}$ after many measurements were used to round off to that value. Values of other properties have been listed in Qiu et al (Qiu et al., 2019).

The flow of plasma in the extravascular tissue is taken to be that given by flow through a porous medium, that is a local volume average is used. Similar volume average is used in the capillary. The flow of blood inside the capillary is taken to be $6 \text{ mPa}\cdot\text{s}$, same as that of whole blood. It is Newtonian even though the volume fraction of red blood cells in the capillary exceed 50%. The red blood cells deform inside the capillary as they flow, but stay away from the walls. Thus, there is a lubricating layer of plasma near the wall and the net result is that blood acts like a Newtonian fluid, same as the plasma.

The permeation through the capillary membrane is split into two parts as the results appear to be better if the pores diameters are considered to be bimodal (Baxter et al., 1995) following Rippe and Haraldsson (1987). Each group has its own permeability and surface area associated with it. It is the penetration of the solute into the extravascular tissue that is very slow. As Qiu and Neogi (2021) showed, it is determined mostly by the convection. The diffusion of BFA is accompanied by binding, some are nonspecific, with an equilibrium constant of about 1, and some are specific with a large equilibrium constant. The specific reaction is applicable only when the solute is BFA and the organ is the tumor. The nonspecific reactions have to be specified in a distributed system as to whether the bound entity is fully mobile (Qiu et al., 2019) or fully immobile (Chauhan et al., 2009). In addition, Chauhan et al (2009) show that presence of impermeable cells in the tissue decreases the diffusivity, which implies that the diffusion

in a tissue should actually be referred to as dispersion. Qiu and Neogi (2021) were able to show that the reactions further slow the progress of BFA into the extravascular tissue. Hence, any increase of convection in the tissue will be of great benefit.

Below, the fluid mechanics and mass transfer formulated previously, their shortcomings and the remedy posed here are discussed below. In that, the project is a complex transport phenomena problem, and it addresses the main issue in pharmacokinetics of effective drug delivery. Because of their lengths, all mathematical details that have appeared elsewhere (Qiu et al., 2019 and 2021) have been omitted. All values of constants used for work below have been tabulated on Qiu and Neogi (2021) and have not been reproduced here.

2. FLUID MECHANICS

Previously, Qiu et al (2019) assumed low Reynolds number flow of a Newtonian fluid inside the capillaries. The problem was expressed in terms of the biharmonic equation in stream function

$$E^4 \hat{\psi} = 0 \quad (1)$$

Henceforth, all quantities inside the capillary will be shown with carats. The general solution for a cylindrical system is known (Rippe and Haraldsson, 1987). The extravascular tissue is modeled as flow through a porous media, using Brinkman equation. Brinkman equation can be converted to an equation for the stream function

$$E^4 \psi = k^{-1} E^2 \psi \quad (2)$$

where k is the permeability and $E^2 = \frac{\partial^2}{\partial r^2} + \frac{\partial}{r \partial r} + \frac{\partial^2}{\partial z^2}$. Here, r and z are the coordinates

in the radial and axial directions. The velocities are $v_r = \frac{1}{r} \frac{\partial}{\partial z} \psi$, $\hat{v}_r = \frac{1}{r} \frac{\partial}{\partial z} \hat{\psi}$ and

$v_z = -\frac{1}{r} \frac{\partial}{\partial r} \psi$, $\hat{v}_z = -\frac{1}{r} \frac{\partial}{\partial r} \hat{\psi}$. The general solution to Eq. (2) for a cylindrical system has

been given by Sane (2002). It is noteworthy that \sqrt{k} / L is a very small number that makes the above problem stiff and difficult to solve numerically. Here L is the length of the cylinder. The equations are still linear and hence an exact solution is possible.

Further, the velocities in the extravascular tissue are the superficial velocities.

Besides the tissue and capillary, the volumetric flux of plasma through the membrane satisfies

$$v = L_p (\hat{p}|_{r_i} - p|_{r_o} - \sigma \Delta \Pi) \quad (3)$$

Here r_i and r_o are the inner and outer radii of the capillary, Figure 1. L_p is the hydraulic permeability, σ is the reflection coefficient and $\Delta \Pi$ is the difference between the inner and outer osmotic pressures taken to be 20 mm of mercury (Guyton and Hall, 2006).

Two measured values were specified. The first is the average velocity of flow into the capillary in the Krogh cylinder at 0.1 cm/s. Now, fluid enters the Krogh cylinder, but exits at a lower flow rate. The fraction representing the loss is ω . The loss happens because the membrane is leaky, and some of the leak finally leaves the Krogh cylinder for the lymphatic system. For the liver $\omega = 10^{-4}$ and 0.1 for the tumor. At first one feature that was stressed was that the flow need to be contained in the cell but it led to some absurdities even though in the main the flow looked reasonable (Sane, 2002). The more relaxed conditions did not specify a transcapillary pressure or limits on circulation.

However, instead of a transcapillary pressure drop of 20 mm of mercury only 3.8 mm was found which is solely the Hagen-Poiseuille pressure drop in a capillary with impermeable walls. The circulation in the extravascular tissue was observed but was negligible in magnitude (Qiu et al., 2019). It was suggested that the compliance of the capillary walls increased the pressure drop to 20 mm of mercury. That is, practically no liquid went past the capillary membrane and thus there was no effect on pressure drop. It was suggested that the compliance of the capillary walls increased the pressure drop to 20 mm of mercury. As mentioned earlier, it is necessary to incorporate the effect of the lymphatic system. It can be done in form of forcing the pressure p on the outer surface of the Krogh cylinder to be a low value, but there is some uncertainty as to where this pressure is to be located because of the architecture (physiology). The alternative is used here is to force the transcapillary pressure drop to 20 mm of mercury and let the pressure of the outer surface develop accordingly. In that case one of the earlier boundary conditions has to be removed. This is the condition that the tangential velocity is zero at the porous medium-capillary membrane interface. There are some indications that flow there may not be zero (Beavers and Joseph, 1967). The cross-sectional averaged pressure in the capillary $\langle \hat{p} \rangle$ at the entrance was set to zero and at the exit to - 20 mm of mercury. In addition, only the first coefficient of a series was given a value and higher coefficients were set to zeros. It is possible to do a more detailed matching using collocation, but the problem was already very large. More details are given below. The pressure is

$$\hat{p} = \sum_n 2 a_n [\hat{c}_{2n} \hat{c}_{5n} I_0(a\xi)] \cos(a\zeta) s^3 \mu - \frac{\Delta p^* \zeta}{\Lambda} + \frac{\Delta p^* \omega}{4\Lambda^2} (\xi^2 + 2\zeta^2) \quad (4)$$

$$- \frac{2\alpha\zeta\Delta p^*}{(2\alpha - \xi_i)} + s^3 \mu p_0$$

and the average is

$$\langle \hat{p} \rangle = \sum_n 4 a_n \hat{c}_2 \hat{c}_5 \frac{I_1(a\xi)}{\xi} \cos(a\zeta) s^3 \mu - \frac{\Delta p^* \zeta}{\Lambda} + \frac{\Delta p^* \omega}{8\Lambda^2} \xi^2 + \frac{\Delta p^* \omega \zeta^2}{2\Lambda^2} \quad (5)$$

$$- \frac{2\alpha\zeta\Delta p^*}{(2\alpha - \xi_i)} + s^3 \mu p_0$$

where

$$p_0 = \frac{1}{2s^3\mu} \left[-\Delta\Pi + \Delta p^* - \frac{\Delta p^* \omega}{4\Lambda^2} \xi^2 - \frac{\Delta p^* \omega}{2} + \frac{2\alpha\Delta p^* \Lambda}{(2\alpha - \xi_i)} \right] \quad (6)$$

$\hat{c}_{2n} \hat{c}_{5n}$ are constants of integration where $\hat{c}_{2n} \hat{c}_{5n}$ are all zeros for n greater than 1 and $\hat{c}_{21} \hat{c}_{51} = 7.546 \times 10^{-6}$. p_0 is a constant term and the value is -8.56 mmHg. Here, the axial position is $\zeta = sz$ and the radial position is $\xi = sr$ where $s = 1/\sqrt{k}$. ξ_i represents to the dimensionless of inner capillary diameter. k is the permeability of the porous extravascular tissue. Δp^* is from Hagen–Poiseuille equation $\Delta p^* = \frac{8 \langle \hat{v}_{zo} \rangle \mu L}{r_i^2}$

$$\alpha = \frac{\text{resistance to flow in the porous medium}}{\text{resistance to flow across the capillary wall}} = L_p s \mu \quad (7)$$

where L_p is the hydraulic coefficient of the capillary wall. We have considered the flow in the model of liver and tumor. The properties of tumor were determined from a 0.7 g tumor grafted in mice, but scaled up to 20 g in humans (70 kg) and considered to be homogeneous as have Baxter et al (1995).

3. MASS TRANSFER

The sequential procedure for drug delivery considered by Baxter et al (1995) is simplified because to analyze the mass transfer, it is necessary to solve partial differential equations. At first, only the introduction of hapten is considered. It is taken to be inert and presents the base case of how fast the penetration is into the extravascular tissue.

The governing equation is

$$\frac{\partial \hat{\theta}}{\partial \tau} + \frac{\hat{v}_z}{\langle \hat{v}_{zo} \rangle} \hat{P}e \frac{\partial \hat{\theta}}{\partial \zeta} + \frac{\hat{v}_r}{\langle \hat{v}_{zo} \rangle} \hat{P}e \frac{\partial \hat{\theta}}{\partial \xi} = \frac{\partial^2 \hat{\theta}}{\partial \xi^2} + \frac{1}{\xi} \frac{\partial \hat{\theta}}{\partial \xi} + \frac{\partial^2 \hat{\theta}}{\partial \zeta^2} \quad (8)$$

in the capillary and

$$\frac{\partial \theta}{\partial \tau} + \frac{v_z}{\langle \hat{v}_{zo} \rangle} \frac{\hat{P}e}{\varepsilon} \frac{\partial \theta}{\partial \zeta} + \frac{v_r}{\langle \hat{v}_{zo} \rangle} \frac{\hat{P}e}{\varepsilon} \frac{\partial \theta}{\partial \xi} = d \left[\frac{\partial^2 \theta}{\partial \xi^2} + \frac{1}{\xi} \frac{\partial \theta}{\partial \xi} + \frac{\partial^2 \theta}{\partial \zeta^2} \right] \quad (9)$$

in the extravascular tissue where the axial and radial positions now are $\zeta = z/r_i$

and $\xi = r/r_i$, as opposed to those in Eq. (4). Further, $\hat{\theta} = \hat{c}/c_o$, $\tau = \hat{D}t/r_i^2$, Peclet

number $\hat{P}e = \frac{\langle \hat{v}_{zo} \rangle r_i}{\hat{D}}$, ε is the volume fraction not occupied by the cells, the concentration

is $\theta = c/c_o$ and c_o is a reference concentration used throughout. In addition, the

diffusivity ratio is $d = D/\hat{D}$. The connection of the intravascular and extravascular fluid exchange and the conditions at the membranes are

$$\left(\hat{\theta} \cdot \frac{\hat{v}_r}{\langle \hat{v}_{zo} \rangle} \cdot \hat{P}e - \frac{\partial \hat{\theta}}{\partial \xi} \right) \Bigg|_{\xi=1} = \frac{j_{v-i}}{c_o \hat{D} / r_i} = \left(\theta \cdot \frac{v_r}{\langle \hat{v}_{zo} \rangle} \cdot \frac{\hat{P}e}{\varepsilon} - d \frac{\partial \theta}{\partial \xi} \right) \Bigg|_{\xi=r_0/r_i} \quad (10)$$

j_{v-i} is the flux that the solute crosses the membrane from the inside of the capillary to the outside of the capillary interstitial space, and $j_{v-i} = J_{v-i} / S$. The equation below is the J_{v-i} is the flow of solute across the membrane in moles per unit time, which is from Rippe and Haraldsson (1987) who have presented a lumped system model.

$$J_{v-i} = J_L (1 - \sigma_L) \hat{c}|_{\xi=1} + PS_L \left(\hat{c}|_{\xi=1} - \frac{c|_{\xi=r_o/r_i}}{R} \right) \frac{Pe_L}{e^{Pe_L} - 1} + J_S (1 - \sigma_S) \hat{c}|_{\xi=1} + PS_S \left(\hat{c}|_{\xi=1} - \frac{c|_{\xi=r_o/r_i}}{R} \right) \frac{Pe_S}{e^{Pe_S} - 1} \quad (11)$$

where R is the rejection coefficient equal to 1.0 here, σ is the reflection coefficient and $J_L = J_{iso} + \alpha_L L_y$ and $J_S = -J_{iso} + \alpha_S L_y$, L_y is the lymphatic flow, J_{iso} is recirculation flow rate in the membrane and $\alpha_L + \alpha_S = 1.0$. The membrane has two different Peclet numbers in large pores and small pores, $Pe_L = J_L(1 - \sigma_L) / PS_L$ and $Pe_S = J_S(1 - \sigma_S) / PS_S$.

The hapten is introduced as a step change from $\hat{\theta} = 0$ at time $t = 0$ to 1.0 at the entrance. Eventually the hapten penetrates the extravascular tissue and the holdup is given by

$$F_h = \frac{2}{(Z^2 - \xi^2) \Lambda} \iint_{\xi=\xi_i, Z \& \zeta=0, \Lambda} \theta \xi d\xi d\zeta \quad (12)$$

which is a function of time t . Here, $Z = R / r_i$ for the boundary of tissue. The present formulation is same as our past one except for the fact that the velocities are two dimensional in the extravascular tissue and all velocities are those that have been calculated in the previous. The solution is obtained by finite difference, forward time and central space. Only the liver and tumor are considered here, as before.

We separately analyze the case where BFA is introduced into a fresh Krogh cylinder. There are two species in the capillary, BFA free and BFA non-specifically bound. This non-specific binding has been considered fully mobile, 1:1 and the molecule that binds has all the properties of human serum albumin (HSA) if not the HSA itself. Now these come a long way before entering the liver or the tumor. As a result we assume that equilibrium binding has been reached and continues that status even afterwards. In the capillary, we assume that the total concentration of BFA is injected $c_o = \hat{c}^f + \hat{c}^B$. \hat{c}^B will only be present on the tissue side, represents the BFA binding it with specific sites in the tumor, \hat{c}^f and \hat{c}^B are the BFA solute in the plasma flow. The resultant balance equation and boundary conditions are

$$\hat{\theta}^f = \frac{1}{1 + K_A} \quad (13)$$

$$\hat{\theta}^B = \frac{K_A}{1 + K_A} \quad (14)$$

at the entrance $\zeta = 0$. In the above equations, $K_A = k^f / k^r$ is the equilibrium constant.

As noted earlier, the values of parameters used and their sources have been tabulated earlier (Qiu and Neogi, 2021). The governing equations for inside of capillaries,

$$\frac{\partial \hat{\theta}^f}{\partial \tau} + \frac{\hat{v}_z}{\langle \hat{v}_{zo} \rangle} \hat{P}e \frac{\partial \hat{\theta}^f}{\partial \zeta} + \frac{\hat{v}_r}{\langle \hat{v}_{zo} \rangle} \hat{P}e \frac{\partial \hat{\theta}^f}{\partial \xi} = \left[\frac{1}{\xi} \frac{\partial}{\partial \xi} \xi \frac{\partial \hat{\theta}^f}{\partial \xi} + \frac{\partial^2 \hat{\theta}^f}{\partial \zeta^2} \right] \quad (15)$$

$$\hat{\theta}^B = K_A \hat{\theta}^f \quad (16)$$

and in the tissue

$$\frac{\partial \theta^f}{\partial \tau} + \frac{v_r}{\langle \hat{v}_{zo} \rangle} \hat{P}e \frac{\partial \theta^f}{\partial \xi} = d_1 \left[\frac{1}{\xi} \frac{\partial}{\partial \xi} \xi \frac{\partial \theta^f}{\partial \xi} + \frac{\partial^2 \theta^f}{\partial \zeta^2} \right] \quad (17)$$

$$\theta^b = K_A \cdot \theta^f \quad (18)$$

$$\theta^b = b_{\max} K'_A \theta^f / [1 + K'_A \theta^f] \quad (19)$$

In order to understand the speed with which the specific sites have reacted,

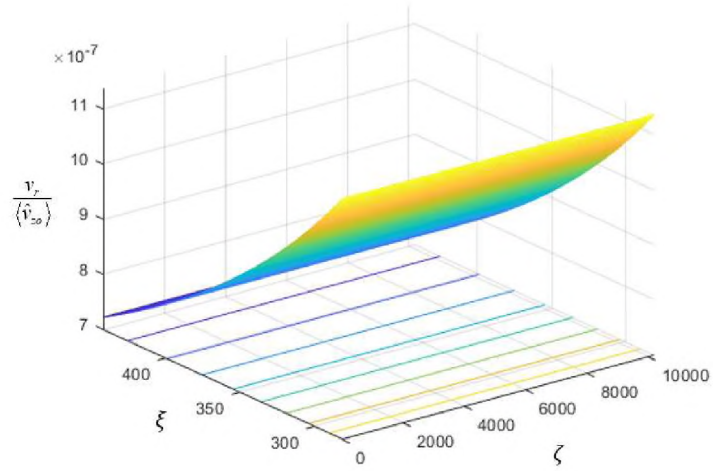
$$F_{BFA} = \frac{\int_0^{\xi_o} \int_{\Lambda}^R \theta_a^b 2\pi\xi d\xi d\zeta}{\pi(R^2 - \xi_o^2) b_{\max} \Lambda} \quad (20)$$

is calculated.

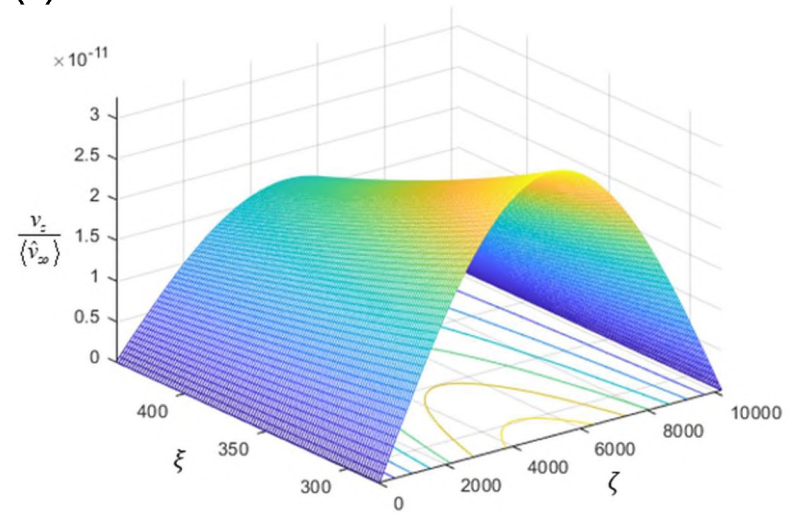
4. RESULTS AND DISCUSSION

First we look at the fluid mechanics, and look at the changes brought about by forcing a transcapillary pressure drop of 20 mm of mercury. In Figures 1(a) and 1(b) are illustrated the radial velocity v_r and the axial velocity v_z of the fluid flow in the liver in the extravascular space. The first has not changed much but v_z has increased by two orders of magnitude over our earlier work (Qiu and Neogi, 2021) upon forcing a transcapillary pressure drop of 20 mm of mercury. Note that v_z , does not affect v_r which flows outward with no apparent variation with the axial direction. The pressure in Figure 1 (c) is high on the entrance side of the extravascular tissue, as a lot of plasma rush out, but only a small amount is allowed to leak into the lymphatic system, that is leave the Krogh cylinder. The convection fluid loss after the reabsorption through the vessel wall, is the loss to the lymphatic system, which is ω in here (Guyton and Hall,

(a)



(b)



(c)

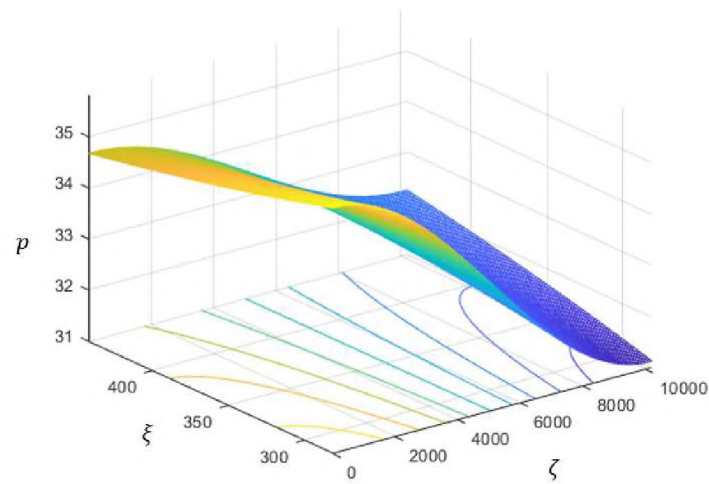


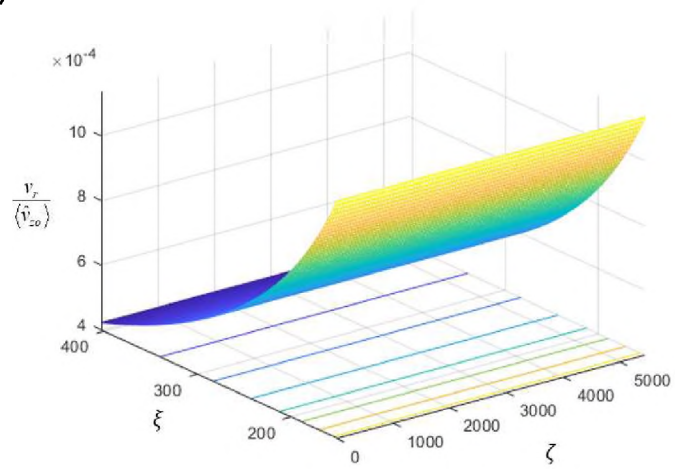
Figure 1. (a) v_r in the liver tissue, (b) v_z in the liver tissue, (c) pressure in the liver tissue

2006; Dewhurst and Secomb, 2017). As a result, there arises a stagnation pressure, which is the conversion of kinetic energy into pressure energy as most of the plasma that tries to get out is stopped. The pressures here are very large. It is probable that both the transcapillary pressure drop and ω are smaller in a real 20g tumor. This is not an artifact of the model. If we have two capillaries in parallel and this outward flow which result in a head on collision in the midspace, and stagnation will arise.

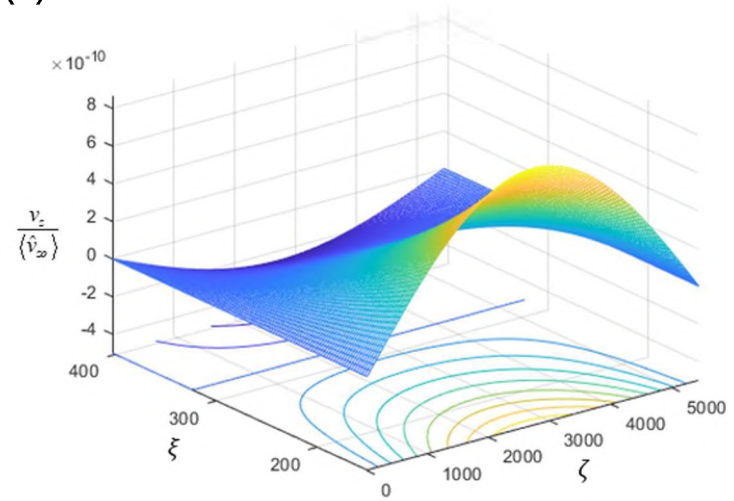
Inside the capillary, the axial velocity profile is nearly parabolic as in Hagen-Poiseuille flow, the radial velocity increases by one order of magnitude over our previous result (Qiu and Neogi, 2021). These figures are not been shown as they do not present significantly new result.

In Figures 2(a) – (c) are shown the flow features in the extravascular tissue in the tumor. The flow out to the lymphatic system here is higher by three orders of magnitude over the liver. As a result the radial flow out in the Figure 2 (a) is higher by three orders of magnitude. The axial velocity in Figure 2 (b) increases by two orders of magnitude over our previous work, however, is capable of showing negative values. There are two vortices here. The first one is the anticipated one where the plasma leaves the capillary at the arteriole end and returns at the venule end. Here we see an additional circulation where fluid enters from outside from the venule end and leaves at arteriole end, all that the far end of the tissue. This flow is a lot weaker. Further, the pressure build up in Figure 2(c) is very high probably because of higher flow in the tumor. In an inhomogeneous tumor, the large pressures are actually observed and attributed to the damage in the lymph ducts which also cause stagnation (Netti et al., 1996). Some capillaries in the tumor are collapsed under the elevated of solid stress, and the blood

(a)



(b)



(c)

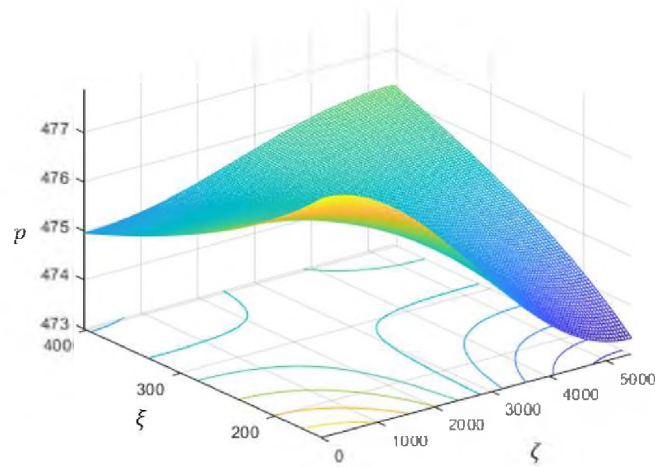


Figure 2. (a) v_r in the tumor tissue, (b) v_z in the tumor tissue, (c) pressure in the tumor tissue

flow is limited (Chauhan et al, 2013). The pressures here are very large. It probable that both the transcapillary pressure drop and ω are smaller in a real 20 g tumor.

Shown in Figures 3 and 4 in the liver and tumor respectively, are the holdup of the hapten which is taken to be an inert. The rates of increase due to improved convection in the extravascular tissue is an order of magnitude larger in the liver and more than two orders of magnitude larger in the tumor due to higher convection over our previous work. As before, the constant rate of increase with time, show the importance of flow in the radial direction in the tissue, v_r , as the main source of mass transfer in the tissue.

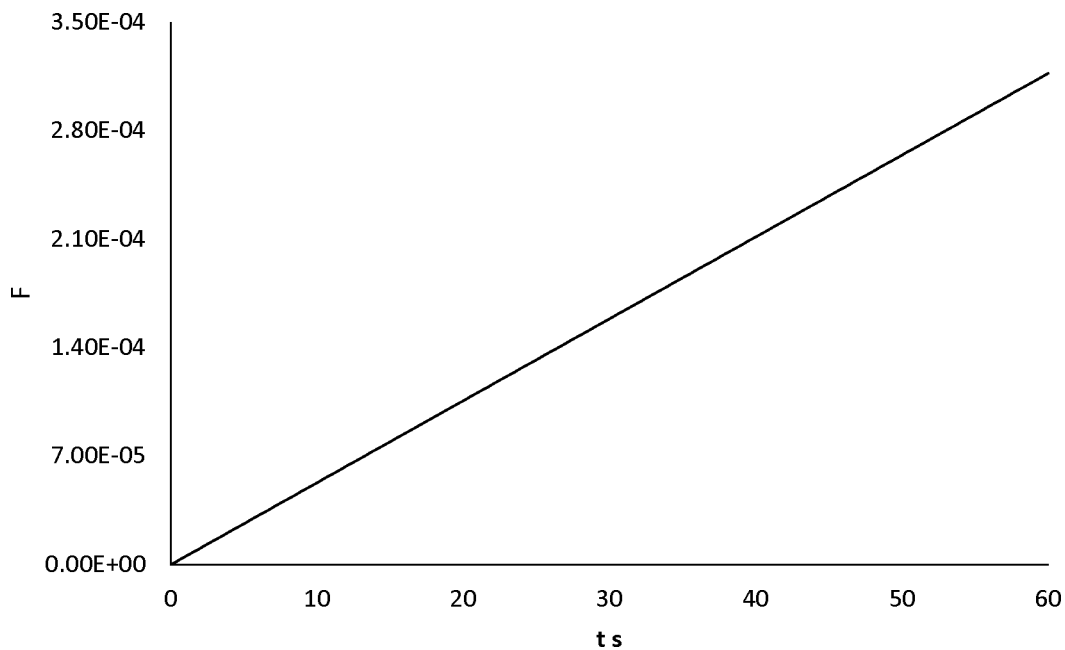


Figure 3. Hapten holdup in the liver tissue as a function of time (s).

The uptake of BFA which reacts, is shown in Figure 5. It is seen that a constant rate of increase is observed at a longer time, but is still faster than in our earlier results due to increased convection. In addition, if non-specific binding to immobile molecules

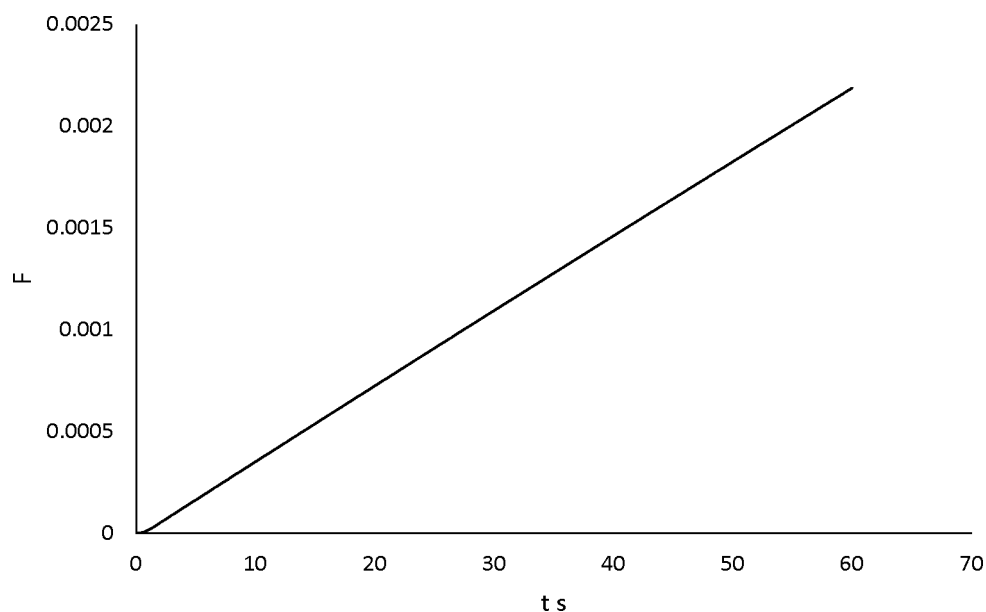


Figure 4. Hapten holdup in the tumor tissue as a function of time (s).

or tissue is considered, that the time in Figure 5 need to be increased by a factor of $(1+K^*)$ where K^* is proportional to the equilibrium constant of the non-specific reaction. To be sure, all the solute molecules are large and heavy and have very low diffusivity. At the other end Krogh (1919) worked with diffusion of oxygen with consumption into the tissue and found that the entire tissue could receive oxygen. Here the diffusivity is very high and no consideration of convection is probably justified. The matter may also change when we look at inhomogeneous tumors (Pluen et al, 2001). The details at the concentrations are shown in Figure 6 and shows more penetration than before.

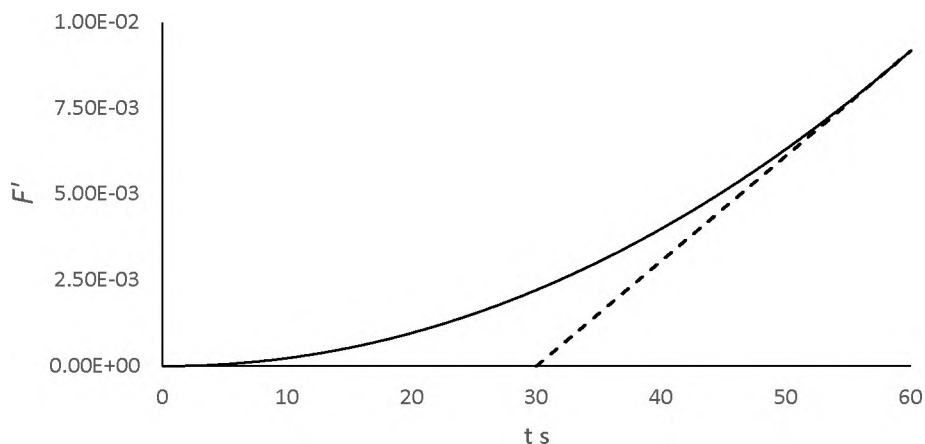


Figure 5. Specifically bound BFA holdup in the tumor as a function of time t (s).

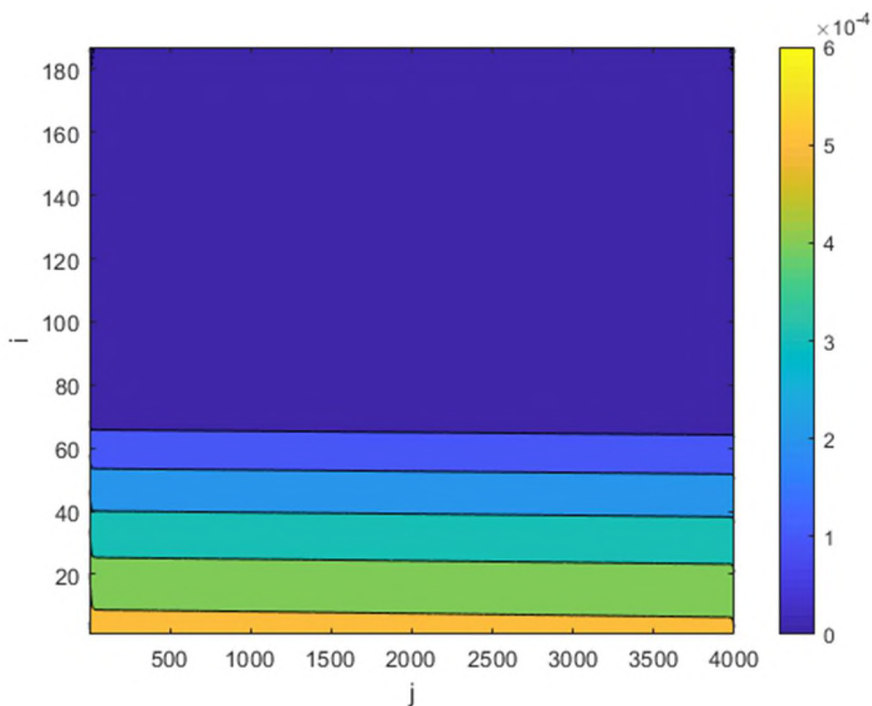


Figure 6. The concentration of θ_a^b in tissue at time 60s after the mixture of free bifunctional antibody fragment \hat{c}_a^f and nonspecifically bound (B) fragment \hat{c}_a^B is injected into the capillary. Here i and j represent the steps in the radial and axial directions. The steps in the radial direction have been made to start from the outer surface of the membrane. Note that the concentration is based on the void volume, though plotted uniformly. The time is 60 s.

5. CONCLUSIONS

The Krogh cylinder model used here contains all the suitable variables and physicochemical parameters. The mass transfer algorithm has involved the convection flow with the solution perfusion and retention in the Krogh cylinder model extravascular space. They show that the penetration rate of a solute depends mainly on the flow and is very low. Some additional measures need to be taken to increase the rate of perfusion. The result indicates the convection has an essential role in drug delivery.

REFERENCES

- Baxter, L.T., Zhu, H., Mackensen, D.G., Butler, W.F., Jain, R.K. (1995). Biodistribution of monoclonal antibodies: Scale-up from mouse to human using a physiologically based pharmacokinetic model. *Cancer Res.* 55. 4611-4622.
<https://doi.org/10.1016/j.dmpk.2018.11.002>
- Beavers, G.S., and Joseph, D.D. (1967) Boundary conditions at a naturally permeable wall. *J. Fluid Mech.* 30, 197-207.
- Dewhirst, M., & Secomb, T. (2017). Transport of drugs from blood vessels to tumour tissue. *Nature Reviews Cancer*, 17(12), 738-750.
<https://doi.org/10.1038/nrc.2017.93>
- Chauhan, V.P., Lanning, R.M., Diop-frimpong, B., Mok, W., Brown, E.B., Padera, T.P., Boucher, Y., Jain, R. (2009) Multiscale measurements distinguish cellular and interstitial hindrances to diffusion in vivo. *Biophys. J.* 97: 330-336.
<https://doi.org/10.1016/j.bpj.2009.03.064>
- Chauhan, V.P., Martin, J. D., Liu, H., Lacorre, D. A., Jain, S. R., Kozin, S. V., Stylianopoulos, T., Mousa, A. S., Han, X., Adstamongkonkul, P., Popović, Z., Huang, P., Bawendi, M. G., Boucher, Y., & Jain, R. K. (2013). Angiotensin inhibition enhances drug delivery and potentiates chemotherapy by decompressing tumour blood vessels. *Nature communications*, 4, 2516.
<https://doi.org/10.1038/ncomms3516>
- Guyton, A.C., Hall, J.E., 2006. Textbook of Medical Physiology, 11th ed., Saunders.

- Haberman, W.L., Sayre, R.M. (1958). Motion of rigid fluid spheres in stationary and moving liquids inside cylindrical tubes. U.S. Department of Navy, David Taylor Model Basin Report. 1143 NS 715-102.
- Krogh A. (1919). The supply of oxygen to the tissues and the regulation of the capillary circulation. *The Journal of physiology*, 52(6), 457–474.
<https://doi.org/10.1113/jphysiol.1919.sp001844>
- Netti, P. A., Roberge, S., Boucher, Y., Baxter, L. T., & Jain, R. K. (1996). Effect of transvascular fluid exchange on pressure-flow relationship in tumors: a proposed mechanism for tumor blood flow heterogeneity. *Microvascular research*, 52(1), 27–46. <https://doi.org/10.1006/mvre.1996.0041>
- Pluen, A., Boucher, Y., McKee, T.D., Gohonghi, T., di Tomaso, E., Brown, E.R., Campbell, R.B., Berk, D.A., and Jain, R.K. (2001) Role of tumor-host interactions in interstitial diffusion of macromolecules: Cranial vs subcutaneous tumors. PNAS 98, 4629.
- Qiu, X., Sane, N., Neogi, P. (2019). Convection in Krogh cylinder: Putting back fluid flow in the extravascular tissue. *AIChE J.* 65. e16720/1-7.
<https://doi.org/10.1002/aic.16720>
- Qiu, X., and Neogi, P. (2021) Effect of flow on mass transfer in a tumor in targeted drug delivery. Manuscript submitted for publication.
- Renkin, E.M. (1977). Multiple pathways of capillary permeability. *Circulation Res.* 41, 735-743. <https://doi.org/10.1161/01.res.41.6.735>
- Rippe, B., Haraldsson, B. (1987). Fluid and protein fluxes across small and large pores in the microvasculatures. Application of two-pore equation. *Acta Physiol Scand.* 131, 411-428. <https://doi.org/10.1111/j.1748-1716.1987.tb08257.x>
- Smaje, L., Zweifach, B.W., Intaglietta, M. (1970) Micropressures and capillary filtration coefficients in single vessels of the cremaster muscle of the rat. *Microvascular Res.* 2, 96-110. [https://doi.org/10.1016/0026-2862\(70\)90055-5](https://doi.org/10.1016/0026-2862(70)90055-5)
- Sane, N. (2002) Convective-diffusive transport in Krogh cylinder. M.S. Thesis, Chemical Engineering, University of Missouri-Rolla, Rolla, MO. 65409, 2002.
- Wideman, M. (2020). Dimensions of Blood Vessels from Distributing Artery to Collecting Vein. *Circulation Research.* Cir. Res. 14.375-378
<https://doi.org/10.1161/01.res.12.4.375>

SECTION

2. CONCLUSIONS AND RECOMMENDATIONS

2.1. CONCLUSIONS

This dissertation has provided the comprehensive theoretical studies and presented the simulation of fluid and mass transfer in Krogh cylinder. We have indicated the convention of fluid dynamics in the extravascular space. The combination of Krogh model and plug flow reactor (PFR) is applied for the pharmacokinetic model. The dosing time in single capillary model showed in mathematical. The result of the theoretical model is capable to estimate the relationship the fluid exchange in microvascular.

To draw a conclusion, we based on the continuity and momentum equations to simulate the blood fluid flow in the intravascular space, and the continuity equation and Brinkman equation govern the interstitial fluid flow in the extravascular space is the first step. The fluid flow in the interstitial space leak to the periphery of the outer cylindrical model owing to the lymphatic system is applied, and the convection in the extravascular space can present. The fluid flow for the microvascular space has mimicked a realistic a single capillary microvessel system.

The study of the pharmacokinetic model in particular organ used to use the stirred tank model, which calculate the concentration in the blood stream. The second step of research is discovery a plug flow reactor in single capillary from the stirred tank model in Jain's experiment (Baxter et al, 1995). The mass transfer of pharmaceutical solute in a microvessel applies in fluid exchange model. The result shows the solute penetrate from

the intervascular space and cross the capillary membrane to the tissue side. The convection appears in the extravascular space even it is small. The macromolecular of bifunction antibody has smaller penetration rate than the micromolecular of haptan.

We two major missions in final step, the first is edit the capillary pressure and re-defined the fluid mechanics, and the second mission is that combine the above two simulation model. The sub-compartment model in pharmacokinetics used to approach the summarized of pharmaceutical solute concentration versus time. The dynamics of drug deliver has considered here. These studies are based on the organ of the intervascular and extravascular compartment model (CM) and convert to a single capillary the plug flow reactor in the Krogh cylinder model. We interpolate the experimental data and apply it to the empirical formula to estimate drug distribution concentration with time. The CM does not include the mass transfer resistance, and the Krogh model lacks the pressure drop information. Our model simulation has presented fluid flow in the short distance of capillary and peripheral space, which analyzes the axial and radial direction in the Krogh cylinder model. The fluid model in the capillary accord with the physiology behavior has redefined some conditions in previous studies (Qiu et al., 2019) and applied with the 20-mmHg capillary pressure to the intravascular space has been mimic simulated and examined the extravascular space pressure dynamic in the liver extravascular space. However, the result of pressure in the tumor extravascular space is too high. Perhaps the 0.7 g tumor in the mouse is heterogeneous. The reality tumor has a complicated circumstance, and the tumor tissue may have different vascular shunts, necrosis, and high interstitial fluid pressure. Our model could find out the different observations to maintain the 0.1 cm/s velocity and 20 mm Hg in capillary cause the high IFP in extravascular

space. The above result of the fluid mechanism was added to the mass transfer study. This study has also considered two solute travel cases in the intervascular and extravascular space: non-reactive system with hapten and reactive system with bifunctional antibody (BFA). The mass transfer algorithm results have involved the convection flow with the solution perfusion and retention in the Krogh cylinder model extravascular space and indicate the convection has an essential role in drug delivery.

2.2. RECOMMENDATIONS

The dissertation has provided a base fluid exchange theoretical simulation method and model in single vessel and its surrounding tissue. The effect of capillary pressure and extravascular space pressure is largely unknown. In order to support and verify the simulation model of intervascular and extravascular space in the tumor tissue, the detailed experimental data are required. It is important step to discover the fluid dynamics in microenvironmental. The result could develop to allometric scaling or multi parallel capillaries structural to an organ, such as the profile of partial pressure in the organ. It also makes it important in the future to study the flow more closely to obtain higher amounts of convection in keeping with discussions in physiology.

APPENDIX

THE SHORT BIOGRAPHICAL OF SCHACK AUGUST STEENBERG KROGH

August Krogh was from Denmark, where he was born in November 1874, and received the Nobel Prize for Physiology or Medicine in 1920. His scientific life is devoted almost fully to the study of capillary.

In his youth, he made an important discovery that the relationship that played the key role of regulation of CO₂ in atmosphere was the ocean, which assisted in studying the mass transfer process between oxygen and the CO₂ in the physiological systems.

Krogh has a significant contribution that studied the mechanism of above gas exchange. The capillaries are connected between the arteries and veins. The walls of the capillaries are very thin, made with only a layer of flat endothelial cells. The capillary diameter is small, the blood flow is very slow, and the permeability is large, which is beneficial to transfer of oxygen and nutrients in the blood, cells, and tissues. The metabolites are exchanged between the extravascular tissue and the capillary.

Krogh created a new direction in capillary research and in that he studied all aspects including neurotransmission and muscular control. He presented his studies in seven lectures at Yale University which is available in form of a book: *The Anatomy and Physiology of Capillaries*, Yale University Press, New Haven, 1922.

Krogh has another important contribution in insulin. His wife, Marie Krogh, had diabetes. Krogh learned the extraction of insulin from Banting (Banting, F.G., 1891-1941) a Canadian surgeon, and returned to Copenhagen with production permit and

healed his wife's illness. The insulin produced in Denmark was used to treat patients in March 1923. This was the beginning of Novo Nordisk's business. He was helped in this venture all through by his wife.

BIBLIOGRAPHY

- Abramowitz, M., Stegun, I. (1968) Handbook of Mathematical Functions. With Formulas, Graphs, and Mathematical Tables. U.S. Dept. of Commerce National Bureau of Standards; 374.
- Bassingthwaighe, J.B., Chan, I.S.J., Wang, C.J. (1992). Computationally efficient algorithms for convection-permeation-diffusion models for blood-tissue exchange. *Annals Biomedical Eng.* 20, 687-725.
<https://doi.org/10.1007/BF02368613>
- Baxter, L.T., Jain, R.K. (1989). Transport of fluid and macromolecules in tumors. I. Role of interstitial pressure and convection. *Microvasc. Res.* 37: 77-104.
- Baxter, L.T., Yuan, F., Jain, R.K. (1992). Pharmokinetic analysis of the perivascular distribution of bifunctional antibodies and haptens: Comparison with experimental data. *Cancer Res.* 52, 5838-5844.
- Baxter, L.T., Zhu, H., Mackensen, D.G., Butler, W.F., Jain, R.K. (1995). Biodistribution of monoclonal antibodies: Scale-up from mouse to human using a physiologically based pharmacokinetic model. *Cancer Res.* 55. 4611-4622.
<https://doi.org/10.1016/j.dmpk.2018.11.002>
- Baxter, L.T., Zhu, H., Mackenson, D.G, Jain, R.K. (1994). Physiologically based pharmacokinetic model for specific and nonspecific monoclonal antibodies and fragments in normal tissue and human tumor xenografts in nude mice. *Cancer Res.* 54, 1517-1528.
- Boucher. Y., Brekken. C., Netti, P.A., Baxter, L.T., Jain, R.K., (1988). Intratumoral infusion of fluid: estimation of hydraulic conductivity and implications for the delivery of therapeutic agents. *Brit. J. Cancer.* 78: 1442-1448.
- Brinkman, H.C. (1947) A calculation of the viscous force exerted by a flowing fluid on a dense swarm of particles. *Applied Scientific Research.* 1:27.
- Cattaneo, L., Zunino, P. (2014). A computational model of drug delivery through microcirculation to compare different tumor treatments. *Int. J. Numer. Meth. Biomed. Engng.* 30. 1347-1371. <https://doi.org/10.1002/cnm.2661>
- Chauhan, V.P., Lanning, R.M., Diop-frimpong, B., Mok, W., Brown, E.B., Padera, T.P., Boucher, Y., Jain, R. (2009) Multiscale measurements distinguish cellular and interstitial hindrances to diffusion in vivo. *Biophys. J.* 97: 330-336.
<https://doi.org/10.1016/j.bpj.2009.03.064>

- Chetty, M., Johnson, T. N., Polak, S., Salem, F., Doki, K. and Rostami-Hodjegan, A. (2020). "Physiologically Based Pharmacokinetic Modelling To Guide Drug Delivery In Older People". *Advanced Drug Delivery Reviews*, vol 135, 2018, pp. 85-96. Elsevier BV, doi:10.1016/j.addr.2018.08.013.
- Cooney, D.O. (1976) *Biomedical Engineering Principles*, Marcel Dekker, N.Y.
- Fenster, A., Laceyfield, J.C., (2015). *Ultrasound Imaging and Therapy*. CRC Press, Taylor & Francis, Boca Raton, Fl; 2015: 67.
- Fournier, R.L. (1999) *Basic Transport in Biomedical Engineering*, Taylor and Francis, Philadelphia. 24, 44, 71.
- Gaehtgens P. (1980). Flow of blood through narrow capillaries: rheological mechanisms determining capillary hematocrit and apparent viscosity. *Biorheology*, 17(1-2), 183–189. <https://doi.org/10.3233/bir-1980-171-220>
- Goldman, D. (2008). Theoretical models of microvascular oxygen transport to tissue. *Microcirculation*. 15, 795-811. <https://doi.org/10.1080/10739680801938289>
- Gullino, P., Grantham, F. (1961). Studies on the exchange of fluids between host and tumor. I. A method for growing “tissue-isolated” tumors in laboratory animals. *J. Natl. Cancer Inst.* 27, 679–693.
- Gullino, P.M., Grantham, F.H. (1961) Studies on the exchange of fluids between host and tumor. II. The blood flow of hepatomas and other tumors in rats and mice. *J. Nat. Cancer Institute.* 27, 1465-1491. <https://doi.org/10.1093/jnci/27.6.1465>
- Guyton, A.C., Hall, J.E. (2000) *Textbook of Medical Physiology*, 10th ed., W.B. Saunders Co., Philadelphia, pp. 163.
- Guyton, A.C., Hall, J.E., 2006. *Textbook of Medical Physiology*, 11th ed., Saunders.
- Haberman, W.L., Sayre, R.M. (1958). Motion of rigid fluid spheres in stationary and moving liquids inside cylindrical tubes. U.S. Department of Navy, David Taylor Model Basin Report. 1143 NS 715-102.
- Happel, J. (1958). Viscous flow in a multiparticle systems: Slow motion of fluids relative to beds of spherical particles. *AIChE J.* 4, 197-201. <https://doi.org/10.1002/aic.690040214>
- Haward, R.N. (1973). Introduction (The nature of polymer glasses, their packing density and mechanical behavior) in *The Physics of Glassy Polymers*, R.N. Haward, ed., Applied Sci. Pub., London; 1-53 (see Table 5, p. 43).
- Iwata, H., Morikawa, N., Ikada, Y. (1996). Permeability of filters used for immunoisolation. *Tissue Eng.* 2, 289-298. <https://doi.org/10.1089/ten.1996.2.289>

- Jain, R.K. (1989) Delivery of novel therapeutic agents in tumors: Physiological barriers and strategies. *J Natl Cancer Inst* 81:570-576
- Jain, R.K. (2013) Normalizing Tumor Microenvironment to Treat Cancer: Bench to Bedside to Biomarkers. *Clinical Oncology*, 31, No. 17, 2205-2218
- Jain, R.K. (2013). Normalizing tumor microenvironment to treat cancer: Bench to biomarkers. *J. Clinical Oncology*. 31, 2205-2218.
<https://doi.org/10.1200/JCO.2012.46.3653>
- Jain, R.K. Stylianopoulos, (2010) *T. Nat. Rev. Clin. Oncol.* 7, 653–664 published online 14 September 2010; doi:10.1038/nrclinonc.2010.139
- Jain, R.K., Tong, R.T., Munn, L.L. (2007) Effect of vascular normalization by antiangiogenic therapy on interstitial hypertension, peritumor edema, and lymphatic metastasis: Insights from a mathematical model. *Cancer Res* 67:2729-2735
- Kojic, M., Milosevic, M., Simic, V., Koay, E.J., Fleming, J.B., Nizzero, S., Kojic, N., Ziemys, A., Ferrari, M. (2017). A composite smeared finite element for mass transport in capillary systems and biological tissue. *Comput. Methods Appli. Mech. Engng.* 324, 413-437. <https://doi.org/10.1016/j.cma.2017.06.019>
- Kojic, M., Milosevic, M., Simic, V., Koay, E.J., Ziemys, A., Ferrari, M. (2018). Multiscale smeared finite element model for mass transport in biological tissue: From blood vessels to cells and cellular organelles. *Comput. Biology Medicine*. 99, 7-23. <https://doi.org/10.1016/j.combiomed.2018.05.022>
- Krogh A. (1919). The number and distribution of capillaries in muscles with calculations of the oxygen pressure head necessary for supplying the tissue. *The Journal of physiology*, 52(6), 409–415. <https://doi.org/10.1113/jphysiol.1919.sp001839>
- Krogh A. (1919). The supply of oxygen to the tissues and the regulation of the capillary circulation. *The Journal of physiology*, 52(6), 457–474.
<https://doi.org/10.1113/jphysiol.1919.sp001844>
- Krogh, A. – Biographical. NobelPrize.org. Nobel Media AB 2020. Sat. 24 Oct 2020.
<<https://www.nobelprize.org/prizes/medicine/1920/krogh/biographical/>>
- Kubínová, L., Mao, X. W., & Janáček, J. (2013). Blood capillary length estimation from three-dimensional microscopic data by image analysis and stereology. *Microscopy and Microanalysis*, 19(4), 898-906.
<http://dx.doi.org/10.1017/S1431927613001487>
- Larsen, M.T., Kuhlmann, M., Hvam, M.L., Howard, K.A. (2016). Albumin-based drug delivery: harnessing nature to cure disease. *Molecular Cellular Therapies*. 4(3), 1-12 <https://doi.org/10.1186/s40591-016-0048-8>

- Løkkegaard, A., Nyengaard, J. R., & West, M. J. (2001). Stereological estimates of number and length of capillaries in subdivisions of the human hippocampal region. *Hippocampus*, 11(6), 726–740. <https://doi.org/10.1002/hipo.1088>
- Mangulis, V., *Handbook of Series for Scientists and Engineers*, Academic Press Inc., New York; 1965: 90, 95.
- Martin J.D., Jain, R.K. (2020) Normalizing the Tumor Microenvironment for Radiosensitization. *Molecular Targeted Radiosensitizers* pp 301-338 chapter 12
- Mascheroni, P., Penta, R. (2017). The role of microvascular network structure on diffusion and consumption of anticancer drugs. *Int. J. Numer. Meth. Biomed. Engng.* 33: e2857. <https://doi.org/10.1002/cnm.2857>
- Netti, P.A., Roberge, S., Boucher, Y., Baxter, L.T., Jain, R.K. (1996). Effect of transvascular fluid exchange on pressure-flow relationship in tumors: a proposed mechanism for tumor blood flow heterogeneity. *Microvasc. Res.* 52. 27-46. <https://doi.org/10.1006/mvre.1996.0041>
- Nugent, L.J., Jain, R.K. (1984). Extravascular diffusion in normal and neoplastic tissues. *Cancer Res.* 44, 238-244.
- Penta, R., Ambrosi, D. (2015) The role of microvascular tortuosity in tumor transport phenomena. *J. Theor. Biol.* 364, 80-97. <https://doi.org/10.1016/j.jtbi.2014.08.007>
- Penta, R., Ambrosi, D., Quateroni, A. (2015) Multiscale homogenization for fluid and drug transport in vascularized malignant tissues. *Math. Models and Methods Appl. Sci.* 25, 79-108. <https://doi.org/10.1142/S0218202515500037>
- Pfeffer, R. (1964). Heat and mass transport in multiparticle systems. *I&EC Fundamentals.* 3, 308-383. <https://doi.org/10.1021/i160012a018>
- Qiu, X., Sane, N., Neogi, P. (2019). Convection in Krogh cylinder: Putting back fluid flow in the extravascular tissue. *AIChE J.* 65. e16720/1-7. <https://doi.org/10.1002/aic.16720>
- Renkin, E.M. (1977). Multiple pathways of capillary permeability. *Circulation Res.* 41, 735-743. <https://doi.org/10.1161/01.res.41.6.735>
- Replogue, R. L., Meiselman, H. J., Merrill, E. W. (1967). SPECIAL ARTICLE: Clinical Implications of Blood Rheology Studies. *Circulation*, 36(1), 148–160. <https://doi.org/10.1161/01.cir.36.1.148>
- Rippe, B., Haraldsson, B. (1987). Fluid and protein fluxes across small and large pores in the microvasculatures. Application of two-pore equation. *Acta Physiol Scand.* 131, 411-428. <https://doi.org/10.1111/j.1748-1716.1987.tb08257.x>

- Roache, J., 1998. *Fundamentals of Computational Fluid Dynamics*. Hermosa Pub.
- Schmid-Schönbein, G.W. (1999) Biomechanics of microcirculatory blood perfusion. *Annual Review of Biomedical Engineering*. 1:73-102.
<https://doi.org/10.1146/annurev.bioeng.1.1.73>.
- Secomb, T.W. (2014). Krogh-cylinder and infinite domain models for washout of an inert diffusible solute from tissue. *Microcirculation*. 22, 91-98.
<https://doi.org/10.1111/micc.12180>
- Secomb, T.W., Hsu, R., Pries, A.R. (2006) Tribology of capillary blood flow. *Proc. IMechE v.220 Part J: J. Engineering Tribology*. 767-774.
<https://doi.org/10.1243/13506501JET121>
- Shiple, R., Chapman, S.J. (2010) Multiscale modelling of fluid and drug transport in vascular tumours. *Bull. Math. Biol.* 72, 1464-1491.
<https://doi.org/10.1007/s11538-010-9504-9>
- Smaje, L., Zweifach, B.W., Intaglietta, M. (1970) Micropressures and capillary filtration coefficients in single vessels of the cremaster muscle of the rat. *Microvascular Res.* 2, 96-110. [https://doi.org/10.1016/0026-2862\(70\)90055-5](https://doi.org/10.1016/0026-2862(70)90055-5)
- Swabb, E.A., Wei, J., Gullinon P.M. (1974). Diffusion and convection in normal and neoplastic tissue. *Cancer Res.* 34: 2814-2822.
- Tao, C., Chuah, Y.J., Xu, C., Wang, D.A. (2019). Albumin conjugates and assemblies as versatile bio-functional additives and carriers for biomedical applications. *J. Material Chemistry B*, 7, 357-367. <https://doi.org/10.1039/c8tb02477d>
- Welling, P.G. (1997) *Pharmacokinetics*. 2nd ed., Amer. Chem. Soc., Washington, D.C.
- Wolinsky, H (1980) A Proposal Linking Clearance of Circulating Lipoproteins to Tissue Metabolic Activity as a Basis for Understanding Atherogenesis. *Journal of the American Heart Association*, 47, NO. 3, 301-311

VITA

Xianjie Qiu is from Guangzhou City, China. He came to the United States of America in Spring 2010 and studied at East Los Angeles College. He transferred to Missouri University of Science and Technology and received the Bachelor of Science in Chemical Engineering in December 2015. He received the Master of Science in Chemical Engineering in August 2018 from Missouri S&T. He received the Doctor of Philosophy in Chemical Engineering from Missouri S&T in May 2021.